Relativistic plane wave description of spin transfer observables for proton knockout reactions

S. M. Wyngaardt

Dissertation presented for the degree of Doctor of Philosophy at the University of Stellenbosch

Supervisor: Prof. A. A. Cowley

Co-supervisor: Dr. G. C. Hillhouse

March 2001

Declaration

I the undersigned hereby declare that the work contained in this dissertation is my own original work and has not previously in its entirety or in part been submitted at any university for a degree.

Abstract

In this dissertation we set out to develop the first relativistic model for calculating complete sets of $(p, 2p)$ spin transfer observables. In addition to this a new technique has been developed which allows us to evaluate the transition amplitude, which is used to calculate the scattering observables for the reaction directly. The influence of various medium-modified parameters on the scattered wave functions and NN interaction have been investigated. Due to ambiguities surrounding the πNN coupling we have included both pseudoscalar and pseudovector coupling into the nucleon-nucleon interaction model. Furthermore we have included two different kinematic prescriptions to obtain the effective NN laboratory kinetic energy and center of mass scattering angle, which are used to obtain the NN scattering amplitudes. The aim of this study is to investigate the effects of the various model parameters on complete sets of scattering observables.

Our investigation has shown that although the analyzing power is not very sensitive to nuclear medium effects, and the various other spin transfer observables such as D_{nn} should provide valuable insight. Further refinements of the model would be to include nuclear distortions as well as the IA2 model of the NN interaction.

Samevatting

In hierdie tesis ontwikkel ons die eerste relatiwistiese model vir die berekening van 'n volledige stel $(p, 2p)$ spin waarneembares. Verder word 'n nuwe tegniek ingevoer wat ons toelaat om die oorgangsamplitude, wat gebruik word in berekening van die verstrooings waarneembares vir die reaksie, direk te evalueer. Die invloed van verskeie medium-gemodifiseerde parameters op die verstrooide golffunksies en die NN wisselwerking word bestudeer. As gevolg van onsekerhede betreffende die πNN koppeling word beide die pseudoskalaar en pseudovektor koppeling in die nukleon-nukleon interaksie model ingesluit. Ons sluit ook twee verskillende kinematiese preskripsies in om die effektiewe NN laboratorium kinetiese energie en die massa middelpunt verstrooiings hoek, wat gebruik word vir die berekening van die NN verstrooiings amplitude, te bereken. Die doel van hierdie studie is om die effek van verskeie model parameters op 'n volledige stel spin waarneembares te ondersoek.

Die studie toon dat alhoewel die analiseervermoë nie baie sensitief is vir medium effekte nie, die ander spin waarneembares soos byvoorbeeld D_{nn} waardevolle insig lewer. Daar word voorgestel dat die model verfyn word deur kerndistorsies as ook die meer algemele IA2 model vir die NN interaksie in te sluit.

Acknowledgements

I would like to express my thanks and appreciation to the following people for their assistance, support and encouragement during the completion of my dissertation:

- First of all, my advisor and co-advisor Prof. A. A. Cowley and Dr. G. C. Hillhouse for their wonderful guidance during the past three year over which my Ph. D project has been developed.
- The National Accelerator Center and the National Research Foundation for their financial support which helped to make this project possible.
- A special word of thanks to Prof. J. Mano of the Prefectural College of Technology for assisting me with the programming of my code which I used in performing the calculations.
- Profs. N. S. Chant and P. G Roos for the five months which I spent at the University of Maryland, College Park, and for their help and the wonderful discussions during this period of time.
- Mrs. H. Kannemeyer and W. Joubert for the binding and copy work.
- My colleague Andrew van Biljon for his help with the Linux computer system.
- The staff of the Physics department at the University of Stellenbosch for their friendliness during my five years which I spent with the department.
- On a more personal note I'd like to thank my parents for laying me a rock solid foundation on which to build on.
- My brother and sister for putting up with your "big" brother, especially on those days when the stress levels were a bit high.
- My four aunts and two uncles, cousins and their families for being such a wonderful bunch of people whose doors are always open for a chat, a question or just a cup of tea.

- Greg Hillhouse, my co-advisor, colleague and dear friend for his guidance not only on the academic front, but also in my personal life.
- My "Physics" friends Faith, Retief, Stanley, Christine, Andrew, Tinus and Gillian, thanks for making these past five years one of the most fun filled experiences of my life.
- My friends Christine Kühl, Marc Schneberger, Esther Hainebach, Deepak Goel, Annette Müller, Tami Frank and Alexandra Kott for all the email's.
- A special word of thanks to my dear friends Christine Kühl and Annette Müller for the post cards and letters throughout the years.

Dedicated to my parents Charles and Dulcie Wyngaardt

Contents

Chapter 1

Scientific motivation

1.1 Introduction and motivation

Historically proton knockout reactions, and in particular $(p, 2p)$ reactions have often been used to study single-particle properties of nuclei and the momentum distributions of bound protons in various nuclei [Kit76]. For such investigations the unpolarized triple differential cross section has usually been adequate to extract the required information. Polarized $(p, 2p)$ experiments are currently being performed at energies above 400 MeV [Nor00], for which nuclear distortion effects on the scattered protons are expected to become negligible. Consequently a plane wave model should provide a reasonable description of the scattering observables at high energies.

Spin observables, being ratios of spin-dependent cross sections, are expected to be relatively insensitive to distortions of the scattering wave functions at energies above 400 MeV and, hence, can provide unique information regarding the modification of the free nucleon-nucleon (NN) interaction by the surrounding nuclear medium in the high energy region. Hence, simple plane wave models of the scattering process should provide an adequate first order description of the spin observables within this energy regime. In particular, the exclusive $(\vec{p}, 2\vec{p})$ reaction, whereby an incident polarized proton knocks out a proton from specific orbital in the nucleus and the two outgoing protons are detected in coincidence, is ideally suited for studying medium modifications of the NN interaction [Kud86].

There are a number of compelling reasons for pursuing relativistic models of nuclear structure and nuclear scattering. For example, it is important to have a manifestly Lorentz covariant formalism [Ser86], especially for reliable extrapolation of nuclear systems to extreme conditions of density, or momentum transfer. Historically, the first great triumph of the Dirac equation was its explanation of the spin and magnetic moment of the electron. The relativistic 4–component

Dirac equation provides a natural explanation of the nuclear spin–orbit force. Simple relativistic models provide an excellent description of spin observables for elastic proton scattering at medium energies [McN83]. On the other hand only very sophisticated state–of–the–art non-relativistic models can describe elastic proton scattering with the same level of accuracy. The above considerations motivate our choice of relativistic Dirac-equation-based models as opposed to conventional non-relativistic Schrödinger-equation-based models.

For $(\vec{p}, 2\vec{p})$ reactions, all existing relativistic (and non-relativistic) distorted wave impulse-approximation models appear to fail to reproduce the analyzing power A_y for knockout of $2s_{1/2}$ protons from ^{40}Ca at incident energies of 200 and 300 MeV [Cow00]. Clues for the latter failure will hopefully be found by comparing calculations to complete sets of spin transfer observables allowed by parity and time-reversal invariance, namely P, A_y, D_{nn}, $D_{s'\ell}$, $D_{\ell's}$, $D_{s's}$ and $D_{\ell'\ell}$. However, current relativistic models [Coo89, Ike95, Man96, Man98] have yet to be extended to include the latter observables. In an effort to systematically investigate the analyzing power problem and also to provide a benchmark for future relativistic distorted wave calculations of complete sets of spin transfer observables, we develop a simple relativistic plane wave model where the NN interaction is parametrized in terms of five Fermi (scalar, pseudo-scalar, vector, axial-vector, tensor) invariants, the so-called IA1 representation [McN83]. This model will allow us to investigate the importance of nuclear medium effects within the context of the relativistic mean field approximation of Serot and Walecka [Ser86], whereby free nucleon masses are replaced by smaller effective nucleon masses in the plane wave Dirac spinors, thus enhancing the lower component contributions of the relativistic four-component scattering wave functions. In addition, we will be able to study the influence of different representations of the NN interaction on effective-mass-type medium modifications of the spin transfer observables. For example, for inclusive quasi-elastic $(\vec{p}, \vec{p}')$ scattering it has been shown that the IA1 representation overestimates the importance of nuclear medium effects compared to a more general Lorentz invariant representation of the NN interaction in terms of 44 invariant amplitudes [Ven99].

By definition the polarization transfer observables are ratios of linear combinations of polarized triple differential cross sections. We have developed a relativistic plane wave model whereby the polarized triple differential cross section is written as a contraction between a hadron tensor and a nuclear response tensor. The hadron tensor contains information about the spin projections of the projectile and outgoing scattering wave functions. The spin-independent nuclear

response tensor, on the other hand, contains information about the nuclear structure of the target nucleus. For the NN amplitudes we use the relativistic Horowitz-Love-Franey model [Hor85] which parameterizes the IA1 representation as a sum of Yukawa-like meson exchanges where both direct and exchange diagrams are considered separately. The relativistic boundstate wave function for the struck nucleon is generated using the self-consistent Dirac-Hartree approach developed by Horowitz and Murdock [Lan91].

The layout of this thesis is as follows: Chapter 2 deals with the relativistic plane wave impulse approximation formalism for calculating complete sets of $(p, 2p)$ spin transfer observables. In chapter 3 we show numerical results of our calculations of these sets of observables. Finally, in chapter 4 we give a summary of this thesis.

Chapter 2

Relativistic plane wave model

2.1 Introduction

In this chapter we present a relativistic plane wave impulse approximation formalism for calculating complete sets of $(p, 2p)$ spin transfer observables.

The following section deals with the $(p, 2p)$ reaction mechanism and a brief discussion of the polarized $(p, 2p)$ reaction. In section (2.3) we define the $(p, 2p)$ scattering observables. The unpolarized triple differential cross section is defined and discussed in section (2.3.1) as an introduction to section (2.3.2) which deals with the polarized triple differential cross section. Polarized spin transfer observables are introduced in section (2.3.3), which are linear combination of polarized triple differential cross sections. In section (2.4) we derive the kinematic quantities which are needed in our model. The wave functions of the various scattered particles are dealt with in section (2.5), which also covers the relativistic plane wave model. A short discussion of the Dirac-Hartree approximation and its implementation for extracting the relativistic boundstate wave function is given in section (2.6.1). The nucleon-nucleon interaction employed is discussed in section (2.7). The relativistic Love-Franey (RLF) model is used to generate Lorentz invariant NN amplitudes. We also include Maxwell's energy dependent parameterization [Max96, Max98] into the RLF model. We will show how nuclear medium effects are included in our model with the inclusion of both pseudoscalar and pseudovector coupling for the πNN vertex. The transition amplitude is evaluated in section (2.9). Section (2.10) gives a summary on this chapter.

2.2 The reaction mechanism

The reaction mechanism for $(p, 2p)$ reactions is depicted schematically in fig. (2.1). The experimental setup is such that the scattering angles of the two ejectiles are fixed at $\theta_{a'}$ and $\theta_{b'}$ to the left and right of the incident beam, respectively. The experiment is set up in such a way that only protons which are detected in coincidence with each other, are counted. In a polarized $(p, 2p)$ experiment the spin polarization of the projectile and left scattered beam (a') are measured along any two combinations of the incident and scattered beam directions represented by the unit vectors $(\hat{l}, \hat{s}, \hat{n})$ and $(\hat{l}', \hat{s}', \hat{n})$ respectively as shown in fig. (2.1), and allowed by parity, time- reversal and rotational invariance.

2.3 Scattering observables

In this section we will give expressions for the scattering observables which are measured in $(p, 2p)$ reactions. All $(p, 2p)$ scattering observables are expressed in terms of the transition amplitude $T_{L_b J_b}(\mu_a, \mu_{a'}, \mu_{b'}, M_b)$, which contains information about the dynamics of the scattered protons in the entrance and exit channels, the nucleon-nucleon interaction as well as the boundstate wave function of the bound proton b, and is defined by the expression

$$\begin{aligned} T_{L_b J_b}(\mu_a, \mu_{a'}, \mu_{b'}, M_b) &= \int\int d\vec{x} d\vec{x'} \bar{\Psi}^-(\vec{k}_{a'}, \vec{x}, \mu_{a'}) \otimes \bar{\Psi}^-(\vec{k}_b, \vec{x'}, \mu_{b'}) \hat{t}_{NN}(|\vec{x} - \vec{x}'|) \\ &\quad \times \Psi^+(\vec{k}_a, \vec{x}, \mu_a) \otimes \Phi_{L_b J_b M_b}(\vec{x}'). \end{aligned} \tag{2.1}$$

The symbols $\Psi(\vec{k}_{a'}, \vec{x}, \mu_{a'})$ and $\Psi(\vec{k}_b, \vec{x'}, \mu_{b'})$ refer to the particle wave functions of the scattered protons (a') and (b') , whereas $\Psi(\vec{k}_a, \vec{x}, \mu_a)$ and $\Phi_{L_b J_b M_b}(\vec{x}')$ represent the particle wave function for the projectile a and boundstate wave function of the target nucleon b in the entrance channel, respectively. The bar notation is used to denote the complex conjugate transpose of a wave function and is related to the adjoint of the wave function by $\bar{\Psi} = \Psi^\dagger \gamma^0$, where $(+)$ and $(-)$ represent incoming and outgoing boundary conditions for the projectile and ejectiles, respectively. The scattering wave functions are expressed as functions of the laboratory momenta $\vec{k}_{a'}$, $\vec{k}_{b'}$ and $\vec{k}_a$ of protons a', b' and a respectively; explicit expressions for the scattering momenta are given in section (2.4.1). The position vectors of the protons are labeled by $\vec{x}$ and $\vec{x'}$. In a plane wave model distortions, due to the proton-nucleus optical potentials, on the projectile and scattered

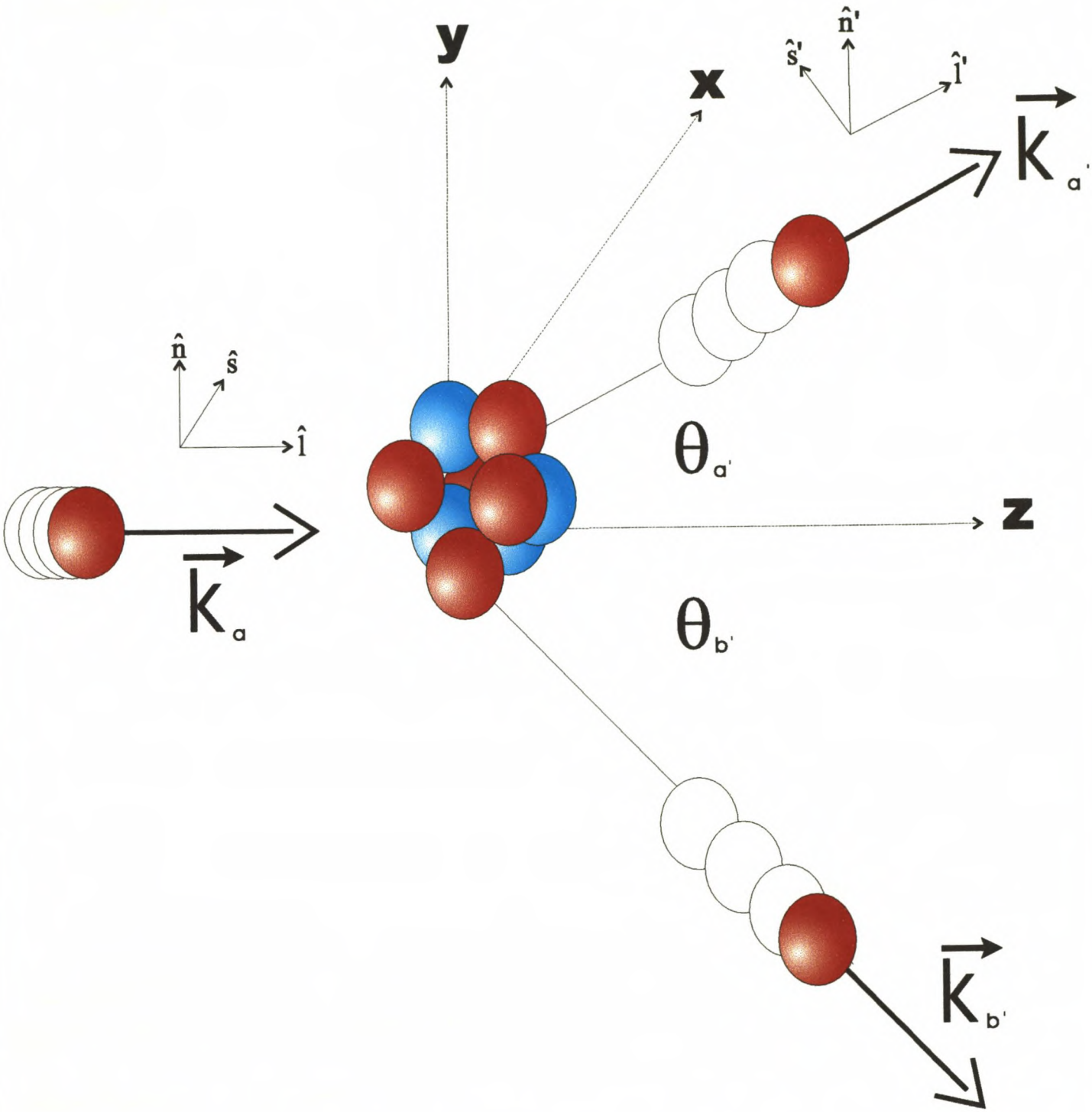

Figure 2.1: A schematic representation of the knockout of the proton b bound in a nucleus by an incident proton a with momentum $\vec{k}_a$ for a $(p, 2p)$ reaction. The left and right scattered protons are labeled a' and b' respectively. The reference axes are chosen such that z points in the incident beam direction with x in the scattering plane. The y-axis is taken to be perpendicular to the scattering plane.

protons are ignored. The scattering wave functions are thus taken to be free plane waves. In section (2.9) we will evaluate the transition amplitude associated with this plane wave model.

2.3.1 Unpolarized triple differential cross section

The probability for a proton knockout reaction to occur is related to the triple differential cross section. In a $(p, 2p)$ reaction this quantity is associated with the probability that an incident proton knocks out a bound proton from a specific orbital in the target nucleus and then detecting these two protons in the exit channel in coincidence with each other. The expression for the unpolarized triple differential cross section is given by [Kud86]

$$\frac{d^3\sigma}{d\Omega_{a'}d\Omega_b dE_{a'}} = \frac{F_{kin}}{(2J_b+1)(2s_a+1)} S_{L_bJ_b} \sum_{\mu_a\mu_{a'}\mu_{b'}M_b} |T_{L_bJ_b}(\mu_{a'}, \mu_a, \mu_b, M_b)|^2 \tag{2.2}$$

where F_{kin} is a kinematic factor

$$F_{kin} = \frac{E_a E_{a'} E_{b'}}{(2\pi)^5} \frac{k_{a'}k_{b'}}{k_a} \left[1 + \frac{E_{b'}}{E_C}\left(1 - \frac{k_a}{k_{b'}}cos\theta_{b'} + \frac{k_{a'}}{k_b}cos(\theta_{a'} + \theta_{b'})\right)\right]^{-1} \tag{2.3}$$

which is a function of the kinetic energies E_i and momenta k_i of the projectile (a), the two scattered protons (a') and (b') and the residual nucleus C in the exit, a spectroscopic factor $S_{L_bJ_b}$, which gives the probability that a proton is found in an orbital specified by the orbital angular momentum and total angular momentum quantum numbers L_b and J_b respectively. The symbols s_a, μ_a, $\mu_{a'}$, $\mu_{b'}$ and M_b represent the spin of the incident proton a, the spin projection of the projectile a, the two ejectiles a' and b', and the total angular momentum projection of the bound particle b respectively. We use $dE_{a'}$, $d\Omega_{a'}$ and $d\Omega_b$ to represent the kinetic energy increment of the scattered proton a' and the solid angles of the detectors fixed at the laboratory scattering angles $\theta_{a'}$ and $\theta_{b'}$ respectively.

2.3.2 Polarized triple differential cross section

In the previous section we have defined the unpolarized triple differential cross section. In the following two sections we define the polarization transfer observables in terms of ratios of linear combinations of polarized triple differential cross sections for various orientations of

spin projections allowed by time reversal, parity and rotational invariance. Polarized triple differential cross sections are obtained by selecting the spin projections of the projectile (μ_a) and the proton which is scattered to the left of the incident beam ($\mu_{a'}$). The polarized triple differential cross section for this particular selection of spin projections is obtained by selecting the particular spin orientations for protons a and a' in Eq. (2.2), hence giving the relationship

$$\frac{d^3\sigma(\mu_a,\mu_{a'})}{d\Omega_{a'}d\Omega_{b'}dE_{a'}} = \frac{F_{kin}}{(2J_b+1)}S_{L_bJ_b}\sum_{\mu_{b'}M_b}|T_{L_bJ_b}(\mu_a,\mu_{a'},\mu_{b'},M_b)|^2. \tag{2.4}$$

In section (2.9) we will look at $|T_{L_bJ_b}(\mu_a,\mu_{a'},\mu_{b'},M_b)|^2$ in greater detail. The $(p,2p)$ polarization transfer observables (or spin observables for short) will be defined in the next section.

2.3.3 Polarization transfer observables

Due to technological advances in the development of polarized proton beams and high resolution spectrometers with focal plane polarimeters, the recent focus has shifted from measuring unpolarized cross sections towards measuring complete sets of polarization transfer observables for various nuclear reactions. These polarization experiments utilize an incident proton beam polarized in an arbitrary orientation to determine the components of the polarization of the scattered protons.

Expressions for calculating complete sets of nucleon-nucleon (NN) spin transfer observables ($D_{i'j}$) in terms of differential cross section are given by [Pal81]

$$D_{i'j} = \frac{\sigma_{\hat{j}\to\hat{i}'} - \sigma_{\hat{j}\to-\hat{i}'} - \sigma_{-\hat{j}\to\hat{i}'} + \sigma_{-\hat{j}\to-\hat{i}'}}{\sigma_{\hat{j}\to\hat{i}'} + \sigma_{\hat{j}\to-\hat{i}'} + \sigma_{-\hat{j}\to\hat{i}'} + \sigma_{-\hat{j}\to-\hat{i}'}} \tag{2.5}$$

where $\hat{j} \in \{\hat{l},\hat{n},\hat{s}\}$ and $\hat{i}' \in \{\hat{l}',\hat{n},\hat{s}'\}$. The unit vectors $\hat{l}$, $\hat{n}$ and $\hat{s}$ are defined in terms of the initial and final laboratory momenta $\vec{k}$ and $\vec{k}'$ as follows

$$\begin{aligned}
\hat{l} &= \frac{\vec{k}}{|\vec{k}|},\\
\hat{l}' &= \frac{\vec{k}'}{|\vec{k}'|},\\
\hat{n} &= \frac{\vec{k}\times\vec{k}'}{|\vec{k}\times\vec{k}'|},\\
\hat{s} &= \frac{\vec{n}\times\vec{l}}{|\vec{n}\times\vec{l}|}.
\end{aligned}$$

$$\hat{s}' = \frac{\vec{n} \times \vec{l}'}{|\vec{n} \times \vec{l}'|}.$$

For the analyzing power (D_{0n}) we measure the probability that an incident beam with polarization direction $\hat{n}$ is unpolarized by the interaction with the target nucleus. Hence, we define D_{0n} as

$$D_{0n} = \frac{\sigma_{\hat{n}\to 0} - \sigma_{-\hat{n}\to 0}}{\sigma_{\hat{n}\to 0} + \sigma_{-\hat{n}\to 0}} \tag{2.6}$$

where

$$\sigma_{\hat{n}\to 0} = \sigma_{\hat{n}\to\hat{n}} + \sigma_{\hat{n}\to -\hat{n}}. \tag{2.7}$$

By imposing rotational, parity and time-reversal invariance on NN scattering only a set of 7 spin transfer observables $\{D_{n0}, D_{0n}, D_{nn}, D_{s'l}, D_{s's}, D_{l's}, D_{l'l}\}$ are allowed. Analogous to NN scattering one can define a set of polarization transfer observables for $(p, 2p)$ reactions in terms of the polarized triple differential cross section as follows:

$$D_{i'j} = \frac{\frac{d^3\sigma_{j\to i'}}{d\Omega_{a'}d\Omega_{b'}dE_{a'}} - \frac{d^3\sigma_{j\to -i'}}{d\Omega_{a'}d\Omega_{b'}dE_{a'}} - \frac{d^3\sigma_{-j\to i'}}{d\Omega_{a'}d\Omega_{b'}dE_{a'}} + \frac{d^3\sigma_{-j\to -i'}}{d\Omega_{a'}d\Omega_{b'}dE_{a'}}}{\frac{d^3\sigma_{j\to i'}}{d\Omega_{a'}d\Omega_{b'}dE_{a'}} + \frac{d^3\sigma_{j\to -i'}}{d\Omega_{a'}d\Omega_{b'}dE_{a'}} + \frac{d^3\sigma_{-j\to i'}}{d\Omega_{a'}d\Omega_{b'}dE_{a'}} + \frac{d^3\sigma_{-j\to -i'}}{d\Omega_{a'}d\Omega_{b'}dE_{a'}}}. \tag{2.8}$$

Similar to Eq. (2.6) we define the analyzing power for the $(p, 2p)$ reaction as follows

$$D_{0n} = \frac{\frac{d^3\sigma_{\hat{n}\to 0}}{d\Omega_{a'}d\Omega_{b'}dE_{a'}} - \frac{d^3\sigma_{-\hat{n}\to 0}}{d\Omega_{a'}d\Omega_{b'}dE_{a'}}}{\frac{d^3\sigma_{\hat{n}\to 0}}{d\Omega_{a'}d\Omega_{b'}dE_{a'}} + \frac{d^3\sigma_{-\hat{n}\to 0}}{d\Omega_{a'}d\Omega_{b'}dE_{a'}}} \tag{2.9}$$

where

$$\frac{d^3\sigma_{\hat{n}\to 0}}{d\Omega_{a'}d\Omega_{b'}dE_{a'}} = \frac{d^3\sigma_{\hat{n}\to\hat{n}}}{d\Omega_{a'}d\Omega_{b'}dE_{a'}} + \frac{d^3\sigma_{\hat{n}\to -\hat{n}}}{d\Omega_{a'}d\Omega_{b'}dE_{a'}}. \tag{2.10}$$

The polarization transfer observables for $(p, 2p)$ reactions are related to the probability that the projectile proton (a) with initial spin projection along the $\hat{j}$ direction, will be scattered into a final spin state with projection along $\hat{i}'$ while at the same time also being detected in coincidence with the second scattered proton (b'). The unit vectors $\hat{j}$ and $\hat{i}$ are taken to be valid combinations of vectors (allowed by certain symmetries) out of the sets $(\hat{l}, \hat{s}, \hat{n})$ and $(\hat{l}', \hat{s}', \hat{n})$ as

shown in fig. (2.1). For our model we define the directions of spin polarization as follows

$$\hat{l} = \frac{\vec{k}_a}{|\vec{k}_a|} \tag{2.11}$$

$$\hat{l}' = \frac{\vec{k'}_a}{|\vec{k'}_a|} \tag{2.12}$$

$$\hat{n} = \frac{\vec{k}_a \times \vec{k}_{a'}}{|\vec{k}_a \times \vec{k}_{a'}|} \tag{2.13}$$

$$\hat{s} = \frac{\hat{n} \times \hat{l}}{|\hat{n} \times \hat{l}|} \tag{2.14}$$

$$\hat{s}' = \frac{\hat{n} \times \hat{l}'}{|\hat{n} \times \hat{l}'|} \tag{2.15}$$

where the laboratory momenta $\vec{k}_a$ and $\vec{k}_{a'}$ are schematically depicted in fig. (2.1). In the discussions which follow we use the symbol $A_y = D_{0n}$ to present the analyzing power. The following sections deal with the $(p, 2p)$ kinematics, the relativistic plane wave scattering functions, the boundstate wave function, the nucleon-nucleon t-matrix and the evaluation of the $(p, 2p)$ scattering amplitude $|T_{L_b J_b}(\mu_a, \mu_{a'}, \mu_{b'}, M_b)|^2$.

2.4 Kinematics for $(p, 2p)$ reactions

The kinematic quantities such as the momenta and scattering angles of the scattered protons, which are required for calculating the wave functions of the scattered particles as well as the kinematic factor which appears in Eq. (2.2), are derived in this section. In addition to this we will derive the kinetic energy, momentum and scattering angle of the recoil particle as well as the center of mass scattering angle and effective laboratory kinetic energy which are required for generating the NN scattering amplitudes in Eq. (2.2) [1].

2.4.1 The laboratory system

We will now derive the momenta and scattering angles which are needed to calculate the scattering wave functions and the kinematic factor which appears in Eq. (2.2). In addition to this we will derive the kinetic energy, momentum and scattering direction of the recoil nucleus.

[1] We use natural units throughout this thesis to simplify many of the derivations. Hence $c = \hbar = 1$

In fig. (2.1) we show a schematic representation of a $(p, 2p)$ reaction in the laboratory frame of reference. The labels a, a', b' A and C are used to represent the projectile, the two ejectiles, the target and residual nucleus respectively. We use the symbols m_a, $m_{a'}$, $m_{b'}$, M_A, M_C, to represent the rest masses of particles a, a', b', A and C respectively. The scattering angles of the two ejectiles a' and b' as well as the residual nucleus are labeled by $\theta_{a'}$, $\theta_{b'}$ and θ_C. The total relativistic energy, kinetic energy and momentum of particle i are represented by ϵ_i, E_i and $\vec{k}_i$. These quantities are related to each other by the following expressions:

$$\epsilon_i = \sqrt{k_i^2 + m_i^2} = E_i + m_i \tag{2.16}$$

and

$$k_i^2 = E_i^2 + 2E_i m_i. \tag{2.17}$$

Due to energy conservation one can write

$$\epsilon_a + M_A = \epsilon_{a'} + \sqrt{k_{b'}^2 + m_{b'}^2} + \sqrt{k_C^2 + M_C^2} + E_x \tag{2.18}$$

where E_x is the excitation energy respectively. Assuming that momentum conservation holds it follows that

$$\vec{k}_a = \vec{k}_{a'} + \vec{k}_{b'} + \vec{k}_C. \tag{2.19}$$

Hence

$$\begin{aligned} \vec{k}_C^2 &= (\vec{k}_a - \vec{k}_{a'} - \vec{k}_{b'})^2 \\ &= k_a^2 + k_{a'}^2 + k_{b'}^2 - 2k_a k_a \cos\theta_{a'} - 2k_a k_{b'} \cos\theta_{b'} + 2k_{a'} k_b \cos(\theta_{a'} + \theta_{b'}). \end{aligned} \tag{2.20}$$

One can eliminate k_C in Eq. (2.18) by substituting Eq. (2.20) to yield

$$\begin{aligned} \epsilon_a + M_A &= \epsilon_{a'} + \sqrt{k_{b'}^2 + (m_{b'})^2} + \\ &\sqrt{k_a^2 + k_{a'}^2 + k_{b'}^2 - 2k_a k_{a'} \cos\theta_{a'} - 2k_a k_{b'} \cos\theta_{b'} + 2k_{a'} k_{b'} \cos(\theta_{a'} + \theta_{b'}) + (M_C)^2} + \\ &E_x. \end{aligned} \tag{2.21}$$

Squaring yields

$$\begin{aligned} &[\epsilon_a + M_A - \epsilon_{a'} - E_x - \sqrt{k_{b'}^2 + (m_{b'})^2}]^2 \\ = \; &[k_a^2 + k_{a'}^2 + k_{b'}^2 - 2k_a k_{a'} \cos\theta_{a'} - 2k_a k_{b'} \cos\theta_{b'} + 2k_{a'} k_{b'} \cos(\theta_{a'} + \theta_{b'})] + (M_C)^2 \end{aligned} \tag{2.22}$$

which one can write as

$$\begin{aligned} 2(\epsilon_a + M_A - \epsilon_{a'} - E_x)\sqrt{k_{b'}^2 + (m_{b'})^2} &= (\epsilon_a + M_A - \epsilon_a - E_x)^2 + (m_{b'})^2 - (M_C)^2 \\ &\quad -[k_a^2 + k_{a'}^2 - 2k_a k_{a'} \cos\theta_{a'} - 2k_a k_{b'} \cos\theta_{b'} \\ &\quad +2k_{a'} k_{b'} \cos(\theta_{a'} + \theta_{b'})] \\ &= 2[k_a \cos\theta_{b'} - k_{a'} \cos(\theta_{a'} + \theta_{b'})]k_{b'} + (\epsilon_a + M_A \\ &\quad -\epsilon_{a'} - E_x)^2 + (m_{b'})^2 - (m_C)^2 + (m_{b'})^2 - (M_C)^2 \\ &\quad -[k_a^2 + k_{a'}^2 - 2k_a k_a \cos\theta_{a'}] \\ &= C_1 k_b + C_2 \end{aligned} \tag{2.23}$$

where

$$C_1 = 2[k_a \cos\theta_{b'} - k_{a'} \cos(\theta_{a'} + \theta_{b'})], \tag{2.24}$$

and

$$C_2 = (\epsilon_a + M_A - \epsilon_{a'} - E_x)^2 + (m_{b'})^2 - (M_C)^2 - [k_a^2 + k_{a'}^2 - 2k_a k_{a'} \cos\theta_{a'}]. \tag{2.25}$$

Squaring Eq. (2.23) yields

$$4[\epsilon_a + M_A - \epsilon_{a'} - E_x]^2[k_{b'}^2 + (m_{b'})^2] = C_1^2 k_{b'}^2 + 2C_1 C_2 k_{b'} + C_2^2 \tag{2.26}$$

or

$$\{C_1^2 - 4[\epsilon_a + M_A - \epsilon_{a'} - E_x]^2\}k_{b'}^2 + 2C_1 C_2 k_{b'} + C_2^2 - 4(m_{b'})^2[\epsilon_a + M_A - \epsilon_{a'} - E_x]^2 = 0 \tag{2.27}$$

which can be written as

$$Ak_{b'}^2 + 2C_1 C_2 k_{b'} + B = 0 \tag{2.28}$$

where

$$A = C_1^2 - 4(\epsilon_a + M_A - \epsilon_a - E_x)^2 \tag{2.29}$$

and

$$B = C_2^2 - 4(m_{b'})[\epsilon_a + M_A - \epsilon_{a'} - E_x]^2. \tag{2.30}$$

Hence from Eq. (2.28) it follows that

$$k_{b'} = \frac{-C_1 C_2 \pm \sqrt{C_1^2 C_2^2 - AB}}{A}. \tag{2.31}$$

The projectile kinetic energy in the entrance and exit channel, labeled (E_a) and ($E_{a'}$), is fixed when running a calculation. The momenta of particles a and a' in the entrance and exit channels can be calculated from the expressions

$$k_a = \sqrt{(E_a + m_{a'})^2 - (m_{a'})^2} \tag{2.32}$$

and

$$k_{a'} = \sqrt{(E_{a'} + m_{a'})^2 - (m_{a'})^2}. \tag{2.33}$$

The momentum of b' is calculated with Eq. (2.31). The total relativistic laboratory energy, kinetic energy and momentum of the residual nucleus C are given by the expressions

$$\begin{aligned} \epsilon_C &= \epsilon_a + M_A - \epsilon_{a'} - \epsilon_{b'} - E_x \\ E_C &= \epsilon_C - M_C \\ k_C &= \sqrt{\epsilon_C - (M_C)^2}. \end{aligned} \tag{2.34}$$

Due to conservation of momentum, it follows that along the incident beam direction, which is chosen as the z-direction,

$$(k_a)_z = (k_{a'})_z + (k_{b'})_z + (k_C)_z \tag{2.35}$$

and

$$k_a = k_{a'} \cos\theta_{a'} + k_{b'} \cos\theta_{b'} + k_C \cos\theta_C. \tag{2.36}$$

Hence

$$\cos\theta_C = \frac{k_a - k_{a'} \cos\theta_{a'} - k_{b'} \cos\theta_{b'}}{k_C}. \tag{2.37}$$

Similarly we have in the y-direction

$$(k_a)_y = (k_{a'})_y + (k_{b'})_y + (k_C)_y \tag{2.38}$$

and

$$0 = k_{a'} \sin\theta_{a'} - k_{b'} \sin\theta_{b'} - k_C \sin\theta_C, \tag{2.39}$$

which yields

$$\sin\theta_C = \frac{k_{a'}\sin\theta_{a'} - k_{b'}\sin\theta_{b'}}{k_C}. \tag{2.40}$$

In the following section we derive the quantities which are needed to calculate the nucleon-nucleon t-matrix.

2.4.2 Kinematics of the nucleon-nucleon system

In this section we derive the kinematic quantities which are needed to obtain the nucleon nucleon t-matrix. These include the nucleon nucleon center of mass scattering angle and effective laboratory kinetic energy which will be used to calculate the NN scattering amplitudes associated with the nucleon nucleon interaction model, which is discussed in section (2.7).

Consider the reaction $A(a, a'b')C$ where (as before) A represents the target nucleus, a labels the projectile, a' and b' represents the two scattering protons to the left and right of the incident beam, and C labels the residual nucleus. Because of the conservation of four momentum in this reaction, one can write

$$P_a + P_A = P_{a'} + P_{b'} + P_C, \tag{2.41}$$

where P_i represents the four momentum of particle i in the laboratory system. We define

$$P_B = P_A - P_C, \tag{2.42}$$

which allows one to write Eq. (2.41) as

$$P_a - P_B = P_{a'} - P_{b'}. \tag{2.43}$$

By using the Mandelstam variables s and t, which are Lorentz invariant quantities, we have that in the laboratory frame

$$s = (P_a + P_B)^2 = (P_{a'} + P_{b'})^2 \tag{2.44}$$

and

$$t = (P_a - P_{a'})^2 = (P_B - P_b)^2. \tag{2.45}$$

We have thus reduced the three body problem to a two body problem. The impulse approximation assumes that the reaction is dominated by the interaction between the projectile and

the struck bound proton in the target nucleus. Therefore the effect of the rest of the nuclear medium is ignored. The proton-proton interaction is essentially a two body interaction, and hence we need to reduce the three body $(p, 2p)$ problem to a two body problem to obtain the kinematic quantities used for the two-body nucleon-nucleon interaction. Because the interaction between the two protons is strictly speaking not between free protons, we make use of two possible kinematic prescriptions to obtain the effective laboratory kinetic energy and center of mass scattering angle at which the NN scattering amplitudes are evaluated. In the case of the initial energy prescription we use

$$\begin{aligned} s_i &= (P_a + P_B)^2 \\ &= (\epsilon_a + \epsilon_B)^2 - (k_a + k_B)^2 \\ &= (\epsilon_a + m_B)^2 - k_a^2 \\ &= m_a^2 + m_B^2 + 2m_B\epsilon_a \\ &= 2E_a m_B + (m_a + m_B)^2, \end{aligned} \tag{2.46}$$

where we assume that m_B is the same as the free proton mass m_p. Hence the effective kinetic energy of the proton in the laboratory frame, which follows from Eq. (2.46), is given by

$$E_a = \frac{s_i - 4m_p^2}{2m_p}. \tag{2.47}$$

In the case of the final energy prescription we use

$$s_f = (P_{a'} + P_{b'})^2 \tag{2.48}$$

to obtain an effective kinetic energy which is given by

$$E_a = \frac{s_f - 4m_p^2}{2m_p}. \tag{2.49}$$

The NN center of mass scattering angle is calculated from the Mandelstam variable t. From Eq. (2.45) it follows that in the laboratory system

$$\begin{aligned} t &= (\epsilon_a - \epsilon_{a'})^2 - (\vec{k}_a - \vec{k}_{a'})^2 \\ &= \epsilon_a^2 - k_a^2 + \epsilon_{a'}^2 - k_{a'}^2 - 2\epsilon_a\epsilon_{a'} + 2\vec{k}_a \cdot \vec{k}_{a'} \\ &= 2m_p^2 - 2\epsilon_a\epsilon_{a'} + 2k_a k_{a'} \cos\theta_{a'}. \end{aligned} \tag{2.50}$$

Within the impulse approximation we assume that the projectile strikes a free proton. Hence, we assume that in the rest frame of the projectile and the struck target proton, the center of

mass momenta of the projectile and the left scattered proton satisfy the condition

$$k_a^{cm} = k_{a'}^{cm} = k^{cm}. \tag{2.51}$$

It therefore follows that

$$\begin{aligned} t &= (P_a^{cm} - P_{a'}^{cm})^2 \\ &= (\epsilon_a^{cm} - \epsilon_{a'}^{cm})^2 - (\vec{k}_a^{cm} - \vec{k}_{a'}^{cm})^2 \\ &= m_a^2 + m_{a'}^2 - 2\epsilon_a^{cm}\epsilon_{a'}^{cm} + 2k_{cm}^2 \cos\theta_{a'}^{cm} \\ &= 2m_p^2 - 2\epsilon_a^{cm}\epsilon_{a'}^{cm} + 2(k^{cm})^2 \cos\theta_{a'}^{cm}. \end{aligned} \tag{2.52}$$

Let $\theta_{a'}^{cm} = \theta^{cm}$, then from Eq. (2.52) we get

$$\cos\theta^{cm} = \frac{t - 2m_p - 2\epsilon_a^{cm}\epsilon_{a'}^{cm}}{2(k^{cm})^2}. \tag{2.53}$$

Because of the assumption made in Eq. (2.51) it follows that

$$\epsilon_a^{cm} = \epsilon_{a'}^{cm} = E_{NN}^{cm} + m_p, \tag{2.54}$$

where E_{NN}^{cm} is defined as the center of mass kinetic energy of both a and a'. Hence Eq. (2.53) can be written as

$$\cos\theta^{cm} = \frac{t + 2(E_{NN}^{cm})^2 + 4m_p E_{NN}^{cm}}{2(k^{cm})^2}. \tag{2.55}$$

If we let $\epsilon^{cm} = \epsilon_a^{cm} = \epsilon_{a'}^{cm}$ then the total relativistic center of mass energy of the protons a or a' is given by the relationship

$$(\epsilon^{cm})^2 = (E_{NN}^{cm} + m_p)^2 = (k^{cm})^2 + m_p^2. \tag{2.56}$$

It therefore follows that

$$2(k^{cm})^2 = 2(E_{NN}^{cm})^2 + 4m_p E_{NN}^{cm}. \tag{2.57}$$

Thus Eq. (2.55) becomes

$$\begin{aligned} \cos\theta^{cm} &= \frac{t + 2(k_{cm})^2}{2(k^{cm})^2} \\ &= \frac{t}{2(k^{cm})^2} + 1. \end{aligned} \tag{2.58}$$

The NN center of mass scattering angle is therefore given by

$$\theta^{cm} = \cos^{-1}\left[\frac{t}{2(k^{cm})^2} + 1\right]. \tag{2.59}$$

We define the quantity k^{cm} in the center of mass frame where $\vec{k}_{a'}^{cm} + \vec{k}_{b'}^{cm} = 0$. In the laboratory we have that, from the Mandelstam variable s_f, we get

$$\begin{aligned} s_f &= (P_{a'} + P_{b'})^2 \\ &= (\epsilon_{a'} + \epsilon_{b'})^2 - (\vec{k}_{a'} + \vec{k}_{b'})^2 \\ &= (\epsilon_{a'} + \epsilon_{b'})^2 - k_{a'}^2 - k_{b'}^2 + k_{a'} k_{b'} \cos\theta(\theta_{a'} + \theta_{b'}) \end{aligned} \tag{2.60}$$

Since s_f is an invariant quantity under a Lorentz transformation it follows that in the $a + a'$ center of mass system

$$\begin{aligned} s_f &= (\epsilon_a^{cm} + \epsilon_{a'}^{cm})^2 - (\vec{k}_a^{cm} + \vec{k}_{a'}^{cm})^2 \\ &= 4\epsilon_{Tot}^{cm}, \end{aligned} \tag{2.61}$$

where ϵ_{Tot}^{cm} represents the total sum energy of the particles a and a' in the $a + a'$ rest system. which is related to the center of mass momentum k^{cm} by the relationship

$$(k^{cm})^2 + m_p^2 = \epsilon_{Tot}^{cm}. \tag{2.62}$$

Thus from Eqs. (2.61)and (2.62) we get

$$(k^{cm})^2 = \frac{s_f}{4} - m_p^2. \tag{2.63}$$

In the following three sections we will discuss the relativistic plane wave model, the boundstate wave function and the nucleon nucleon t-matrix.

2.5 Relativistic plane wave model

In the following three sections we will discuss the relativistic plane wave functions, the bound state wave function and nucleon nucleon t-matrix which enters in the definition of the $(p, 2p)$ transition amplitude defined by Eq. (2.1). In this section we focus on the relativistic plane wave functions which describe the dynamics of the projectile and scattered protons.

The model presented in this dissertation ignores distortions of the incident and outgoing protons. Spin transfer observables, being ratios of polarized triple differential cross sections, are expected to be relatively insensitive to distortions of the scattered wave functions (especially at high

energies) and hence all proton scattering wave functions in both the entrance and exit channel satisfy the free Dirac equation [Bjo64]

$$(i\not{\nabla} - m)\phi(\vec{k}, \vec{x}, \mu) = 0, \tag{2.64}$$

where $\not{\nabla} = \gamma^\mu \partial_\mu$. In terms of the free Dirac spinors, the plane wave scattering wave functions associated with the incoming and two outgoing protons in Eq. (2.1) are given by [Gre90, Bjo64]

$$\begin{aligned} \Psi(\vec{k}_a, \vec{x}, \mu_a) &= e^{-i\vec{k}_a \cdot \vec{x}} u(\vec{k}_a, \mu_a) \\ \Psi(\vec{k}_{a'}, \vec{x}, \mu_{a'}) &= e^{-i\vec{k}_{a'} \cdot \vec{x}} u(\vec{k}_{a'}, \mu_{a'}) \\ \Psi(\vec{k}_{b'}, \vec{x}, \mu_{b'}) &= e^{-i\vec{k}_{b'} \cdot \vec{x}} u(\vec{k}_{b'}, \mu_{b'}), \end{aligned} \tag{2.65}$$

where

$$u(\vec{k}, \mu) = N \begin{pmatrix} \chi_\mu \\ \frac{\vec{\sigma} \cdot \vec{k}}{\epsilon + m} \chi_\mu \end{pmatrix}, \tag{2.66}$$

is the Dirac spinor for a particle with mass m, total relativistic energy ϵ, momentum $\vec{k}$ and spin projection μ respectively. The normalization condition

$$u_\alpha^\dagger(\vec{k}, \mu)\gamma^0 u_\alpha(\vec{k}, \mu) = 1, \tag{2.67}$$

where α is the index of the 4-component vector $u(\vec{k}, \mu)$, and

$$\gamma^0 = \begin{pmatrix} 1 & 0 & 0 & 0 \\ 0 & 1 & 0 & 0 \\ 0 & 0 & -1 & 0 \\ 0 & 0 & 0 & -1 \end{pmatrix},$$

yields

$$N = \left[\frac{\epsilon + m}{2m}\right]^{\frac{1}{2}}. \tag{2.68}$$

The Pauli spinors for spin projections along the z-axis are explicitly given by

$$\chi_{\frac{1}{2}} = \binom{1}{0} \text{ and } \chi_{-\frac{1}{2}} = \binom{0}{1}, \text{ respectively.}$$

In the following section we will discuss the relativistic bound state wave function.

2.6 Bound state wave function

In order to derive the $(p, 2p)$ transition amplitude, which is defined by Eq. (2.1), we need to define the bound state wave function for the bound proton in the target nucleus. In a relativistic model this involves generating the upper and lower component radial bound state wave functions. To generate these wave functions, we employ the program Timora [Lan91] which in based on the Dirac-Hartree approximation. In this section we will briefly discuss the ingredients of this model.

2.6.1 The Dirac-Hartree Approximation

The Dirac-Hartree equation for a finite nucleus can be derived from an interacting relativistic field theory of mesons and baryons by approximating the meson field operators by classical fields. In the discussion which follows, only the contributions from the neutral scalar (ϕ) and vector (V^μ) meson field, as in the Walecka model [Wal74], will be considered. The code however also contains contributions from a neutral (isovector) ρ meson and the coulomb potential [Hor81]. Considering only static, spherically symmetric nuclei, the meson fields depend only on the radius, and only the V^0 component of the vector field contributes. Thus the Dirac equation for the baryon field (ψ) is

$$\{i\gamma_\mu\partial^\mu - g_v\gamma^0 V^0(r) - [M - g_s\phi(r)]\}\psi(\vec{x}) = 0, \tag{2.69}$$

where γ^μ represents the Dirac gamma matrices as defined by Bjorken and Drell [Bjo64] and the appropriate values for the scalar and vector coupling constants g_s and g_v are given below. Although the baryon field is still an operator, the meson fields are classical; hence Eq. (2.69) is linear, and one may seek normal mode solutions of the form $\psi(x) = \psi(\vec{x})e^{-i\epsilon t}$. This leads to

$$h\psi(\vec{x}) = \epsilon\psi(\vec{x}), \tag{2.70}$$

which defines the Hamiltonian h

$$h \equiv -i\vec{\alpha}\cdot\vec{\nabla} + g_v V^0(r) + \beta[M - g_s\phi(r)]. \tag{2.71}$$

Both positive and negative solutions $U(\vec{x})$ and $V(\vec{x})$ are obtained from Eq. (2.70), and thus the field operator is given by the expansion

$$\hat{\psi}(\vec{x}) = \sum_\alpha [\hat{A}^\dagger_\alpha U_\alpha(\vec{x}) + \hat{B}^\dagger_\alpha(\vec{x})V_\alpha(\vec{x})], \tag{2.72}$$

where $\hat{A}^{\dagger}_{\alpha}$ and $\hat{B}^{\dagger}_{\alpha}$ are the baryon and antibaryon creation operators which satisfy the standard anti-commutation relations. The label α specifies the full set of single particle quantum numbers. Since it is assumed that the system is spherically symmetric and parity conserving, α contains the orbital angular momentum (L_b), total angular momentum (J_b), total angular momentum projection (M_b) and spin projection quantum numbers (μ_b), as described in refs. [Bjo64] and [Ser86]. Using the well-known properties of the relativistic angular momentum operator, it is easy to show that the angular and spin solutions are spin spherical harmonics [Var88]:

$$\mathcal{Y}_{L_b J_b M_b}(\theta,\phi) = \sum_{M_{L_b},\mu_b} C^{L_b \frac{1}{2} M_{L_b} \mu_b}_{J_b M_b} Y_{L_b,M_{L_b}}(\theta,\phi)\chi_{\mu_b}, \tag{2.73}$$

where $Y_{L_b,M_{L_b}}$ is a spherical harmonic, $C^{L_b \frac{1}{2} M_{L_b} \mu_b}_{J_b M_b}$ presents a Clebsch coefficient and χ_{μ_b} is a two component Pauli spinor. It follows that the four component Dirac wave functions can be divided into its upper and lower two component pieces. Thus the positive-energy spinors can be written as

$$U_{\alpha}(\vec{x}) \equiv \Phi^{B}_{L_b J_b M_b}(\vec{x}) = \frac{1}{r}\begin{pmatrix} u^{B}_{L_b J_b}(r)\mathcal{Y}_{L_b J_b M_b}(\theta,\phi) \\ \\ iw^{B}_{L_b J_b}(r)\mathcal{Y}_{\tilde{L}_b J_b M_b}(\theta,\phi) \end{pmatrix}. \tag{2.74}$$

The normalization is given by the expression

$$\int_0^{\infty} dr(|u^{B}_{L_b J_b}(r)|^2 + |w_{L_b J_b}(r)|^2) = 1. \tag{2.75}$$

With the general form for the spinors in Eq. (2.74), one can evaluate the nuclear densities, which serve as source terms in the meson field equations. For the discussion which follows we will introduce the quantum number κ which is related to the orbital and total angular momentum by the following relations

$$\kappa = \begin{cases} l, \text{ if } j = l - \frac{1}{2} \\ \\ -(l+1), \text{ if } j = l + \frac{1}{2} \end{cases}. \tag{2.76}$$

Assume that the nuclear ground state consists of filled shells up to some values of n, and κ, which may be different for protons and neutrons; this is appropriate for double magic nuclei. In addition, assume that all bilinear products of baryon operators are normal ordered, which

removes contributions from the negative-energy spinors $V_\alpha(\vec{x})$. This amounts to neglecting contributions from the filled Dirac sea of baryons. These contributions are however beyond the scope of the work presented in my thesis and will therefore not be discussed. With these assumptions, the local baryon (ρ_B) and scalar (ρ_s) densities become

$$\left.\begin{array}{l}\rho_B(\vec{x}) \\ \\ \rho_s(\vec{x})\end{array}\right\} = \sum_\alpha^{occ} \bar{\Phi}_\alpha^B(\vec{x}) \begin{pmatrix} \gamma^0 \\ \\ 1 \end{pmatrix} \Phi_\alpha^B(\vec{x})$$

$$= \sum (\frac{2J_b+1}{4\pi r^2}(|u_\beta(r)|^2 \pm |w_\beta(r)|^2), \tag{2.77}$$

where we have used the identity

$$\sum_{M_b=-J_b}^{J_b} \mathcal{Y}^\dagger_{\kappa M_b} \mathcal{Y}_{\kappa' M_b} = (\frac{2J_b+1}{4\pi})\delta_{\kappa\kappa'} \qquad \kappa' = \pm\kappa. \tag{2.78}$$

which holds for filled shells, and the remaining quantum numbers are denoted by $\{\alpha\} \equiv \{\kappa, M_b\}$ and $\{\beta\} \equiv \{\kappa\}$. Note that since the shells are filled, the sources are spherically symmetric. The sources produce the meson fields, which satisfy the static Klein-Gordon equation

$$\frac{d^2}{dr^2}\phi(r) + \frac{2}{r}\frac{d}{dr}\phi(r) - m_s^2\phi(r) = -g_s\rho_s(r), \tag{2.79}$$

$$\frac{d^2}{dr^2}V^0(r) + \frac{2}{r}\frac{d}{dr}V^0(r) - m_v^2V^0(r) = -g_v\rho_B(r). \tag{2.80}$$

The symbols m_v and m_s in Eq. (2.80) represent the vector and scalar meson masses. For the Coulomb potential, one uses the contribution to ρ_B arising from protons only, while for the ρ meson one uses half the proton and neutron densities [Hor81].

The equations for the baryon follow upon substituting Eq. (2.74) into (2.70), which produces

$$\frac{d}{dr}u_a(r) + \frac{\kappa}{r}u_a(r) - [\epsilon_\beta - g_vV^0(r) + M - g_s\phi(r)]w_a(r) = 0 \tag{2.81}$$

$$\frac{d}{dr}w_a(r) - \frac{\kappa}{r}w_a(r) - [\epsilon_\beta - g_vV^0(r) + M - g_s\phi(r)]u_a(r) = 0, \tag{2.82}$$

with M representing the hadron mass of the protons or neutrons. Thus the spherical nuclear ground state is described by coupled, one dimensional differential equations that may be solved by an iterative procedure which is discussed in ref. [Lan91]. Once the solution has been found, the total energy of the system is given by

$$\epsilon = \sum_a^{odd} \epsilon_\beta(2J_b+1) - \frac{1}{2}\int d^3[-g_s\phi(r)\rho_s(r) + g_vV^0(r)\rho_B(r)]. \tag{2.83}$$

Solutions of the preceding equations depend on the parameters g_s, g_v, m_s and g_s (when the ρ meson is included). The experimental values $M = 939MeV$, $m_v = m_\omega = 783MeV$, $m_\rho = 770MeV$ and $e^2/4\pi = \alpha = 1/137.036$ (which determines the Coulomb potential) are taken as fixed values. The free parameters are solved in the limit of infinite nuclear matter, the empirical equilibrium density ($\rho_0^0 = 0.1484$ fm^{-3}), binding energy (15.75 MeV), and symmetric energy (35 MeV) are produced. In the next section we will discuss the nucleon nucleon t-matrix.

2.7 The nucleon nucleon t-matrix

2.7.1 Introduction

We use the relativistic Love-Franey model to evaluate $t_{NN}(|\vec{x} - \vec{x}'|)$ in Eq. (2.1). Various phenomenological forms have in the past been used to fit the free nucleon-nucleon t-matrix. A non-relativistic model of the NN t-matrix was developed by Love and Franey [LF81], in which the NN t-matrix is presented as the sum of Yakawa terms. While providing good fits to (p, p') and (p, n) amplitudes, the non-relativistic Love-Franey t-matrix suffers from some disadvantages of a non-relativistic treatment. Since it is not Lorentz invariant, it cannot be used in relativistic calculations based on the Dirac impulse approximation. Large cancellations between the direct and exchange contributions to the amplitudes are found. Such cancellations do not occur in relativistic treatments. Finally, comparisons between the non-relativistic Love-Franey t-matrix and microscopic NN potentials are hampered by the fact that the parameters of the fit and the meson parameterization of the potentials are not related in any simple fashion.

Subsequent to the work by Love and Franey, a Lorentz covariant treatment of the NN amplitude was developed by McNeil, Ray and Wallace (MRW) [McN83] to study elastic proton-nucleus scattering. One disadvantage of this work is that the Lorentz invariant amplitudes are obtained by a transformation from the Wolfenstein amplitudes, so that there is no separation into direct and exchange amplitudes. As a result, the MRW t-matrix cannot be used in calculations where one wishes to treat the direct and exchange contributions explicitly, such as in relativistic treatments of $(p, 2p)$ reactions [Coo89, Ike95]. As pointed out by Horowitz [Hor85], the MRW t-matrix does not incorporate the non-localities associated with the exchange terms and consequently must fail at energies well below 500 MeV, where exchange contributions have been

shown to be important [Hil99].

In an attempt to resolve some of the difficulties associated with existing fits, Horowitz [Hor85] introduced a relativistic version of the Love-Franey parameterization in which the NN t-matrix is parametrized in terms of phenomenological relativistic "meson" exchanges: we refer to this model as the relativistic Love-Franey model. Such a form combines several desirable features. Since it is Lorentz invariant, it can be readily incorporated in calculations based on the Dirac impulse approximation. The various meson exchange amplitudes, with form factors included, can be written analytically in both momentum space and position space, so that calculations using the t-matrix can be carried out in either space. Direct and exchange contributions to the t-matrix are explicitly separated, thereby eliminating some of the difficulties associated with the MRW amplitudes. Finally, the meson-exchange parameters of the fit can be directly compared with those occurring in microscopic one-boson-exchange potentials.

2.7.2 The relativistic Love-Franey model

A Lorentz invariant representation of the NN scattering amplitude ($\hat{F}$), commonly called the IA1 representation, is given by [McN83]:

$$\hat{F}(q) = F^S(q)(I_1 \otimes I_2) + F^V(q)(\gamma_1^\mu \otimes \gamma_{2\mu}) + F^P(q)(\gamma_1^5 \otimes \gamma_{25}) + F^A(q)(\gamma^5\gamma_1^\mu \otimes \gamma_5\gamma_{2\mu}) + F^T(q)(\sigma_1^{\mu\nu} \otimes \sigma_{2\mu\nu}), \tag{2.84}$$

where the superscripts $\mathbf{S}, \mathbf{V}, \mathbf{P}, \mathbf{A}$ and $\mathbf{T}$ refer to the **S**calar-**P**seudoscalar-**V**ector-**A**xialvector-**T**ensor parameterization of the relativistic NN amplitudes. The latter representation is related to the commonly used Wolfenstein representation of the NN scattering amplitude

$$(2ik_{cm})^{-1}[\chi_{\mu_a'} \otimes \chi_{\mu_b'} \hat{M} \chi_{\mu_a} \otimes \chi_{\mu_b}] = \bar{u}(\vec{k}_{a'}, \mu_{a'}) \otimes \bar{u}(\vec{k}_{b'}, \mu_{b'}) \hat{F} \bar{u}(\vec{k}_a, \mu_a) \otimes \bar{u}(\vec{k}_b, \mu_b) \tag{2.85}$$

via

$$\begin{aligned}(2ik_{cm})^{-1}\hat{M} \;=\; & A(I_1 \otimes I_2) + i|\vec{m}|C(\vec{\sigma}_1 \otimes I_2 + I_1 \otimes \vec{\sigma}_2) \cdot \hat{n} + (B + Dm^2)(\vec{\sigma}_1 \otimes I_2) \cdot \hat{m}(I_1 \otimes \vec{\sigma}_2) \cdot \hat{m} + \\ & (B + E)(\vec{\sigma}_1 \otimes I_2) \cdot \hat{l}(I_1 \otimes \vec{\sigma}_2) \cdot \hat{l} + B(\vec{\sigma}_1 \otimes I_2) \cdot \hat{n}(I_1 \otimes \vec{\sigma}_2) \cdot \hat{n} \; . \end{aligned} \tag{2.86}$$

The orthogonal unit vectors $\hat{m}$, $\hat{n}$ and $\hat{q}$ in Eq. (2.86) are defined in terms of the initial ($\vec{k}_i$) and final ($\vec{k}_f$) center of mass momenta of the projectile and ejectile nucleon which are given by the

expressions

$$\begin{aligned} \hat{m} &= \frac{\vec{k}_f - \vec{k}_i}{|\vec{k}_f - \vec{k}_i|}, \\ \hat{l} &= \frac{\vec{k}_f + \vec{k}_i}{|\vec{k}_f + \vec{k}_i|}, \end{aligned} \tag{2.87}$$

and

$$\hat{n} = \frac{\vec{k}_f \times \vec{k}_i}{|\vec{k}_f \times \vec{k}_i|}. \tag{2.88}$$

Adopting the ansatz of Horowitz [Hor85], one can divide F^L into two parts: a direct term and an exchange term. Thus

$$F^L(q) = i\frac{M_N}{2k_{cm}E_{cm}}[F_D^L(q) + F_X^L(Q)], \tag{2.89}$$

where the index L labels the corresponding Dirac gamma matrices and the symbols D and X distinguish between the direct and exchange terms of F^L. The direct momentum transfer (q) for the scattering angle θ_{cm} is

$$q = 2k_{cm}\sin(\frac{\theta_{cm}}{2}), \tag{2.90}$$

while the exchange momentum transfer Q is

$$Q = 2k_{cm}\sin\left[\frac{\pi - \theta_{cm}}{2}\right]. \tag{2.91}$$

The direct and exchange terms are given by the expressions

$$F_D^L(q) = \sum_{j=1}^{N} \delta_{L,type_j}(\tau_1 \cdot \tau_2)^{I_j} f^j(q) \tag{2.92}$$

and

$$F_X^L(Q) = (-1)^{I_{NN}} \sum_{j=1}^{N} C_{type_j,L}(\tau_1 \cdot \tau_2)^{I_j} f^j(Q), \tag{2.93}$$

respectively, where

type_j = kind of meson-N coupling for the jth meson, (S,V,P,A,T),

N = number of mesons used in fit,

I_j = isospin of jth meson (0 or 1),

I_{NN} = 1 for pp scattering

and

$$C_{type_j,L} \equiv \begin{pmatrix} 2 & 2 & 1 & -2 & 2 \\ 8 & -4 & 0 & -4 & -8 \\ 24 & 0 & -4 & 0 & 24 \\ -8 & -4 & 0 & -4 & 8 \\ 2 & -2 & 1 & 2 & 2 \end{pmatrix}. \tag{2.94}$$

In the Relativistic Love-Franey model, the $f^j(q)$'s are separated into real and imaginary parts

$$f^j(q) = f^j_R(q) - if^j_I(q) \tag{2.95}$$

which are given explicitly by the expressions

$$f^j_R = \frac{g_j^2}{q^2 + m_j^2}(1 + q^2/2\Lambda_j^2)^{-2}, \tag{2.96}$$

$$f^j_I = \frac{\bar{g}_j^2}{q^2 + \bar{m}_j^2}(1 + q^2/2\bar{\Lambda}_j^2)^{-2}, \tag{2.97}$$

with the real and imaginary meson masses m_j, $\bar{m}_j$, coupling constants g_j^2, $\bar{g}_j^2$ and cutoff parameter Λ_j $\bar{\Lambda}_j$ obtained by fitting to data (see ref. [Hor85] for information on the fitting procedure). Note that imaginary meson masses $\bar{m}_i$ are chosen arbitrarily, and the coupling constants $\bar{g}_i$ and cutoff parameters $\bar{\Lambda}_i$ are included simply as fitting parameters.

2.7.3 Maxwell's Energy Dependent Parameterization

The Lorentz invariant Horowitz parameterization has been used successfully in proton-nucleus studies through the $(p, 2p)$ reaction. It, however, suffers from the disadvantage that the various amplitudes were fitted separately at each individual energy (135, 200, 400 and 800 MeV), rather than as functions of energy. This is not only inconvenient from the numerical point of view,

since it necessitates interpolation between the energies used in the fit, but it also rules out any meaningful comparison of off-shell properties of the t-matrix at different energies, since the fits at different energies are not related to one another. The cutoff parameters obtained by Horowitz vary dramatically from one energy to the next. Since the NN amplitudes themselves vary smoothly with energy, one might expect that a fit could be found in which the individual coupling constants and cutoff parameters also vary smoothly with energy.

An energy-dependent parameterization of the cutoff parameters and coupling constants are presented by Maxwell [Max96]. Two sets of parameters have been generated for the energy regions 200-500 MeV and 500-800 MeV respectively. A linear energy dependence proved to be adequate for the cutoff parameters, while in the case of the coupling strengths a quadratic term is required, namely

$$\Lambda(E) = \Lambda_0(1 + \gamma T_{rel}) \tag{2.98}$$

and

$$g^2 = g_0 + g_1 T_{rel} + g_2 T_{rel}^2 \tag{2.99}$$

were used for both the real and imaginary parts of the amplitudes, with

$$T_{rel} = \frac{T - T_0}{T_0}, \tag{2.100}$$

where $T_0 = 200$ MeV for incident energies 200-500 MeV and $T_0 = 500$ MeV for the energy range 500 - 800 MeV. The parameterization is carried out in terms of the laboratory energy T, rather than the center of mass energy E_{cm}. The quantities Λ_0, g_0, g_1, g_2, $\bar{\Lambda}_0$, $\bar{g}_0$, $\bar{g}_1$ and $\bar{g}_2$ are parameters to be fitted [Max96, Max98].

We now discuss the effects of the nuclear medium on the scattered protons and nucleon-nucleon interaction.

2.8 Medium effects

The impulse approximation assumes that the interaction between the projectile and the struck target proton is essentially between two free particles. This assumption ignores the influence of the rest of the nucleons on both protons as they propagate through the nuclear medium. However, according to the Walecka model [Ser86], the nucleon mass in the nuclear medium is modified (reduced relative to the free value) by an attractive scalar potential S which results

from the interactions of the nucleon with the other nucleons in the nucleus. The effective nucleon mass M_N^* is calculated from relativistic mean field theory and is related to it's free value M_N by

$$M_N^* = M_N + < S >, \tag{2.101}$$

where $< S >$ represents the average scalar field experienced by the nucleon as it propagates through the nuclear medium. Since the projectile and scattered protons in the $(p, 2p)$ reaction move under the influence of scattering potentials in the nucleus, their masses will be modified by the medium according to Eq. (2.101). We hence include medium effects in the incident and scattered wave functions by replacing the free proton mass with an effective mass in the Dirac spinor in Eq. (2.66).

In recent years numerous models have also been developed which incorporate medium modifications of coupling constants, meson masses and nucleon masses in the nuclear medium. In particular, we use the Brown-Rho scaling law [Bro91] to include the latter medium effects in our formalism. According to this the hadron mass scales as

$$\frac{m_N^*}{m_N} = \frac{m_\sigma^*}{m_\sigma} = \frac{m_\rho^*}{m_\rho} = \frac{m_\omega^*}{m_\omega} = \xi, \tag{2.102}$$

where m_σ, m_ρ and m_ω are the masses of the σ, ρ and ω mesons, respectively; the starred quantities refer to the corresponding medium-modified values. The nucleon-meson coupling constants for the σ and ω mesons are also assumed to be modified by the nuclear medium according to the relationship

$$\frac{g_{\sigma NN}^*}{g_{\sigma NN}} = \frac{g_{\omega NN}^*}{g_{\omega NN}} = \chi, \tag{2.103}$$

where $g_{\sigma NN}$ and $g_{\omega NN}$ are the coupling constants for the σ and ω mesons respectively.

Medium effects to the NN-interaction are included by replacing the free proton mass, σ, ρ and ω meson masses and σ and ω meson-nucleon coupling constants with their corresponding medium-modified values via Eqs. (2.102) and (2.103). The optimal choice for ξ and χ is found to be 0.70 and 0.75 respectively [Kre95]. We only include medium effects on the real meson masses and coupling constants (and not on the imaginary meson masses and coupling constants) since these are physical quantities.

2.8.1 Pseudoscalar versus pseudovector coupling

In the past, concern has been expressed about the ambiguities in the form of the relativistic NN scattering operator $\hat{\mathcal{F}}$ given by Eq. (2.84) [Mat82, Ser86, Hor88, Lan91]. There are many other possible operators with the same five on-shell matrix elements, but different $4 \times 4 \otimes 4 \times 4$ matrix structures [Ven99]. Furthermore the impulse approximation assumes the same form for the free and medium modified NN scattering. The question arises as to how the medium modified scattering matrix, and the polarization transfer observables, change when other forms of $\hat{\mathcal{F}}$, different to that specified by Eq. (2.84) are used.

One of the major ambiguities concerns the choice of the πNN vertex in the amplitudes [Mat82, Ser86, Mur87, Hor88, Lan91]. We will investigate how these ambiguities will manifest itself in our model by using the prescription of [Hil99] for the pseudoscalar and pseudovector vertex. This involves using a pseudoscalar vertex which simply implies using the free pion coupling constant g_π^2 for the πNN vertex or a pseudovector vertex which implies replacing the free pion coupling constant in the relativistic Love-Franey model with

$$g_\pi^2 \longrightarrow g_\pi^2 \xi^2 \tag{2.104}$$

where ξ is the fraction with which the proton mass is modified in the nuclear medium relative to it's free value. We will now do a further evaluation of $|T_{L_b J_b}(\mu_a, \mu_{a'}, \mu_{b'}, M_b)|^2$.

2.9 Evaluating $|T_{L_b J_b}(\mu_{a'}, \mu_{a'}, \mu_{b'}, M_b)|^2$ within a relativistic plane wave approximation

In the $(p, 2p)$ formalism information about nucleon-nuclear distortions and the nucleon-nucleon interaction are contained in the transition amplitude $|T_{L_b J_b}(\mu_{a'}, \mu_{a'}, \mu_{b'}, M_b)|^2$ which is defined by Eq. (2.1). We will present two techniques for evaluating the transition amplitude. The first technique involves writing $|T_{L_b J_b}(\mu_{a'}, \mu_{a'}, \mu_{b'}, M_b)|^2$ as a contraction between 2 tensor covariants. This approach is similar to that used in high energy electron knockout reactions. In the alternative method, which we call the brute force method, we evaluate $T_{L_b J_b}(\mu_a, \mu_{a'}, \mu_{b'}, M_b)$ first by using relativistic plane wave functions for our scattered wave function in which the spin polarizations are obtained by performing Wigner transformations on the Dirac spinors. The

transition amplitude is then obtained by multiplying $T_{L_b,J_b}(\mu_a,\mu_{a'},\mu_{b'},M_b)$ with its complex conjugate transpose. The trace method is preferred above the brute force method because $|T_{L_bJ_b}(\mu_a,\mu_{a'},\mu_{b'},M_b)|^2$ is computed directly. We will simply use the brute force approach as a numerical check for the trace method.

2.9.1 The trace method

In the plane wave approximation all nucleon-nuclear scattering potentials are assumed to be zero, thus the wave function $\psi(\vec{k}_i,\vec{x},\mu_i)$ for the various protons found in the entrance and exit channels are replaced by plane waves which are given by Eqs. (2.65). Hence in the plane wave approximation, substitution of the plane wave scattering wave functions given by Eq. (2.65) into the expression for the transition amplitude $T_{L_bJ_b}(\mu_a,\mu_{a'},\mu_{b'},M_b)$ given by Eq. (2.1), yields

$$\begin{aligned} T_{L_bJ_b}(\mu_a,\mu_{a'},\mu_{b'},M_b) &= \int\int d\vec{x}_1 d\vec{x}_2 e^{-i\vec{k}_{a'}\cdot\vec{x}_1}\bar{u}(\vec{k}_{a'},\mu_{a'})\otimes e^{-i\vec{k}_{b'}\cdot\vec{x}_2}\bar{u}(\vec{k}_{b'},\mu_{b'})\hat{t}_{NN}(\vec{x}_1-\vec{x}_2) \\ &\quad\times e^{i\vec{k}_a\cdot\vec{x}_1}u(\vec{k}_a,\mu_a)\otimes\Phi_{L_bJ_bM_b}(\vec{x}_2). \end{aligned} \tag{2.105}$$

The quantities $\vec{k}_{a'}$, $\vec{k}_{b'}$ and $\vec{k}_a$ represent the momenta of the two outgoing protons a' and b' as well as the projectile a in the laboratory frame of reference. The positions of the projectile a and struck proton relative to the center of mass of the target nucleus is labeled by $\vec{x}_1$ and $\vec{x}_2$i respectively. The nucleon-nucleon t-matrix in position space is represented by $t_{NN}(|\vec{x}_1-\vec{x}_2|)$. For convenience we define the coordinates $\vec{r}$ and $\vec{r}'$ such that

$$\vec{r} = \vec{x}_1-\vec{x}_2 \tag{2.106}$$

and

$$\vec{r}' = \vec{x}'.$$

The position of the projectile relative to the center of mass of the target nucleus is therefore given by

$$\vec{x} = \vec{x}_1-\frac{m_b}{M_A}\vec{x}_2 \tag{2.107}$$

$$= \vec{r}+\frac{M_C}{M_A}\vec{r}'. \tag{2.108}$$

If $m_b << M_A$, then $\vec{x} \sim \vec{x}_1$. Hence, one can write Eq. (2.105) as

$$T_{L_bJ_b}(\mu_a, \mu_{a'}, \mu_{b'}, M_b) = \int\int d\vec{r}d\vec{r}' e^{-i\vec{q}\cdot\vec{r}} e^{i(\vec{k}_a - \vec{k}_{a'} - \vec{k}_{b'})\cdot\vec{r}'} \bar{u}(\vec{k}_{a'}, \mu_{a'}) \otimes \bar{u}(\vec{k}_{b'}, \mu_{b'}) \hat{t}_{NN}(\vec{r}) u(\vec{k}_a, \mu_a) \otimes \Phi_{L_bJ_bM_b}(\vec{r}'), \tag{2.109}$$

where

$$\vec{q} = \vec{k}_{a'} - \vec{k}_a \tag{2.110}$$

is the momentum transfer for the reaction. From Eq. (2.19) we have that the recoil momentum of the residual nucleus is given by

$$\vec{k}_C = \vec{k}_a - \vec{k}_{a'} - \vec{k}_{b'}. \tag{2.111}$$

Thus Eq. (2.109) becomes

$$\begin{aligned} T_{L_bJ_b}(\mu_a, \mu_{a'}, \mu_{b'}, M_b) &= [\bar{u}(\vec{k}_{a'}, \mu_{a'}) \otimes \bar{u}(\vec{k}_{b'}, \mu_{b'})] \int d\vec{r} e^{-i\vec{q}\cdot\vec{r}} \hat{t}_{NN}(\vec{r}) \\ &\quad [u(\vec{k}_a, \mu_a) \otimes \int d\vec{r}' e^{i(\vec{k}_C)\cdot\vec{r}'} \Phi_{L_bJ_bM_b}(\vec{r}')]. \end{aligned} \tag{2.112}$$

Using the Fourier transforms [Math70]

$$t_{NN}(\vec{q}) = \int d\vec{r} e^{-i\vec{q}\cdot\vec{r}} \hat{t}_{NN}(\vec{r}) \tag{2.113}$$

and

$$\Phi_{L_bJ_bM_b}(-\vec{k}_C) = \int d\vec{r} e^{i\vec{k}_C\cdot\vec{r}} \Phi_{L_bJ_bM_b}(\vec{r}), \tag{2.114}$$

we get

$$T_{L_bJ_b}(\mu_a, \mu_{a'}, \mu_{b'}, M_b) = [\bar{u}(\vec{k}_{a'}, \mu_{a'}) \otimes \bar{u}(\vec{k}_{b'}, \mu_{b'})] \hat{t}_{NN}(\vec{q}) [u(\vec{k}_a, \mu_a) \otimes \Phi_{L_bJ_bM_b}(-\vec{k}_C)]. \tag{2.115}$$

We use the relativistic Love-Franey model, discussed in section (2.7), to obtain the nucleon-nucleon t-matrix [Hor85, LF81], that is

$$\hat{t}_{NN}(q) = \frac{-i8\pi k_{cm}}{E_{cm}} \sum_{i=s}^{t} F^i(q)(\lambda_1^i \otimes \lambda_{2i}), \tag{2.116}$$

where the λ^i's are the five Dirac matrices $(1, \gamma^\mu, \gamma^5, \gamma^5\gamma^\mu, \sigma^{\mu\nu})$ and the indices 1 and 2 refer to the projectile and target nucleon respectively. Substituting Eq. (2.116) into Eq. (2.115) yields

$$T_{L_bJ_b}(\mu_a, \mu_{a'}, \mu_{b'}, M_b) = \sum_{i=S}^{T} F^i(q)[\bar{u}(\vec{k}_{a'}, \mu_{a'}) \otimes \bar{u}(\vec{k}_{b'}, \mu_{b'})][\lambda^i \otimes \lambda_i][u(\vec{k}_a, \mu_a) \otimes \Phi_{L_bJ_bM_b}(-\vec{k}_C)]. \tag{2.117}$$

Using the identity [Zha99]

$$(A \otimes B)(C \otimes D) = (AC) \otimes (BD), \tag{2.118}$$

we get

$$T_{L_b J_b}(\mu_a, \mu_{a'}, \mu_{b'}, M_b) = \sum_{i=S}^{T} (F^i)(q)([\bar{u}(\vec{k}_{a'}, \mu_{a'})\lambda_1^i u(\vec{k}_a, \mu_a)] \otimes [u(\vec{k}_{b'}, \mu_{b'})\lambda_{2i}\Phi_{L_b J_b M_b}(-\vec{k}_C)]. \tag{2.119}$$

Terms of the form $\bar{u}(\vec{k}, \mu)\lambda u(\vec{k}, \mu)$ are complex numbers. Thus one can write

$$T_{L_b J_b}(\mu_a, \mu_{a'}, \mu_{b'}, M_b) = \sum_{i=S}^{T} (F^i)(q)([\bar{u}(\vec{k}_{a'}, \mu_{a'})\lambda_1^i u(\vec{k}_a, \mu_a)][u(\vec{k}_{b'}, \mu_{b'})\lambda_{2i}\Phi_{L_b J_b M_b}(-\vec{k}_C)]. \tag{2.120}$$

The complex conjugate of Eq. (2.120) yields

$$T^*_{L_b J_b}(\mu_a, \mu_{a'}, \mu_{b'}, M_b) = \sum_{i=S}^{T} (F^i)^*(q)([\bar{u}(\vec{k}_{a'}, \mu_{a'})\lambda_1^i u(\vec{k}_a, \mu_a)][u(\vec{k}_{b'}, \mu_{b'})\lambda_{2i}\Phi_{L_b J_b M_b}(-\vec{k}_C)])^*. \tag{2.121}$$

Using the identity [Fra90] $(AB)^* = B^* A^*$ we get

$$T^*_{L_b J_b}(\mu_a, \mu_{a'}, \mu_{b'}, M_b) = \sum_{i=S}^{T} (F^i)^*(q)[u(\vec{k}_{b'}, \mu_{b'})\lambda_{2i}\Phi_{L_b J_b M_b}(-\vec{k}_C)]^*[\bar{u}(\vec{k}_{a'}, \mu_{a'})\lambda_1^i u(\vec{k}_a, \mu_a)]^*. \tag{2.122}$$

Since $\bar{u}(\vec{k}, \mu)\lambda u(\vec{k}', \mu)$ are complex numbers for which the operation of taking the complex conjugate and the adjoint are identical it follows that

$$K = [\bar{u}(\vec{k}', \mu')\lambda^i u(\vec{k}, \mu)]^* = [\bar{u}(\vec{k}', \mu')\lambda^i u(\vec{k}, \mu)]^\dagger. \tag{2.123}$$

Using the identity [Gre90]

$$\bar{u}(\vec{k}, \mu) = u^\dagger(\vec{k}, \mu)\gamma^0, \tag{2.124}$$

one gets

$$[\bar{u}(\vec{k}', \mu')\lambda^i u(\vec{k}, \mu)]^\dagger = [u^\dagger(\vec{k}', \mu')\gamma^0\lambda^i u(\vec{k}, \mu)]^\dagger. \tag{2.125}$$

The identity $[AB]^\dagger = B^\dagger A^\dagger$ of adjoint yields

$$K = u^\dagger(\vec{k}, \mu)(\lambda^i)^\dagger\gamma^{0\dagger}u^{\dagger\dagger}(\vec{k}', \mu'). \tag{2.126}$$

Making use of Eq. (2.124), and introducing the notation $\bar{\lambda}^i = \gamma^0(\lambda^i)^\dagger\gamma^0$, yields

$$\begin{aligned} K &= \bar{u}(\vec{k}, \mu)\gamma^0(\lambda^i)^\dagger\gamma^0 u(\vec{k}', \mu') \\ &= \bar{u}(\vec{k}, \mu)\bar{\lambda}^i u(\vec{k}', \mu'). \end{aligned} \tag{2.127}$$

Hence

$$[\bar{u}(\vec{k'},\mu')\bar{\lambda}^i u(\vec{k},\mu)]^* = \bar{u}(\vec{k},\mu)\bar{\lambda}^i u(\vec{k'},\mu'). \tag{2.128}$$

Using the identity given by Eq. (2.128), one can write Eq. (2.122) as

$$T^*_{L_bJ_b}(\mu_a,\mu_{a'},\mu_{b'},M_b) = \sum_{i=S}^{T}(F^i)^*(q)[\bar{\Phi}_{L_bJ_bM_b}(-\vec{k}_C)\bar{\lambda}_{2i}u(\vec{k}_{b'},\mu_{b'})][\bar{u}(\vec{k}_a,\mu_a)\bar{\lambda}^i_1 u(\vec{k}_{a'},\mu_{a'})] \tag{2.129}$$

One can find $|T_{L_bJ_b}(\mu_a,\mu_{a'},\mu_{b'},M_b)|^2$ by taking the product of Eqs. (2.120) and (2.129) to yield

$$\begin{aligned}
|T_{L_bJ_b}(\mu_a,\mu_{a'},\mu_{b'},M_b)|^2 &= \sum_{i,j=S}^{T} F^i(F^j)^*[\bar{u}(\vec{k}_{a'},\mu_{a'})\lambda^j_1 u(\vec{k}_a,\mu_a)][\bar{u}(\vec{k}_{b'},\mu_{b'})\lambda_{2j}\Phi_{L_bJ_bM_b}(-\vec{k}_C)] \\
&\quad\times[\bar{\Phi}_{L_bJ_bM_b}(-\vec{k}_C)\bar{\lambda}_{2i}u(\vec{k}_{b'},\mu_{b'})][\bar{u}(\vec{k}_a,\mu_a)\bar{\lambda}^i_1 u(\vec{k}_{a'},\mu_{a'})] \\
&= \sum_{i,j=S}^{T} F^i(F^j)^* \sum_{\alpha,\beta,\delta,\epsilon=1}^{4}\sum_{\rho,\sigma,\tau,\lambda=1}^{4}[\bar{u}_\alpha(\vec{k}_{a'},\mu_{a'})(\lambda^j_1)_{\alpha\beta}u_\beta(\vec{k}_a,\mu_a)] \\
&\quad\times[\bar{u}_\delta(\vec{k}_b,\mu_b)(\lambda_{2j})_{\delta\epsilon}\{\Phi_{L_bJ_bM_b}(-\vec{k}_C)\}_\epsilon][\{\bar{\Phi}_{L_bJ_bM_b}(-\vec{k}_C)\}_\rho(\bar{\lambda}_{2i})_{\rho\sigma}u_\sigma(\vec{k}_{b'},\mu_{b'})] \\
&\quad\times[\bar{u}_\tau(\vec{k}_a,\mu_a)(\bar{\lambda}_1)^i_{\tau\lambda}u_\lambda(\vec{k}_{a'},\mu_{a'})] \\
&= \sum_{i,j=S}^{T} F^i(F^j)^* \sum_{\alpha,\beta,\delta,\epsilon=1}^{4}\sum_{\rho,\sigma,\tau,\lambda=1}^{4}[u_\lambda(\vec{k}_{a'},\mu_{a'})\bar{u}_\alpha(\vec{k}_{a'},\mu_{a'})](\lambda^j_1)_{\alpha\beta}u_\beta(\vec{k}_a,\mu_a) \\
&\quad\times\bar{u}_\tau(\vec{k}_a,\mu_a)](\bar{\lambda}^i_1)_{\tau\lambda}[u_\sigma(\vec{k}_{b'},\mu_{b'})\bar{u}_\delta(\vec{k}_{b'},\mu_{b'})](\lambda_{2j})_{\delta\epsilon} \\
&\quad\times\{\Phi_{L_bJ_bM_b}(-\vec{k}_C)\}_\epsilon\{\bar{\Phi}_{L_bJ_bM_b}(-\vec{k}_C)\}_\rho\bar{\lambda}_{2i\rho\sigma}.
\end{aligned} \tag{2.130}$$

Using the definition of the energy projection operator [Bjo64, Gre92]

$$\sum_\mu u_\alpha(\vec{k},\mu)\bar{u}_\beta(\vec{k},\mu) = \left(\frac{\not{p}+m}{2m}\right)_{\alpha\beta}, \tag{2.131}$$

where p represents the four momentum vector of the particle in question and the spin projection operator $\hat{\Sigma}$ [Bjo64, Gre92]

$$\hat{\Sigma}(\mu_i) = \frac{1+\gamma_5\not{S}_i}{2}, \tag{2.132}$$

where $S_i = (S^0_i, \vec{S}_i)$ is the four component spin polarization vector of particle i (associated with the spin projection quantum number μ_i), one can express $|T_{L_bJ_b}(\mu_a,\mu_{a'},\mu_{b'},M_b)|^2$ in the desired form. In Eq. (2.131) and (2.132) we make use of the Feynman slach notation namely $\not{A} = \gamma^\mu A_\mu$. Performing a Lorentz boost from the rest system of the particle to a frame of reference in which the particle moves with a momentum of $\vec{p}$, one can show that the zeroth component of S_i will be given by $\frac{\vec{p}\cdot\hat{t}}{m}$ [Gre92] where $\hat{t} \in \{\hat{l},\hat{l}',\hat{s},\hat{s}',\hat{n}\}$. The spatial components of the four component spin vector are chosen to be any one of the directions $(\hat{l},\hat{l}',\hat{s},\hat{s}')$ or $\hat{n}$.

In a polarized $(p, 2p)$ experiment the spins projections of the projectile (a) and scattered particle (a') are fixed, while the spin projections of the bound proton (b) and the other scattered proton (b') are not. In the case of Eq. (2.130) the spin projections are all fixed values. To obtain the desired form for $|T_{L_bJ_b}(\mu_a, \mu_{a'}, \mu_{b'}, M_b)|^2$ one has to sum over the spin projections of b and b' while keeping the spin projections of a and a' constant. For the bound proton one has to sum over all possible spin projections which a proton in a state with total orbital angular momentum of J_b can have. This implies taking the sum over the total angular momentum projection M_b and the spin projection $\mu_{b'}$. Thus

$$\begin{aligned}\sum_{M_b\mu_{b'}} |T_{L_bJ_b}(\mu_a, \mu_{a'}, \mu_{b'}, M_b)|^2 &= \sum_{i,j=S}^{T} \sum_{M_b\mu_{b'}} \sum_{\alpha,\beta,\delta,\epsilon=1}^{4} \sum_{\rho,\sigma,\tau,\lambda=1}^{4} F^i(F^j)^*[u_\lambda(\vec{k}_{a'}, \mu_{a'})\bar{u}_\alpha(\vec{k}_{a'}, \mu_{a'})](\lambda_1^j)_{\alpha\beta} \\ &\times [u_\beta(\vec{k}_a, \mu_a)\bar{u}_\tau(\vec{k}_a, \mu_a)](\bar{\lambda}_1^i)_{\tau\lambda}[u_\sigma(\vec{k}_{b'}, \mu_{b'})\bar{u}_\delta(\vec{k}_{b'}, \mu_{b'})](\lambda_{2i})_{\delta\epsilon} \\ &\times \{\Phi_{L_bJ_bM_b}(-\vec{k}_C)\}_\epsilon\{\bar{\Phi}_{L_bJ_bM_b}(-\vec{k}_C)\}_\rho(\bar{\lambda}_{2i})_{\rho\sigma}. \end{aligned} \tag{2.133}$$

In ref. [Gre90] it is shown that the spin projection operator satisfies the relationship

$$\hat{\Sigma}(\mu)u(\vec{k}, \mu') = \delta_{\mu'\mu}u(\vec{k}, \mu)\,. \tag{2.134}$$

Using identity (2.134) one can write

$$\begin{aligned}\sum_{M_b\mu_{b'}} |T_{L_bJ_b}(\mu_a, \mu_{a'}, \mu_{b'}, M_b)|^2 &= \sum_{i,j=S}^{T} \sum_{M_b\mu_b} \sum_{\mu_F\mu_I} \sum_{\alpha,\beta,\delta,\epsilon=1}^{4} \sum_{\rho,\sigma,\tau,\lambda=1}^{4} F^i(F^j)^*[u_\lambda(\vec{k}_{a'}, \mu_F)u_\alpha(\vec{k}_{a'}, \mu_F)] \\ &\times \{\hat{\Sigma}(\mu_{a'})(\lambda_1^j)_{\alpha\beta}u_\beta(\vec{k}_a, \mu_I)\bar{u}_\tau(\vec{k}_a, \mu_I)]\{\hat{\Sigma}(\mu_a)(\bar{\lambda}_1^i)_{\tau\lambda}[u_\sigma(\vec{k}_{b'}, \mu_{b'}) \\ &\times [u_\sigma(\vec{k}_b, \mu_{b'})(\lambda_{2i})_{\delta\epsilon}]\{\Phi_{L_bJ_bM_b}(-\vec{k}_C)\}_\epsilon\{\bar{\Phi}_{L_bJ_bM_b}(-\vec{k}_C)\}_\rho\{\bar{\lambda}_{2i}\}_{\rho\sigma}, \end{aligned} \tag{2.135}$$

where the indices μ_F and μ_I represent all possible combinations of spin projections over a' and a respectively. Using the identity given by Eq. (2.131), one can rewrite the previous equation as

$$\begin{aligned}\sum_{M_b\mu_{b'}} |T_{L_bJ_b}(\mu_a, \mu_{a'}, \mu_{b'}, M_b)|^2 &= \sum_{M_b} \sum_{i,j=S}^{T} \sum_{\alpha,\beta,\delta,\epsilon=1}^{4} F^i(F^j)^* \left(\frac{\not{p}_{a'} + m}{2m}\right)_{\lambda\alpha} \{\hat{\Sigma}(\mu_{a'})\lambda_1^j\}_{\alpha\beta} \left(\frac{\not{p}_a + m}{2m}\right)_{\beta\tau} \\ &\times \{\hat{\Sigma}(\mu_a)\bar{\lambda}\}_1^i\}_{\tau\lambda} \sum_{\rho,\sigma,\tau,\lambda=1}^{4} \left(\frac{\not{p}_{b'} + m}{2m}\right)_{\sigma\delta} \{\lambda_2^j\}_{\delta\epsilon}\{\Phi_{L_bJ_bM_b}(-\vec{k}_C)\}_\epsilon \\ &\times \{\bar{\Phi}_{L_bJ_bM_b}(-\vec{k}_C)\}_\rho\{\bar{\lambda}_{2i}\}_{\rho\sigma}. \end{aligned} \tag{2.136}$$

Thus

$$\sum_{M_b\mu_{b'}} |T_{L_bJ_b}(\mu_a,\mu_{a'},\mu_{b'},M_b)|^2 = \sum_{M_b}\sum_{i,j=S}^{T} F^i(F^j)^* Tr[\left(\frac{\not p_{a'}+m}{2m}\right)\bar\Sigma(\mu_{a'})\lambda_1^j\left(\frac{\not p_a+m}{2m}\right)\bar\Sigma(\mu_a)\bar\lambda_1^i]$$
$$\times Tr[\left(\frac{\not p_{b'}+m}{2m}\right)\lambda_{2j}\Phi_{L_bJ_bM_b}(-\vec k_C)\bar\Phi_{L_bJ_bM_b}(-\vec k_C)\lambda_{2i}]. \quad (2.137)$$

Note that with the spin-projection operators the spin projections of particles a and a' in the entrance and exit channels are fixed. Substitution of Eq. (2.132) into Eq. (2.137) yields

$$\sum_{M_b\mu_{b'}} |T_{L_bJ_b}(\mu_a,\mu_{a'},\mu_{b'},M_b)|^2 = \sum_{M_b}\sum_{i,j=S}^{T} F^i(F^j)^* Tr[\left(\frac{\not p_{a'}+m}{2m}\right)\left(\frac{1+\gamma^5\not S_{a'}}{2}\right)\lambda_1^j\left(\frac{\not p_a+m}{2m}\right)$$
$$\times\left(\frac{1+\gamma^5\not S_a}{2}\right)(\bar\lambda_1^i)]Tr[\left(\frac{\not p_{b'}+m}{2m}\right)\lambda_{2j}$$
$$\Phi_{L_bJ_bM_b}(-\vec k_C)\bar\Phi_{L_bJ_bM_b}(-\vec k_C)\{\lambda_{2i}\}. \quad (2.138)$$

Defining

$$K_1 = \frac{p_{a'}}{m}$$
$$P_1 = \frac{p_a}{m}$$
$$K_2 = \frac{p_{b'}}{m}, \quad (2.139)$$

Eq. (2.138) can be written as

$$\sum_{M_b\mu_{b'}} |T_{L_bJ_b}(\mu_a,\mu_{a'},\mu_{b'},M_b)|^2 = \sum_{M_b}\sum_{i,j=S}^{T}(F^j)^*F^i\frac{1}{32}Tr[(\not K_1+1)(1+\gamma^5\not S_{a'})\lambda_1^j$$
$$\times(\not P_1+1)(1+\gamma^5\not S_a)\bar\lambda_1^i]$$
$$\times Tr[(\not K_2+1)\lambda_{2j}\Phi_{L_bJ_bM_b}(-\vec k_C)\bar\Phi_{L_bJ_bM_b}(-\vec k_C)\bar\lambda_{2i}]. \quad (2.140)$$

In a more compact notation Eq. (2.140) can be written as

$$\sum_{M_b\mu_{b'}} |T_{L_bJ_b}(\mu_a,\mu_{a'},\mu_{b'},M_b)|^2 = \sum_{i,j=S}^{T}(F^j)^*F^iL^{ji}(K_1,P_1,S_a,S_{a'})\sum_{M_b}H_{ji}(\vec x,\vec{x'},M_b,K_2), \quad (2.141)$$

where

$$L^{ji}(K_1,P_1,S_a,S_{a'}) = \frac{1}{16}Tr[(\not K_1+1)\left(1+\gamma^5\not S_{a'}\right)\lambda_1^j(\not P_1+1)\left(1+\gamma^5\not S_a\right)\bar\lambda_1^i] \quad (2.142)$$

defines the projectile tensor and

$$H_{ji}(K_2, M_b, K_2) = \frac{1}{2} Tr[(\not{K}_2 \quad + 1)\, \Phi_{L_b J_b M_b}(-\vec{k}_C) \bar{\Phi}_{L_b J_b M_b}(-\vec{k}_C) \bar{\lambda}_{2i}], \tag{2.143}$$

the target tensor which is often also referred to as the nuclear response function. In the following two sections we will write down explicit expressions for both $L^{ji}(K_1, P_1, S_a, S_{a'})$ and $H_{ji}(K_2, M_b, K_2)$.

2.9.2 The hadronic tensor

Information about the polarization of the protons in the entrance and exit channels of a polarized $(p, 2p)$ reaction is contained in the spin-dependent hadronic tensor defined by Eq.(2.142). Further evaluation of the hadronic tensor is performed so as to write it in a form which is contractable with the response function. The hadronic tensor defined by Eq.(2.142) can be written in the form

$$L^{ji}(K_1, P_1, S_a, S_{a'}) = \frac{1}{16} Tr[X^+ \lambda^j X^- \bar{\lambda}^i], \tag{2.144}$$

where

$$X^+(K_1, S_{a'}) \quad = \quad (\not{K}_1 \quad + 1)(1 + \gamma^5 \not{S}_{a'} \quad) \tag{2.145}$$

and

$$X^-(P_1, S_a) \quad = \quad (\not{P}_1 \quad + 1)(1 + \gamma^5 \not{S}_a \quad). \tag{2.146}$$

In the case where one works with unpolarized beams, the spin vectors S_a and $S_{a'}$ can be set equal to zero, yielding

$$X^+(K_1) \quad = \quad (\not{K}_1 \quad + 1) \tag{2.147}$$

and

$$X^-(P_1) \quad = \quad (\not{P}_1 \quad + 1). \tag{2.148}$$

It is shown in the appendix that any 4×4 matrix X can be written as

$$X = \sum_{i,j=1}^{2} (e_i^\dagger \otimes e_j) \otimes X_{ij}, \tag{2.149}$$

where e_1 and e_2 are the two component unit row vectors $(1,0)$ and $(0,1)$, $\otimes$ denotes a Kronecker product, and X_{ij} is a 2×2 matrix. It therefore follows that Eq. (2.144) can be written as

$$L^{ji}(K_1, P_1, S_a, S_{a'}) = Tr[(\sum_{m,n=1}^{2} (e_m^\dagger \otimes e_n) \otimes X_{mn}^{+})\lambda_j (\sum_{q,r=1}^{2} (e_q^\dagger \otimes e_r) \otimes X_{qr}^{-})\lambda_i]. \tag{2.150}$$

Any 2×2 matrix M_{ij} can be expanded in terms of the set of 2×2 matrices consisting of the 2×2 identity matrix I_2 and the three Pauli matrices $\{\sigma_x, \sigma_y, \sigma_z\}$. Thus

$$X_{ij}^{+} = \sum_{R=I_2}^{\sigma_z} G_R^{ij} \Gamma_R \tag{2.151}$$

and

$$X_{ij}^{-} = \sum_{T=I_2}^{\sigma_z} P_T^{ij} \Gamma_T. \tag{2.152}$$

Hence

$$L^{ji}(K_1, P_1, S_a, S_{a'}) = \frac{1}{16} \sum_{m,n=1}^{2} \sum_{q,r=1}^{2} \sum_{R,T=I_2}^{\sigma_z} G_R^{mn} P_T^{qr} Tr[((e_m^\dagger \otimes e_n) \otimes \Gamma_R)\lambda_j ((e_{qr}^\dagger \otimes e_r) \otimes \Gamma_T)\bar{\lambda}_i]. \tag{2.153}$$

In ref. [Its80] it is shown that the bilinear gamma matrices λ_i can be constructed by taking the Kronecker product of various combinations of the Pauli matrices so that one can write

$$\lambda_j = A_j^1 \otimes A_j^2, \tag{2.154}$$

where A_i^1 and A_i^2 represents the two Pauli matrices which gives us the matrix λ_i. Similarly one can write

$$\bar{\lambda}_j = B_i^1 \otimes B_i^2. \tag{2.155}$$

Using the latter two identities one can write Eq. (2.153) as

$$L^{ji}(K_1, P_1, S_a, S_{a'}) = \frac{1}{16} \sum_{m,n=1}^{2} \sum_{q,r=1}^{2} \sum_{R,T=I_2}^{\sigma_z} G_R^{mn} P_T^{qr} Tr[(e_m^\dagger \otimes e_n) \otimes \Gamma_R)(A_i^1 \otimes A_i^2)(e_{qr}^\dagger \otimes e_r) \otimes \Gamma_T)(B_i^1 \otimes B_i^2)]. \tag{2.156}$$

Using the identity given by Eq. (2.118) and the fact that $\mathrm{Tr}[AB] = \mathrm{Tr}[A]\mathrm{Tr}[B]$ yields

$$L^{ji}(K_1, P_1, S_a, S_{a'}) = \frac{1}{16} \sum_{m,n=1}^{2} \sum_{q,r=1}^{2} \sum_{R,T=I_2}^{\sigma_z} G_R^{mn} P_T^{qr} Tr[(e_m^\dagger \otimes e_n) A_j^1 (e_{qr}^\dagger \otimes e_r) B_i^1] Tr[\Gamma_R A_j^2 \Gamma_T B_i^2]. \tag{2.157}$$

One can further simplify the expression (2.157) by using the trace identity

$$Tr[(u^\dagger \otimes v) X (x^\dagger \otimes y) Y] = (u^\dagger X y)(x^\dagger Y v), \tag{2.158}$$

yielding

$$L^{ji}(K_1, P_1, S_a, S_{a'}) = \frac{1}{16} \sum_{m,n=1}^{2} \sum_{q,r=1}^{2} \sum_{R,T=I_2}^{\sigma_z} G_R^{mn} P_T^{qr} [(e_m^\dagger A_j^1 e_r)(e_q^\dagger B_i^1 e_n)] Tr[\Gamma_R A_j^2 \Gamma_T B_i^2]. \tag{2.159}$$

The expansion coefficients G_R^{mn} and P_T^{qr} in Eq. (2.159) can be derived as follows. One can write Eqs. (2.145) and (2.146) explicitly as

$$X^+(K_{1\mu}, S_{a'\nu}) = \gamma^\mu K_{1\mu} + \gamma^5 \gamma^\nu S_{a'\nu} + \gamma^\mu K_{1\mu} \gamma^5 \gamma^\nu S_{a'\nu} + I_4 \tag{2.160}$$

and

$$X^-(P_{1\rho}, S_{a\sigma}) = \gamma^\rho P_{1\rho} + \gamma^5 \gamma^\sigma S_{a\sigma} + \gamma^\rho P_{1\rho} \gamma^5 \gamma^\sigma S_{a\sigma} + I_4, \tag{2.161}$$

where

$$\begin{aligned} I_4 &= \begin{bmatrix} I_2 & 0 \\ 0 & I_2 \end{bmatrix} \\ \gamma^0 &= \begin{bmatrix} I_2 & 0 \\ 0 & -I_2 \end{bmatrix} \\ \gamma^i &= \begin{bmatrix} 0 & \sigma^i \\ \sigma^i & 0 \end{bmatrix} \\ \gamma^5 &= \begin{bmatrix} 0 & I_2 \\ I_2 & 0 \end{bmatrix}. \end{aligned} \tag{2.162}$$

Substituting the latter expressions into Eqs. (2.160) and (2.161) yields

$$X^+ = \begin{bmatrix} X_{11}^+ & X_{12}^+ \\ X_{21}^+ & X_{22}^+ \end{bmatrix}, \tag{2.163}$$

where

$$\begin{aligned} X_{11}^+ &= (K_{10} + 1) I_2 + S_{a'j} \sigma^j \\ X_{12}^+ &= (K_{1i} S_{a'i} - (1 + K_{10}) S_{a'0}) I_2 - (K_{1i} - i(K_{1j} S_{a'k} + K_{1k} S_{a'j})) \sigma^i \\ X_{21}^+ &= (K_{1i} S_{a'i} + (1 - K_{10}) S_{a'0}) I_2 - (K_{1i} + i(K_{1j} S_{a'k} + K_{1k} S_{a'j})) \sigma^i \\ X_{22}^+ &= (1 - K_{10}) I_2 - S_{a'j} \sigma^i. \end{aligned} \tag{2.164}$$

Similarly one can write

$$X^- = \begin{bmatrix} X_{11}^- & X_{12}^- \\ X_{21}^- & X_{22}^- \end{bmatrix}, \tag{2.165}$$

where

$$\begin{aligned} X_{11}^{-} &= (P_{10}+1)I_2 + S_{aj}\sigma^j \\ X_{12}^{-} &= (P_{1i}S_{ai} - (1+P_{10})S_{a0})I_2 - (P_{1i} - iP_{1j}S_{ak})\sigma^i \\ X_{21}^{-} &= (P_{1i}S_{ai} + (1-P_{10})S_{a0})I_2 - (P_{1i} + iP_{1j}S_{ak})\sigma^i \\ X_{22}^{-} &= (1-P_{10})I_2 - S_{ai}\sigma^i. \end{aligned} \tag{2.166}$$

Thus from identities (2.151, 2.152) and Eqs. (2.164) and (2.166), it follows that

$$\begin{aligned} G_{I_2}^{11} &= K_{10}+1 \\ G_{\sigma_i}^{11} &= S_{a'i} \\ G_{I_2}^{12} &= -(1+K_{10})S_{a'0} \\ G_{\sigma_i}^{12} &= -(K_{1i} - iK_{1j}S_{a'k}) \\ G_{I_2}^{21} &= (1-K_{10})S_{a'0} \\ G_{\sigma_i}^{21} &= -(K_{1i} + iK_{1j}S_{a'k}) \\ G_{I_2}^{22} &= 1-K_{10} \\ G_{\sigma_i}^{22} &= -S_{a'i} \end{aligned} \tag{2.167}$$

and

$$\begin{aligned} P_{I_2}^{11} &= P_{10}+1 \\ P_{\sigma_i}^{11} &= S_{ai} \\ P_{I_2}^{12} &= -(1+P_{10})S_{a0} \\ P_{\sigma_i}^{12} &= -(P_{1i} - iP_{1j}S_{ak}) \\ P_{I_2}^{21} &= (1-P_{10})S_{a0} \\ P_{\sigma_i}^{21} &= -(P_{1i} + iP_{1j}S_{ak}) \\ P_{I_2}^{22} &= 1-P_{10} \\ P_{\sigma_i}^{22} &= -S_{ai}. \end{aligned} \tag{2.168}$$

2.9.3 The response function

We now proceed to write down simplified expressions for the response function which is defined by Eq. (2.143). The relativistic boundstate wave function (see also section (2.6.1)) is given by [Ike95]

$$\Phi^B_{L_bJ_bM_b}(\vec{r}) = \frac{1}{r}\sum_{M_{L_b}} \begin{bmatrix} u^B_{L_bJ_b}(r) C^{L_b\frac{1}{2}M_{L_b}\mu_b}_{J_bM_b} Y_{L_bM_{L_b}}(\hat{r}) \\ iw^B_{L_bJ_b}(r) C^{\widetilde{L}_b\frac{1}{2}M_{\widetilde{L}_b}\mu_b}_{J_bM_b} Y_{\widetilde{L}_bM_{L_b}}(\hat{r}) \end{bmatrix} \otimes \chi_{\mu_b}, \tag{2.169}$$

where the labels $C^{L_b\frac{1}{2},M_{L_b}\mu_b}_{J_bM_b}$, $Y_{L_bM_{L_b}}(\hat{x})$ and χ_{μ_b} represent the Clebsch-Gordon coefficients, the spherical harmonics and the two component spin vectors associated with the bound proton (b). We first evaluate Eq. (2.114). A partial wave expansion of $e^{i\vec{k}_C\cdot\vec{r}}$ yields

$$e^{i\vec{k}_C\cdot\vec{r}} = 4\pi\sum_{L=0}^{\infty}\sum_{M_L=L}^{L} = -i^{L_b}i^{L_b}j_{L_b}(k_Cr)Y_{L_bM_{L_b}}(\hat{k}_C)Y^*_{L_bM_{L_b}}(\hat{r}), \tag{2.170}$$

where $j_n(r)$ represents the spherical Bessel function of order n. Hence

$$e^{i\vec{k}_c\cdot\vec{r}}\Phi^B_{L_bJ_bM_b}(\vec{r}) = \frac{4\pi}{r}\sum_{L=0}^{\infty}\sum_{M_L=-L}^{L} \begin{bmatrix} i^L j_L(k_Cr)u^B_{L_bJ_b}(r)C^{L_b\frac{1}{2}M_{L_b}\mu_b}_{J_bM_b}Y_{LM_L}(\hat{k}_C)Y^*_{LM_L}(\hat{r})Y_{L_bM_{L_b}}(\hat{r})\chi_{\mu_b} \\ i^{L_b+1}j_L(k_Cr)w^B_{L_bJ_b}(r)C^{\widetilde{L}_b\frac{1}{2}M_{\widetilde{L}_b}\mu_b}_{J_bM_b}Y_{LM_L}(\hat{k}_C)Y^*_{LM_L}(\hat{r})Y_{\widetilde{L}_bM_{L_b}}(\hat{r})\chi_{\mu_b} \end{bmatrix}. \tag{2.171}$$

Furthermore the Clebsch-Gordon coefficients are non-zero only if $M_{L_b} = M_b - \mu_b$. Integrating over all space yields

$$\int_0^\infty d\vec{r}e^{i\vec{k}_c\cdot\vec{x}}\Phi^B_{L_bJ_bM_b}(\vec{r}) = \frac{4\pi}{r}\sum_{L=0}^{\infty}\sum_{M_L=-L}^{L} \begin{bmatrix} i^{L_b}j_{L_b}(k_Cr)C^{L_b\frac{1}{2}(M_b-\mu_b)\mu_b}_{J_bM_b}Y_{L_bM_{L_b}}(\hat{k}_C)\chi_{\mu_b}\mathcal{I}_{L_bJ_b}(k_C,M_{L_b}) \\ i^{L_b+1}j_{L_b}(k_Cr)C^{\widetilde{L}_b\frac{1}{2}(M_b-\mu_b)\mu_b}_{J_bM_b}Y_{L_bM_{L_b}}(\hat{k}_C)\chi_{\mu_b}\mathcal{J}_{L_bJ_b}(k_C,M_{L_b}) \end{bmatrix}. \tag{2.172}$$

where

$$\mathcal{I}_{L_bJ_b}(k_C,M_{L_b}) = \int_0^\infty dr\, rj_L(k_Cr)u^B_{L_bJ_b}(r)\int_0^{4\pi}d\Omega Y^*_{LM_L}(\hat{r})Y_{L_bM_b-\mu_b}(\hat{r}) \tag{2.173}$$

and

$$\mathcal{J}_{L_bJ_b}(k_C,M_{L_b}) = \int_0^\infty dr\, rj_L(k_Cr)w^B_{L_bJ_b}(r)\int_0^{4\pi}d\Omega Y^*_{LM_L}(\hat{r})Y_{\widetilde{L}_bM_b-\mu_b}(\hat{r}). \tag{2.174}$$

The identity $\int_0^{4\pi}d\Omega Y^*_{LM_L}(\hat{r})Y_{L'M_{L'}}(\hat{r}) = \delta_{LL'}$ [Sak85] allows us to write

$$\mathcal{I}_{L_bJ_b}(k_C,M_{L_b}) = \int_0^\infty dr\, rj_{L_b}(k_Cr)u^B_{L_bJ_b}(r)\delta_{M_L,M_b-\mu_b}\delta_{L,L_b} \tag{2.175}$$

and

$$\mathcal{J}_{L_bJ_b}(k_C, M_{L_b}) = \int_0^\infty dr\, r j_{L_b}(k_C r) w^B_{L_bJ_b}(r) \delta_{M_L, M_b-\mu_b} \delta_{L,\tilde{L}_b}. \tag{2.176}$$

We define

$$u^B_{L_bJ_b}(k_C) = \int_0^\infty dr\, r j_{L_b}(k_C r) u^B_{L_bJ_b}(r) \tag{2.177}$$

$$w^B_{L_bJ_b}(k_C) = \int_0^\infty dr\, r j_{L_b}(k_C r) w^B_{L_bJ_b}(r). \tag{2.178}$$

Hence

$$\Phi^B_{L_bJ_bM_b}(-\vec{k}_C) = 4\pi \sum_{\mu_b} \begin{bmatrix} i^{L_b} u^B_{L_bJ_b}(k_C) C^{L_b, M_b-\mu_b, \frac{1}{2}, \mu_b}_{J_bM_b} Y_{L_bM_b-\mu_b}(\hat{k}_C)\chi_{\mu_b} \\ i^{L_b+1} w^B_{L_bJ_b}(k_C) C^{\tilde{L}_b, M_b-\mu_b, \frac{1}{2}, \mu_b}_{J_bM_b} Y_{\tilde{L}_bM_b-\mu_b}(\hat{k}_C)\chi_{\mu_b} \end{bmatrix}, \tag{2.179}$$

where $\tilde{L}_b = 2J_b - L_b$. Substituting

$$\chi_{\frac{1}{2}} = \begin{pmatrix} 1 \\ 0 \end{pmatrix}$$

and

$$\chi_{-\frac{1}{2}} = \begin{pmatrix} 0 \\ 1 \end{pmatrix}$$

into Eq. (2.179) gives

$$\Phi^B_{L_bJ_bM_b}(-\vec{k}_C) = 4\pi \begin{bmatrix} i^{L_b} u^B_{L_bJ_b}(k_C) C^{L_b, M_b-\frac{1}{2}, \frac{1}{2}, \frac{1}{2}}_{J_bM_b} Y_{L_bM_b-\frac{1}{2}}(\hat{k}_C) \\ i^{L_b} u^B_{L_bJ_b}(k_C) C^{L_b, M_b+\frac{1}{2}, \frac{1}{2}, -\frac{1}{2}}_{J_bM_b} Y_{L_bM_b+\frac{1}{2}}(\hat{k}_C) \\ i^{\tilde{L}_b+1} w^B_{L_bJ_b}(k_C) C^{L_b, M_b-\frac{1}{2}, \frac{1}{2}, \frac{1}{2}}_{J_bM_b} Y_{\tilde{L}_bM_b-\frac{1}{2}}(\hat{k}_C) \\ i^{\tilde{L}_b+1} w^B_{L_bJ_b}(k_C) C^{L_b, M_b+\frac{1}{2}, \frac{1}{2}, -\frac{1}{2}}_{J_bM_b} Y_{\tilde{L}_bM_b+\frac{1}{2}}(\hat{k}_C) \end{bmatrix}. \tag{2.180}$$

Let

$$\begin{aligned} \phi^B_{1L_bJ_b}(-\vec{k}_C) &= i^{L_b} u^B_{L_bJ_b}(k_C) C^{L_b, M_b-\frac{1}{2}, \frac{1}{2}, \frac{1}{2}}_{J_bM_b} Y_{L_bM_b-\frac{1}{2}}(\hat{k}_C) \\ \phi^B_{2L_bJ_b}(-\vec{k}_C) &= i^{L_b} u^B_{L_bJ_b}(k_C) C^{L_b, M_b+\frac{1}{2}, \frac{1}{2}, -\frac{1}{2}}_{J_bM_b} Y_{L_bM_b+\frac{1}{2}}(\hat{k}_C) \\ \phi^B_{3L_bJ_b}(-\vec{k}_C) &= i^{\tilde{L}_b+1} w^B_{L_bJ_b}(k_C) C^{L_b, M_b-\frac{1}{2}, \frac{1}{2}, \frac{1}{2}}_{J_bM_b} Y_{\tilde{L}_bM_b-\frac{1}{2}}(\hat{k}_C) \\ \phi^B_{4L_bJ_b}(-\vec{k}_C) &= i^{\tilde{L}_b+1} w^B_{L_bJ_b}(k_C) C^{L_b, M_b+\frac{1}{2}, \frac{1}{2}, -\frac{1}{2}}_{J_bM_b} Y_{\tilde{L}_bM_b+\frac{1}{2}}(\hat{k}_C). \end{aligned} \tag{2.181}$$

Thus one can write Eq. (2.180) as

$$\bar{\Phi}^B_{L_bJ_bM_b}(-\vec{k}_C) = \begin{bmatrix} \phi^B_{1L_bJ_b}(\vec{k}_C) \\ \phi^B_{2L_bJ_b}(\vec{k}_C) \\ \phi^B_{3L_bJ_b}(\vec{k}_C) \\ \phi^B_{4L_bJ_b}(\vec{k}_C) \end{bmatrix}. \tag{2.182}$$

The complex conjugate transpose of the boundstate wave function is given by

$$\bar{\Phi}^B_{L_bJ_bM_b}(-\vec{k}_C) = \Phi^{B\dagger}_{L_bJ_bM_b}(-\vec{k}_C)\gamma^0, \tag{2.183}$$

where the matrix γ^0 is given by the relationship [Its80]

$$\gamma^0 = \begin{bmatrix} 1 & 0 & 0 & 0 \\ 0 & 1 & 0 & 0 \\ 0 & 0 & -1 & 0 \\ 0 & 0 & 0 & -1 \end{bmatrix}. \tag{2.184}$$

Using Eqs. (2.182), (2.183) and (2.184) one can write

$$\bar{\Phi}^B_{L_bJ_bM_b}(-\vec{k}_C) = [\phi^{B*}_{1L_bJ_b}(\vec{k}_C), \phi^{B*}_{2L_bJ_b}(\vec{k}_C), -\phi^{B*}_{3L_bJ_b}(\vec{k}_C), -\phi^{B*}_{4L_bJ_b}(\vec{k}_C)]. \tag{2.185}$$

We define

$$x^B(\vec{k}_C, M_b) = \Phi^B_{L_bJ_bM_b}(-\vec{k}_C)\bar{\Phi}^B_{L_bJ_bM_b}(-\vec{k}_C). \tag{2.186}$$

Substituting Eqs.(2.183) and (2.185) into Eq.(2.186) yields

$$\begin{aligned} x^B(\vec{k}_C, M_b') &= \begin{bmatrix} \phi^B_{1L_bJ_b}(-\vec{k}_C) \\ \phi^B_{2L_bJ_b}(-\vec{k}_C) \\ \phi^B_{3L_bJ_b}(-\vec{k}_C) \\ \phi^B_{4L_bJ_b}(-\vec{k}_C) \end{bmatrix} \begin{bmatrix} \phi^{B*}_{1L_bJ_b}(-\vec{k}_C), & \phi^{B*}_{2L_bJ_b}(-\vec{k}_C), & -\phi^{B*}_{3L_bJ_b}(-\vec{k}_C), & -\phi^{B*}_{4L_bJ_b}(-\vec{k}_C) \end{bmatrix} \\ &= \begin{bmatrix} x^B_{11}(-\vec{k}_C) & x^B_{12}(-\vec{k}_C) \\ x^B_{21}(-\vec{k}_C) & x^B_{22}(-\vec{k}_C) \end{bmatrix}, \end{aligned} \tag{2.187}$$

where

$$\begin{aligned} x^B_{11}(\vec{k}_C, M_b) &= \begin{bmatrix} \phi^B_{1L_bJ_b}(-\vec{k}_C)\phi^{B*}_{1L_bJ_b}(-\vec{k}_C) & \phi^B_{1L_bJ_b}(-\vec{k}_C)\phi^{B*}_{2L_bJ_b}(-\vec{k}_C) \\ \phi^B_{2L_bJ_b}(-\vec{k}_C)\phi^{B*}_{1L_bJ_b}(-\vec{k}_C) & \phi^B_{2L_bJ_b}(-\vec{k}_C)\phi^{B*}_{2L_bJ_b}(-\vec{k}_C) \end{bmatrix} \\ x^B_{12}(\vec{k}_C, M_b) &= \begin{bmatrix} \phi^B_{1L_bJ_b}(-\vec{k}_C)\phi^{B*}_{3L_bJ_b}(-\vec{k}_C) & \phi^B_{1L_bJ_b}(-\vec{k}_C)\phi^{B*}_{4L_bJ_b}(-\vec{k}_C) \\ \phi^B_{2L_bJ_b}(-\vec{k}_C)\phi^{B*}_{3L_bJ_b}(-\vec{k}_C) & \phi^B_{2L_bJ_b}(-\vec{k}_C)\phi^{B*}_{4L_bJ_b}(-\vec{k}_C) \end{bmatrix} \\ x^B_{21}(\vec{k}_C, M_b) &= \begin{bmatrix} \phi^B_{3L_bJ_b}(-\vec{k}_C)\phi^{B*}_{1L_bJ_b}(-\vec{k}_C) & \phi^B_{3L_bJ_b}(-\vec{k}_C)\phi^{B*}_{2L_bJ_b}(-\vec{k}_C) \\ \phi^B_{4L_bJ_b}(-\vec{k}_C)\phi^{B*}_{1L_bJ_b}(-\vec{k}_C) & \phi^B_{4L_bJ_b}(-\vec{k}_C)\phi^{B*}_{2L_bJ_b}(-\vec{k}_C) \end{bmatrix} \\ x^B_{22}(\vec{k}_C, M_b) &= \begin{bmatrix} \phi^B_{3L_bJ_b}(-\vec{k}_C)\phi^{B*}_{3L_bJ_b}(-\vec{k}_C) & \phi^B_{3L_bJ_b}(-\vec{k}_C)\phi^{B*}_{4L_bJ_b}(-\vec{k}_C) \\ \phi^B_{4L_bJ_b}(-\vec{k}_C)\phi^{B*}_{3L_bJ_b}(-\vec{k}_C) & \phi^B_{4L_bJ_b}(-\vec{k}_C)\phi^{B*}_{4L_bJ_b}(-\vec{k}_C) \end{bmatrix}. \end{aligned} \tag{2.188}$$

Using the unit vectors $\hat{e}_1 = \binom{1}{0}$ and $\hat{e}_2 = \binom{0}{1}$ one can show that

$$x^B(\vec{x}, \vec{x}', \mu_b, \mu_b') = \sum_{i,j=1}^{2} (e_j^\dagger \otimes e_i) \otimes x_{ij}^B. \tag{2.189}$$

For particle b in the exit channel one defines

$$\begin{aligned} y(K_2, \mu_b) &= \frac{1}{2}(\not{K}_2 + 1) \\ &= \frac{1}{2}(K_2^0\gamma_0 - \vec{K}_2 \cdot \vec{\gamma} + I_4) \\ &= \frac{1}{2}\begin{bmatrix} (K_2^0 + 1)I_2 & -\vec{K}_2^i \cdot \vec{\sigma}_i \\ \vec{K}_2^i \cdot \vec{\sigma}_i & (-K_2^0 + 1)I_2 \end{bmatrix} \\ &= \begin{bmatrix} y_{11} & y_{12} \\ y_{21} & y_{22} \end{bmatrix}, \end{aligned} \tag{2.190}$$

where y_{kl} are 2x2 matrices which are related to the momentum and mass of b by

$$\begin{aligned} y_{11} &= \frac{K_2^0 + 1}{2} I_2 \\ y_{12} &= -\frac{K_2^i \sigma^i}{2} \\ y_{21} &= \frac{K_2^i \sigma^i}{2} \\ y_{22} &= \frac{-K_2^0 + 1}{2} I_2. \end{aligned} \tag{2.191}$$

As in the case of the boundstate wave function one can show that

$$y(K_2, \mu_b) = \sum_{i,j=1}^{2} (e_j^\dagger \otimes e_i) \otimes y_{ij}. \tag{2.192}$$

Employing Eq. (2.192) and Eq.(2.187) one can write

$$y(K_2, \mu_b)\lambda_{2j} x^B(\vec{k}_C, M_b)\lambda_{2i} = \frac{1}{rr'} \sum_{r,s,k,l}^{2} [(e_r^\dagger \otimes e_s) \otimes x_{rs}^B]\lambda_{2j}[(e_k^\dagger \otimes e_l) \otimes y_{kl}]\lambda_{2i} \tag{2.193}$$

using the identity which states that any 2×2 matrix can be expanded in terms of the four linearly independent 2×2 matrices consisting of I_2, together with the three Pauli matrices σ_x,

σ_y and σ_z, that is

$$\begin{bmatrix} a & b \\ c & d \end{bmatrix} = AI_2 + B\sigma_x + C\sigma_y + D\sigma_z, \tag{2.194}$$

where

$$\begin{aligned} A &= \frac{1}{2}(a+d) \\ B &= \frac{1}{2}(b+c) \\ C &= -\frac{i}{2}(c-b) \\ D &= \frac{1}{2}(a-d). \end{aligned} \tag{2.195}$$

One can therefore expand the matrices x^B_{rs} and y_{kl} in terms of I_2 and the Pauli matrices. Hence

$$x^B_{rs} = \sum_{R=I_2}^{\sigma_z} [{}^{rs}_{R}G'_{L_bJ_b}(\vec{x},\vec{x}',M_b)]\Gamma_R \tag{2.196}$$

$$y_{kl} = \sum_{T=I_2}^{\sigma_z} P'^{kl}_{T}\Gamma_T. \tag{2.197}$$

Using Eq. [2.195], the expansion coefficients ${}^{rs}_{R}G'_{L_bJ_b}(\vec{x},\vec{x}')$ can be found to be

$$\begin{aligned}
{}^{11}_{I_2}G'_{L_bJ_b}(-\vec{k}_C,M_b) &= \frac{1}{2}[\phi^B_{1L_bJ_b}(-\vec{k}_C)\phi^{B*}_{1L_bJ_b}(-\vec{k}_C) + \phi^B_{2L_bJ_b}(-\vec{k}_C)\phi^{B*}_{2L_bJ_b}(-\vec{k}_C)] \\
{}^{11}_{\sigma_x}G'_{L_bJ_b}(\vec{x},\vec{x}',M_b) &= \frac{1}{2}[\phi^B_{1L_bJ_b}(-\vec{k}_C)\phi^{B*}_{2L_bJ_b}(-\vec{k}_C) + \phi^B_{2L_bJ_b}(-\vec{k}_C)\phi^{B*}_{1L_bJ_b}(-\vec{k}_C)] \\
{}^{11}_{\sigma_y}G'_{L_bJ_b}(\vec{x},\vec{x}',M_b) &= -\frac{i}{2}[\phi^B_{1L_bJ_b}(-\vec{k}_C)\phi^{B*}_{2L_bJ_b}(-\vec{k}_C) - \phi^B_{2L_bJ_b}(-\vec{k}_C)\phi^{B*}_{2L_bJ_b}(-\vec{k}_C)] \\
{}^{11}_{\sigma_z}G'_{L_bJ_b}(\vec{x},\vec{x}',M_b) &= \frac{1}{2}[\phi^B_{1L_bJ_b}(-\vec{k}_C)\phi^{B*}_{1L_bJ_b}(-\vec{k}_C) - \phi^B_{2L_bJ_b}(-\vec{k}_C)\phi^{B*}_{2L_bJ_b}(-\vec{k}_C)] \\
{}^{12}_{I_2}G'_{LbJ_b}(\vec{x},\vec{x}',M_b) &= \frac{1}{2}[\phi^B_{1L_bJ_b}(-\vec{k}_C)\phi^{B*}_{3L_bJ_b}(-\vec{k}_C) + \phi^B_{2L_bJ_b}(-\vec{k}_C)\phi^{B*}_{4L_bJ_b}(-\vec{k}_C)] \\
{}^{12}_{\sigma_x}G'_{L_bJ_b}(\vec{x},\vec{x}',M_b) &= \frac{1}{2}[\phi^B_{1L_bJ_b}(-\vec{k}_C)\phi^{B*}_{4L_bJ_b}(-\vec{k}_C) + \phi^B_{2L_bJ_b}(-\vec{k}_C)\phi^{B*}_{4L_bJ_b}(-\vec{k}_C)] \\
{}^{12}_{\sigma_y}G'_{L_bJ_b}(\vec{x},\vec{x}',M_b) &= -\frac{i}{2}[\phi^B_{2L_bJ_b}(-\vec{k}_C)\phi^{B*}_{3L_bJ_b}(-\vec{k}_C) - \phi^B_{2L_bJ_b}(-\vec{k}_C)\phi^{B*}_{4L_bJ_b}(-\vec{k}_C)] \\
{}^{12}_{\sigma_z}G'_{L_bJ_b}(\vec{x},\vec{x}',M_b) &= \frac{1}{2}[\phi^B_{1L_bJ_b}(-\vec{k}_C)\phi^{B*}_{3L_bJ_b}(-\vec{k}_C) - \phi^B_{2L_bJ_b}(-\vec{k}_C)\phi^{B*}_{4L_bJ_b}(-\vec{k}_C)] \\
{}^{21}_{I_2}G'_{L_bJ_b}(\vec{x},\vec{x}',M_b) &= \frac{1}{2}[\phi^B_{3L_bJ_b}(-\vec{k}_C)\phi^{B*}_{1L_bJ_b}(-\vec{k}_C) + \phi^B_{4L_bJ_b}(-\vec{k}_C)\phi^{B*}_{2L_bJ_b}(-\vec{k}_C)] \\
{}^{21}_{\sigma_x}G'_{L_bJ_b}(\vec{x},\vec{x}',M_b) &= \frac{1}{2}[\phi^B_{3L_bJ_b}(-\vec{k}_C)\phi^{B*}_{2L_bJ_b}(-\vec{k}_C) + \phi^B_{4L_bJ_b}(-\vec{k}_C)\phi^{B*}_{1L_bJ_b}(-\vec{k}_C)] \\
{}^{21}_{\sigma_y}G'_{L_bJ_b}(\vec{x},\vec{x}',M_b) &= -\frac{i}{2}[\phi^B_{4L_bJ_b}(-\vec{k}_C)\phi^{B*}_{1L_bJ_b}(-\vec{k}_C) - \phi^B_{4L_bJ_b}(-\vec{k}_C)\phi^{B*}_{2L_bJ_b}(-\vec{k}_C)] \\
{}^{21}_{\sigma_z}G'_{L_bJ_b}(\vec{x},\vec{x}',M_b) &= \frac{1}{2}[\phi^B_{3L_bJ_b}(-\vec{k}_C)\phi^{B*}_{1L_bJ_b}(-\vec{k}_C) - \phi^B_{4L_bJ_b}(-\vec{k}_C)\phi^{B*}_{2L_bJ_b}(-\vec{k}_C)]
\end{aligned}$$

$$
\begin{aligned}
{}^{22}_{I_2}G'_{L_bJ_b}(\vec{x},\vec{x}',M_b) &= \frac{1}{2}[\phi^B_{3L_bJ_b}(-\vec{k}_C)\phi^{B*}_{3L_bJ_b}(-\vec{k}_C) + \phi^B_{4L_bJ_b}(-\vec{k}_C)\phi^{B*}_{4L_bJ_b}(-\vec{k}_C)] \\
{}^{22}_{\sigma_x}G'_{L_bJ_b}(\vec{x},\vec{x}',M_b) &= \frac{1}{2}[\phi^B_{3L_bJ_b}(-\vec{k}_C)\phi^{B*}_{4L_bJ_b}(-\vec{k}_C) + \phi^B_{4L_bJ_b}(-\vec{k}_C)\phi^{B*}_{3L_bJ_b}(-\vec{k}_C)] \\
{}^{22}_{\sigma_y}G'_{L_bJ_b}(\vec{x},\vec{x}',M_b) &= -\frac{i}{2}[\phi^B_{4L_bJ_b}(-\vec{k}_C)\phi^{B*}_{3L_bJ_b}(-\vec{k}_C) - \phi^B_{4L_bJ_b}(-\vec{k}_C)\phi^{B*}_{4L_bJ_b}(-\vec{k}_C)] \\
{}^{22}_{\sigma_z}G'_{L_bJ_b}(\vec{x},\vec{x}',M_b) &= \frac{1}{2}[\phi^B_{3L_bJ_b}(-\vec{k}_C)\phi^{B*}_{3L_bJ_b}(-\vec{k}_C) - \phi^B_{4L_bJ_b}(-\vec{k}_C)\phi^{B*}_{4L_bJ_b}(-\vec{k}_C)]. \quad (2.198)
\end{aligned}
$$

Similarly it can be shown that the $P_T^{\prime kl}$'s are explicitly given by

$$
\begin{aligned}
P^{\prime 11}_{I_2} &= \frac{K_2^0+1}{2} \\
P^{\prime 11}_{\sigma_x} &= 0 \\
P^{\prime 11}_{\sigma_y} &= 0 \\
P^{\prime 11}_{\sigma_z} &= 0 \\
P^{\prime 12}_{I_2} &= 0 \\
P^{\prime 12}_{\sigma_x} &= -\frac{K_2^i}{2} \\
P^{\prime 12}_{\sigma_y} &= -\frac{K_2^i}{2} \\
P^{\prime 12}_{\sigma_z} &= -\frac{K_2^i}{2} \\
P^{\prime 21}_{I_2} &= 0 \\
P^{\prime 21}_{\sigma_x} &= \frac{K_2^i}{2} \\
P^{\prime 21}_{\sigma_y} &= \frac{K_2^i}{2} \\
P^{\prime 21}_{\sigma_z} &= \frac{K_2^i}{2} \\
P^{\prime 22}_{I_2} &= \frac{-K_2^0+1}{2} \\
P^{\prime 22}_{\sigma_x} &= 0 \\
P^{\prime 22}_{\sigma_y} &= 0 \\
P^{\prime 22}_{\sigma_z} &= 0,
\end{aligned}
\quad (2.199)
$$

where $K_2^\mu = p_{b'}^\mu/m$. It can be shown that the 16×16 matrices represented by $\lambda_{\alpha\beta}$ are constructed

by taking Kronecker products of the matrices in the set $\{I_2, \sigma_x, \sigma_y, \sigma_z\}$ [Its80]. Hence

$$\lambda_{2j} = A^1_{2j} \otimes A^2_{2j}, \tag{2.200}$$

where A^1_{2j} and A^2_{2j} represents the two particular Pauli matrices which construct λ_{2j}. Similarly it follows that one can write

$$\bar{\lambda}_{2i} = B^1_{2i} \otimes B^2_{2i}. \tag{2.201}$$

Using Eqs. (2.200) and (2.201) in conjunction with the identity $(A \otimes B)(C \otimes D) = (AC \otimes BC)$ allows one to write the righthand side of Eq. (2.193) as

$$\begin{aligned} &\frac{1}{rr'} \sum_{r,s,k,l=1}^{2} \sum_{R,T=I_2}^{\sigma_z} G^{lrs}_R(\vec{x}, \vec{x}', M_b) P^{lkl'}_T(K_2)[(e^\dagger_r \otimes e_s) \otimes \Gamma_R](A^1_{2j} \otimes A^2_{2j})[(e^\dagger_k \otimes e_l) \otimes \Gamma_T](B^1_{2i} \otimes B^2_{2i}) \\ = &\frac{1}{rr'} \sum_{r,s,k,l=1}^{2} \sum_{R,T=I_2}^{\sigma_z} G^{lrs}_R(\vec{x}, \vec{x}', M_b) P^{lkl}_T(K_2)[(e^\dagger_r \otimes e_s) A^1_{2j} (e^\dagger_k \otimes e_l) B^1_{2i}] \otimes [\Gamma_R A^2_{2j} \Gamma_T B^2_{2i}]. \end{aligned} \tag{2.202}$$

The trace of Eq. (2.202) yields

$$\frac{1}{rr'} \sum_{r,s,k,l=1}^{2} \sum_{R,T=I_2}^{\sigma_z} G^{lrs}_R(\vec{x}, \vec{x}', M_b) P^{lkl}_T(K_2) Tr\Big[(e^\dagger_r \otimes e_s) A^1_{2j} (e^\dagger_k \otimes e_l) B^1_{2i}] \otimes [\Gamma_R A^2_{2j} \Gamma_T B^2_{2i}]\Big]. \tag{2.203}$$

Applying the trace identity $Tr(A \otimes B) = Tr(A)Tr(B)$ yields

$$\frac{1}{rr'} \sum_{r,s,k,l=1}^{2} \sum_{R,T=I_2}^{\sigma_z} G^{lrs}_R P^{lkl}_T Tr[(e^\dagger_r \otimes e_s) A^1_{2j} (e^\dagger_k \otimes e_l) B^1_{2i}] Tr[\Gamma_R A^2_{2j} \Gamma_T B^2_{2i}]. \tag{2.204}$$

With the identity $Tr[(u^\dagger \otimes v)X(x^\dagger \otimes y)Y] = (u^\dagger X y)(x^\dagger Y v)$ one arrives at the desired expression for the nuclear response, namely

$$H_{ji} = \frac{1}{rr'} \sum_{r,s,k,l=1}^{2} \sum_{R,T=I_2}^{\sigma_z} G^{lrs}_R P^{lkl}_T [(e^\dagger_r A^1_{2j} e_l)(e^\dagger_k B^1_{2i} e_s)] Tr[\Gamma_R A^2_{2j} \Gamma_T B^2_{2i}]. \tag{2.205}$$

2.9.4 The brute force method

The brute force method involves direct computation of $T_{L_b J_b}(\mu_a, \mu_{a'}, \mu_{b'}, M_b)$ as given by Eq. (2.119), namely

$$T_{L_b J_b}(\mu_a, \mu_{a'}, \mu_{b'}, M_b) = \sum_{i=S}^{T} F^i(q)[\bar{u}(\vec{k}_{a'}, \mu_{a'}) \lambda^i_1 u(\vec{k}_a, \mu_a)][u(\vec{k}_{b'}, \mu_{b'}) \lambda_{2i} \Phi_{L_b J_b M_b}(-\vec{k}_C)]. \tag{2.206}$$

The choice of spin polarizations of the scattered protons is selected in the two component Pauli spinors χ_s in the Dirac spinors given by Eq. (2.66). The orientation of spin polarization

is obtained by performing a Wigner transformation on χ_s. Assuming the x-z plane as the scattering plane and θ_k as the scattering angle of a particle with momentum $\vec{k}$, one can write $\vec{\sigma}\cdot\vec{k}$ in Eq. (2.66) as

$$\begin{aligned}\vec{\sigma}\cdot\vec{k} &= \sigma_x k_x + \sigma_y k_y + \sigma_z k_z \\ &= k\sin\theta_k\sigma_x + k\cos\theta_k\sigma_z \\ &= k\sin\theta_k\begin{pmatrix}0 & 1\\ 1 & 0\end{pmatrix} + k\cos\theta_k\begin{pmatrix}1 & 0\\ 0 & -1\end{pmatrix} \\ &= k\begin{bmatrix}\cos\theta_k & \sin\theta_k\\ \sin\theta_k & -\cos\theta_k\end{bmatrix}. \end{aligned} \tag{2.207}$$

Thus one can write Eq.(2.66) as

$$u(\vec{k},s) = N\begin{bmatrix}\begin{pmatrix}1 & 0\\ 0 & 1\end{pmatrix}\chi_s \\ \frac{k}{\epsilon+m}\begin{pmatrix}\cos\theta_k & \sin\theta_k\\ \sin\theta_k & -\cos\theta_k\end{pmatrix}\chi_s\end{bmatrix}. \tag{2.208}$$

We expand the polarized 2 component spin vectors in terms of the base vectors $\chi_\uparrow = \binom{1}{0}$ and $\chi_\downarrow = \binom{0}{1}$ such that

$$\begin{aligned}\chi_s &= a\chi_\uparrow + b\chi_\downarrow \\ &= \begin{pmatrix}a\\ b\end{pmatrix}. \end{aligned} \tag{2.209}$$

Hence

$$u(\vec{k},s) = N\begin{bmatrix}a\\ b\\ \frac{k}{\epsilon+m}(a\cos\theta_k + b\sin\theta_k)\\ \frac{k}{\epsilon+m}(a\sin\theta_k - b\cos\theta_k)\end{bmatrix}. \tag{2.210}$$

We now have to find the coefficients a and b associated with the polarization directions $\hat{l}$, $\hat{s}$ and $\hat{n}$. For a particle scattered in the x-z plane with scattering angle θ_k relative to the z-axis we have

- for the polarization direction $\hat{l}(\uparrow)$, we rotate the spin basis $\chi_\uparrow$ with θ_k around the y-axis,

- for the polarization direction $\hat{l}(\downarrow)$, we rotate the spin basis $\chi_{\downarrow}$ with θ_k around the y-axis,
- for the polarization direction $\hat{s}(\uparrow)$, we rotate the spin basis $\chi_{\uparrow}$ with $\theta_k + \frac{\pi}{2}$ around the y-axis,
- for the polarization direction $\hat{s}(\downarrow)$, we rotate the spin basis $\chi_{\downarrow}$ with $\theta_k + \frac{\pi}{2}$ around the y-axis,
- for the polarization direction $\hat{n}(\uparrow)$, we rotate the spin basis $\chi_{\uparrow}$ with $\frac{\pi}{2}$ around the y-axis,
- for the polarization direction $\hat{n}(\downarrow)$, we rotate the spin basis $\chi_{\downarrow}$ with $\frac{\pi}{2}$ around the y-axis.

The Euler angles associated with the rotations mentioned above are

$$\text{for } \hat{l}, \quad \alpha = 0 \qquad \beta = \theta_k, \qquad \gamma = 0$$

$$\text{for } \hat{s}, \quad \alpha = 0 \quad \beta = \theta_k + \tfrac{\pi}{2}, \quad \gamma = 0$$

$$\text{for } \hat{n}, \quad \alpha = \tfrac{\pi}{2} \qquad \beta = \tfrac{\pi}{2}, \qquad \gamma = 0.$$

Using the Wigner rotation function represented by the 2×2 matrix [Sak85]

$$\begin{bmatrix} e^{-i(\alpha+\gamma)/2}\cos(\beta/2) & -e^{-i(\alpha-\gamma)/2}\sin(\beta/2) \\ e^{i(\alpha-\gamma)/2}\sin(\beta/2) & e^{i(\alpha+\gamma)/2}\cos(\beta/2) \end{bmatrix}, \tag{2.211}$$

where the angles α, β and γ represent the Euler angles associated with rotations around the z-,y, and x-axes respectively, the rotation matrices used to find the two component spins $\binom{a}{b}$ associated with the polarization directions $\hat{l}$, $\hat{s}$ and $\hat{n}$ are

$$\begin{bmatrix} \cos\frac{\theta_k}{2} & -\sin\frac{\theta_k}{2} \\ \sin\frac{\theta_k}{2} & \cos\frac{\theta_k}{2} \end{bmatrix} \quad \text{for } \hat{l}$$

$$\begin{bmatrix} \frac{1}{\sqrt{2}}(\cos\frac{\theta_k}{2} - \sin\frac{\theta_k}{2}) & \frac{1}{\sqrt{2}}(\sin\frac{\theta_k}{2} + \cos\frac{\theta_k}{2} \\ \frac{1}{\sqrt{2}}(\sin\frac{\theta_k}{2} + \cos\frac{\theta_k}{2}) & \frac{1}{\sqrt{2}}(\cos\frac{\theta_k}{2} - \sin\frac{\theta_k}{2}) \end{bmatrix} \quad \text{for } \hat{s}$$

$$\begin{bmatrix} \frac{1-i}{2} & -\frac{1-i}{2} \\ \frac{1+i}{2} & \frac{1+i}{2} \end{bmatrix} \quad \text{for } \hat{n}.$$

The 2 component spin vectors $\binom{a}{b}$ are obtained by letting the rotation matrices operate on the basis vectors $\chi_\uparrow$ or $\chi_\downarrow$ to give

$$\begin{bmatrix} \cos\frac{\theta_k}{2} & \cos\frac{\theta_k}{2} \\ \sin\frac{\theta_k}{2} & \sin\frac{\theta_k}{2} \end{bmatrix} \begin{pmatrix} 1 \\ 0 \end{pmatrix} = \begin{pmatrix} \cos\frac{\theta_k}{2} \\ \sin\frac{\theta_k}{2} \end{pmatrix} \quad \text{for } \hat{l}(\uparrow)$$

$$\begin{bmatrix} \cos\frac{\theta_k}{2} & -\sin\frac{\theta_k}{2} \\ \sin\frac{\theta_k}{2} & \cos\frac{\theta_k}{2} \end{bmatrix} \begin{pmatrix} 0 \\ 1 \end{pmatrix} = \begin{pmatrix} -\sin\frac{\theta_k}{2} \\ \cos\frac{\theta_k}{2} \end{pmatrix} \quad \text{for } \hat{l}(\downarrow)$$

$$\begin{bmatrix} \frac{1}{\sqrt{2}}(\cos\frac{\theta_k}{2} - \sin\frac{\theta_k}{2}) & \frac{1}{\sqrt{2}}(\sin\frac{\theta_k}{2} + \cos\frac{\theta_k}{2} \\ \frac{1}{\sqrt{2}}(\sin\frac{\theta_k}{2} + \cos\frac{\theta_k}{2}) & \frac{1}{\sqrt{2}}(\cos\frac{\theta_k}{2} - \sin\frac{\theta_k}{2}) \end{bmatrix} \begin{pmatrix} 1 \\ 0 \end{pmatrix} = \begin{pmatrix} \frac{1}{\sqrt{2}}(\cos\frac{\theta_k}{2} - \sin\frac{\theta_k}{2}) \\ \frac{1}{\sqrt{2}}(\sin\frac{\theta_k}{2} + \cos\frac{\theta_k}{2}) \end{pmatrix} \quad \text{for } \hat{s}(\uparrow)$$

$$\begin{bmatrix} \frac{1}{\sqrt{2}}(\cos\frac{\theta_k}{2} - \sin\frac{\theta_k}{2}) & \frac{1}{\sqrt{2}}(\sin\frac{\theta_k}{2} + \cos\frac{\theta_k}{2} \\ \frac{1}{\sqrt{2}}(\sin\frac{\theta_k}{2} + \cos\frac{\theta_k}{2}) & \frac{1}{\sqrt{2}}(\cos\frac{\theta_k}{2} - \sin\frac{\theta_k}{2}) \end{bmatrix} \begin{pmatrix} 0 \\ 1 \end{pmatrix} = \begin{pmatrix} -\frac{1}{\sqrt{2}}(\sin\frac{\theta_k}{2} + \cos\frac{\theta_k}{2}) \\ \frac{1}{\sqrt{2}}(\cos\frac{\theta_k}{2} - \sin\frac{\theta_k}{2}) \end{pmatrix} \quad \text{for } \hat{s}(\downarrow)$$

$$\begin{bmatrix} \frac{1-i}{2} & -\frac{1-i}{2} \\ \frac{1+i}{2} & \frac{1+i}{2} \end{bmatrix} \begin{pmatrix} 1 \\ 0 \end{pmatrix} = \begin{pmatrix} \frac{1-i}{2} \\ \frac{1+i}{2} \end{pmatrix} \quad \text{for } \hat{n}(\uparrow)$$

$$\begin{bmatrix} \frac{1-i}{2} & -\frac{1-i}{2} \\ \frac{1+i}{2} & \frac{1+i}{2} \end{bmatrix} \begin{pmatrix} 0 \\ 1 \end{pmatrix} = \begin{pmatrix} -\frac{1-i}{2} \\ \frac{1+i}{2} \end{pmatrix} \quad \text{for } \hat{n}(\downarrow).$$

The desired form for the transition amplitude is obtained by calculating

$$|T_{L_bJ_b}(\mu_a, \mu_{a'}, \mu_{b'}, M_b)|^2 = T_{L_bJ_b}(\mu_a, \mu_{a'}, \mu_{b'}, M_b)T^*_{L_bJ_b}(\mu_a, \mu_{a'}, \mu_{b'}, M_b). \quad (2.212)$$

and summing over the unpolarized protons to obtain $\sum_{\mu_{b'}M_b} |T_{L_bJ_b}(\mu_a, \mu_{a'}, \mu_b, M_b)|^2$ which is substituted into Eq. (2.4) to calculate the polarized triple differential cross sections.

2.10 Synopsis of theoretical formulation

In this chapter we have presented the relativistic plane wave impulse approximation model for calculating complete sets of $(p, 2p)$ spin transfer observable. A short review of the $(p, 2p)$ reaction mechanism was given. Next we defined the transition amplitude in terms of the scattered particle wave functions, the nucleon-nucleon t-matrix and a boundstate wave function. Expressions of the unpolarized triple differential cross section and spin transfer observables for the $(p, 2p)$ reaction were given. This is followed by the $(p, 2p)$ kinematics which is used to calculate the wave functions for the scattered protons and the NN interaction. Furthermore Dirac plane wave functions were used for the scattered particle wave functions. Radial boundstate wave functions were generated with the self consistent Dirac-Hartree approximation. The relativistic Love-Franey model, based on the IA1 representation, was used to obtain Lorentz invariant NN amplitudes. We have also included Maxwell's energy dependent parameterization to obtain the meson coupling constants and cutoff parameters for the RLF model. In addition to this, medium effects were introduced through the Brown-Rho scaling law. We have also looked at pseudoscalar and pseudovector couplings for the πNN vertex. Radial boundstate wave functions were generated with the self consistent Dirac-Hartree approximation. Thus we have developed a new method for evaluating the modulus-square of the transition amplitude directly. Finally we have reduced the modulus-square of the transition amplitude to the product of two traces. This procedure allowed us to separate the information about the polarized proton beams and struck protons. Using the properties of the energy-momentum projection operator and spin projection operator, we could replace the projectiles wave function and scattered wave functions with terms containing four-momentum and spin vectors. Further simplification was introduced by writing the five covariant matrices $(I_4, \gamma_\mu, \gamma_5, \gamma_5\gamma_\mu, \sigma_{\mu\nu})$ in their Pauli form.

Clearly some refinements to our model are needed. In future models we will include nuclear

distortion effects and a more general IA2 representation of the NN interaction.

In the next chapter numerical results for complete sets of $(p, 2p)$ spin transfer observables will be shown based on the formalism developed in this chapter. We will also discuss numerical checks which we have performed on our code.

Chapter 3

Numerical analysis

3.1 Introduction

In this chapter we will present numerical results of unpolarized triple differential cross sections and complete sets of spin transfer observables which have been obtained with our relativistic plane wave code. Calculations are based on the trace method, previously discussed in Chapter 2. In addition results of various numerical checks of the accuracy of our code are provided. The choice of kinematic conditions for which calculations are performed is based on a $(p, 2p)$ experiment underway at RCNP (Osaka, Japan) [Nor99] in which unpolarized triple differential cross sections and analyzing powers on ^{40}Ca at 392 MeV were measured. However, since the analysis of this experiment has not been completed yet, it will not be possible to compare our results to data. Nevertheless, we will compare results obtained with our newly developed trace technique to that of the traditional "brute force" method which is discussed in section (2.9.4) at an incident energy of 400 MeV on ^{40}Ca. We compare results of $(p, 2p)$ scattering observables based on both the initial and final energy prescriptions, which were discussed in section (2.4.2), to see whether any differences in these prescriptions for the nucleon-nucleon kinematics are reflected in any of the observables. Medium modifications to the NN-interaction and the incident and scattered wave functions based on the Brown-Rho scaling law [Bro91] have been included in our calculations as described in section (2.8). In this way a systematic study showing the contributions of various medium modifications to the calculated scattering observables is presented. The results of the medium-modified observables are then also compared to results calculated with free quantities. These calculations include both pseudoscalar and pseudovector coupling to investigate the ambiguities surrounding the medium effects on the πNN vertex.

3.2 Numerical checks

We now discuss the numerical checks performed on our computer code to the theoretical formulation. To ensure that the algorithm for the scattering observables is programmed correctly, we calculate the free nucleon-nucleon differential cross section and spin observables by replacing the boundstate wave function and momenta in Eq. (2.122) with a relativistic plane wave function and NN center-of-mass momenta respectively. The NN scattering amplitudes are obtained with the relativistic Love-Franey model [Hor85]. Our results are compared to spin observables calculated directly from Arndt phases [Arn86]. Due to differences in the choice of directions for the $(p, 2p)$ and NN spin polarization vectors $\hat{l}$, $\hat{l}'$, $\hat{s}$ and $\hat{s}'$, only the triple differential cross section, analyzing power (A_y) and D_{nn} are compared. Results of our calculations for an incident energy of 400 MeV are shown in fig. (3.1). Good agreement between our calculations and the experimental observables are obtained, hence we are confident that our formulation for calculating these spin observables is programmed correctly.

We use a Gauss-Kronrod integration [Num92] method to perform the integration over the upper and lower radial boundstate wave functions. The integration limit on the radial boundstate wave function is obtained by plotting both the upper and lower radial boundstate wave functions as a function of the distance between the bound nucleon and the center of mass of the residual nucleus for the knockout states $1d_{\frac{5}{2}}$, $1d_{\frac{3}{2}}$ and $2s_{\frac{1}{2}}$ respectively. From fig. (3.2) one can see that all radial wave functions are negligible beyond 20 fm. We take the upper integration limit to be 30 fm. We have also checked that the radial wave functions successfully satisfy the normalization condition given by Eq. (2.75)

3.3 Calculations of $(p, 2p)$scattering observables

In this section we will show results of calculations of unpolarized $(p, 2p)$ triple differential cross sections and complete sets of spin transfer observables which are derived from Eqs. (2.2), (2.8) and (2.9). The NN scattering amplitude is calculated with the relativistic Love-Franey code of Horowitz [Lan91]. We use the code TIMORA [Lan91] to calculate the radial boundstate wave functions. Calculations are done for a ^{40}Ca target nucleus, with projectile energy of 400 MeV, scattering angles of $32.5°$ and $-50.0°$, and knockout of protons from $1d_{\frac{3}{2}}$ and $2s_{\frac{1}{2}}$ shell model

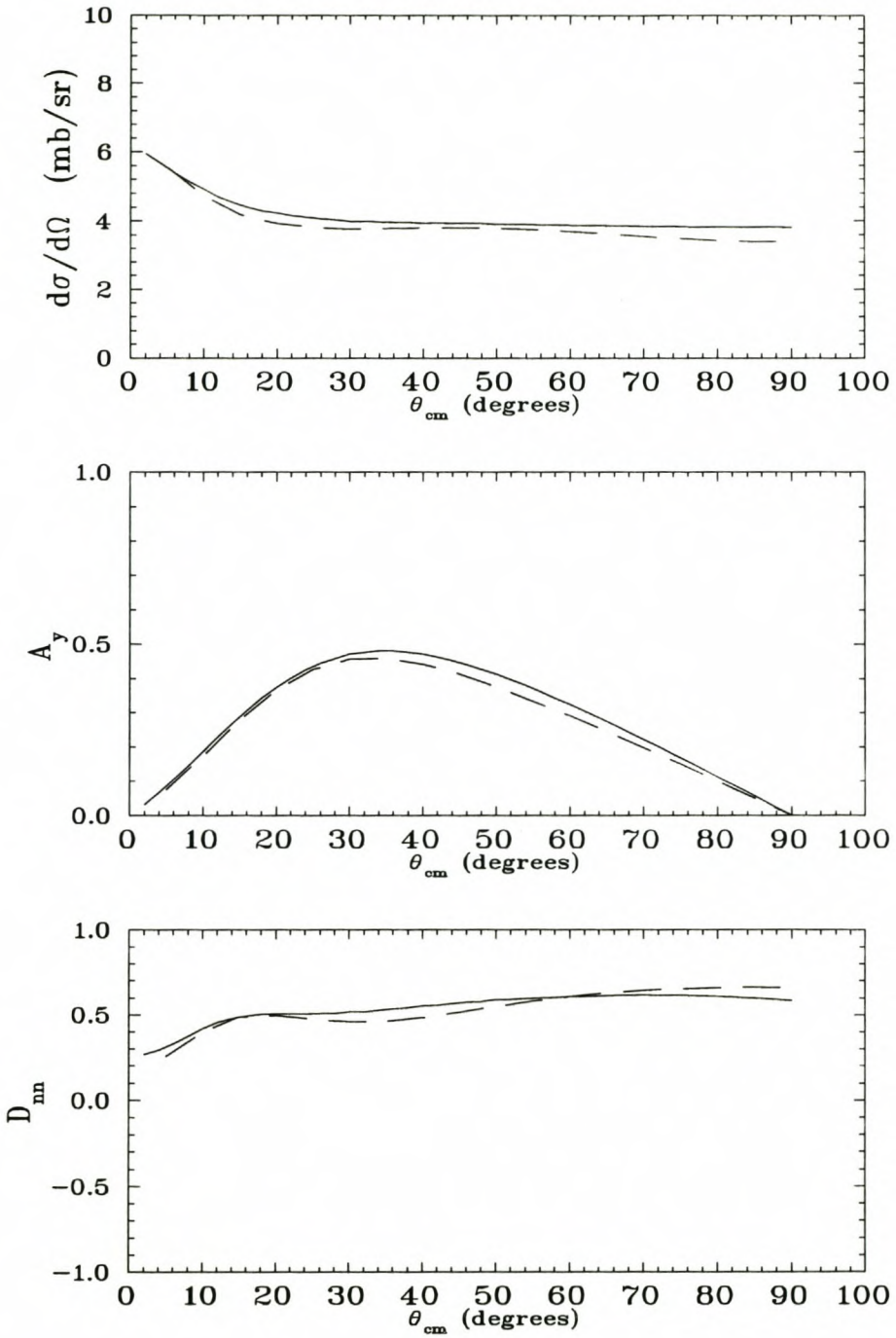

Figure 3.1: Comparisons between the experimental and calculated free NN cross section and spin observables at an incident laboratory energy of 400 MeV, plotted as a function of the center-of-mass scattering angle θ_{cm}. The solid line shows observables calculated from pp Arndt amplitudes while the dashed line shows our calculation values.

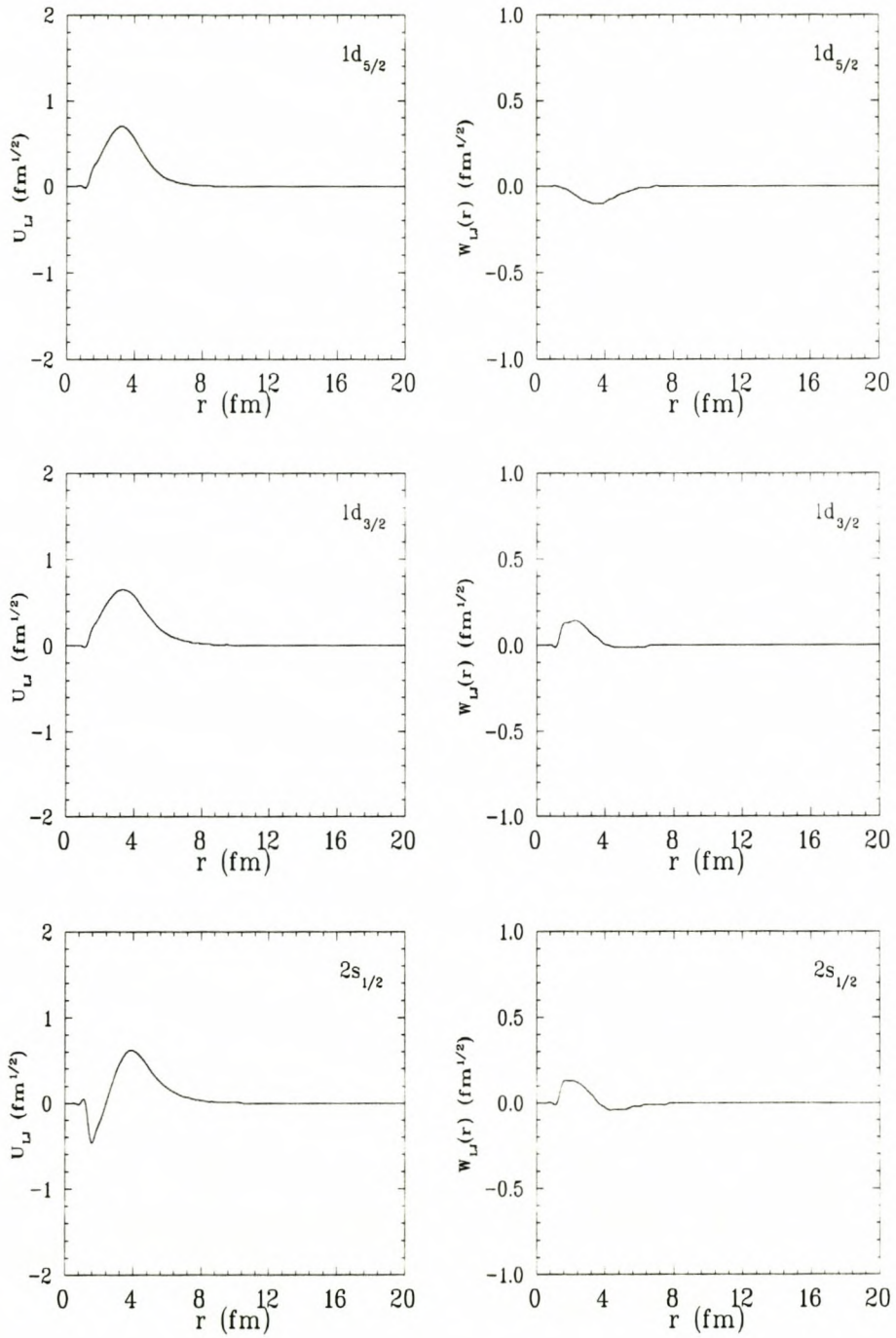

Figure 3.2: The figures on the right and left show the upper (u_{LJ}) and lower (w_{LJ}) radial wave functions as function of the separation distance between the residual nucleus and the bound proton respectively for the $1d_{\frac{5}{2}}$, $1d_{\frac{3}{2}}$ and $2s_{\frac{1}{2}}$.

orbitals. As was mentioned before, these kinematic conditions are dictated by an experiment which is underway at RCNP [Nor99]. In addition we also include calculations for the $1d_{\frac{5}{2}}$ state with the same kinematic constraints as for the $1d_{\frac{3}{2}}$ and $2s_{\frac{1}{2}}$ states. In the following sections we will show comparisons between calculations based on our trace technique and the brute force method. We will also investigate nuclear medium effects on the scattered particles and the NN-interaction based on the Brown-Rho scaling relations [Bro91]: see section (2.8). Various contribution to the medium effects will be examined.

3.3.1 Brute force versus trace technique

Calculations of the unpolarized triple differential cross section and spin transfer observables are presented which show comparisons between results obtained with the trace method to that of the brute force approach. The trace method has the advantage that it allows one to evaluate the modulus-squared of the transition amplitude directly, which is used in calculating the scattering observables, directly whereas this is not the case when using the brute force method. These two methods are formulated in sections (2.9.1) and (2.9.4). The projectile kinetic energy is 400 MeV and the scattering angles of 32.5° and -50.0° are used for the calculations. A free nucleon-nucleon interaction is taken in both cases, i.e. medium effects are excluded. In fig. (3.3) we compare triple differential cross sections calculated with the brute force and trace method for the $1d\frac{5}{2}$, $1d_{\frac{3}{2}}$ and $2s_{\frac{1}{2}}$ states. In figs. (3.4) to (3.6) we show comparisons between the two methods for polarization transfer observables for the various knockout states. The methods are in prefect agreement with each other and hence we cannot distinguish between the curves shown in fig. (3.3).

3.3.2 Initial versus final energy prescription

The plots in figs. (3.7) to (3.10) show comparisons between results of calculated unpolarized triple differential cross sections and spin transfer observables obtained with both initial and final energy prescriptions. All quantities are plotted as a function of the kinetic energy of the proton scattered towards the smaller angle (32.5°). We use Eqs. (2.47) and (2.49) to calculate the effective NN laboratory energy with the initial or final energy prescription respectively. Again the calculations are done for knockout from the $1d_{\frac{5}{2}}$, $1d_{\frac{3}{2}}$ and $2s_{\frac{1}{2}}$ states. The unpolarized triple

differential cross sections predicted with the initial energy prescription are strongly reduced relative to those predicted by the final energy prescription. However, both predictions give the same shape for the cross sections. We see the same trends for all three knockout states. On the other hand, the values of the final and initial energy predictions for spin observables are very close. We nevertheless see a small reduction in the prediction of $D_{s'l}$ for all three states for the final energy prescription compared to the initial energy prescription. The analyzing power predicted by the initial energy prescription is observed to be higher than the values obtained with the final energy prescription for knockout from the $1d_{\frac{5}{2}}$ and $2s_{\frac{1}{2}}$, but there is no apparent trend of the results in general.

3.3.3 Medium effects

In this section we investigate nuclear medium effects on unpolarized triple differential cross sections and spin transfer observables. Medium modifications are included to the projectile and the scattered wave functions as well as the NN-interaction. We use the Brown-Rho scaling law [Bro91], which is discussed in section (2.8) with optimum scaling parameters of $\xi = 0.7$ and $\chi = 0.75$ for the proton mass, meson mass, and coupling constants; as shown by Krein et. al. [Kre95]. In order to get insight into the sensitivity of the various scattering observables to the different medium modified parameters we systematically replaced the free parameters with the medium modified parameters. We will use the symbols M_p, m_{meson} and g_{meson} to represent the free proton mass, σ, ρ and ω meson masses and meson coupling constants respectively and M_p^*, m_{meson}^* and g_{meson}^* to represent the medium modified quantities. Pseudoscalar and pseudovector coupling are included to investigate medium effects on the πNN vertex as discussed in section (2.8.1). All results are calculated with the trace method. As before the reaction considered involves an incident energy of 400 MeV and scattering angles of 32.5° and -50.0° on a target of ^{40}Ca. Knockout from the $1d_{\frac{5}{2}}$, $1d_{\frac{3}{2}}$ and $2s_{\frac{1}{2}}$ states are considered. All observables are plotted as a function of the left-scattered (small angle) proton kinetic energy. For comparisons of the unpolarized triple differential cross sections we take the spectroscopic factor $S_{L_bJ_b}$ to be unity: see Eq. (2.2).

In addition to the spin transfer observables we have also calculated free and medium modified unpolarized triple differential cross sections for all states. In figs. (3.11) to (3.13) we

compare results of unpolarized triple differential cross sections calculated with various medium modified terms and a pseudoscalar πNN coupling to corresponding calculations with free parameters. Furthermore our results of spin transfer observables which were calculated with the same type of medium-modifications are compared to calculations performed with free parameters are shown in figs. (3.14) to (3.28). Similar calculations have been performed with a pseudovector πNN coupling and the results are shown in figs. (3.29) to (3.46).

In the following section we will compare the results obtained with the pseudoscalar and pseudovector πNN coupling.

3.3.4 Pseudoscalar versus pseudovector coupling

We will now give some general trends observed in the results shown in the previous section for calculation of complete sets of $(p, 2p)$ scattering observables with medium effect included. Referring to figs. (3.11) to (3.13) and figs. (3.29) to (3.31) we see that with pseudoscalar and pseudovector coupling the calculated cross sections with and without medium effect are similar in shape for all knockout states. Both pseudoscalar and pseudovector calculations of the unpolarized triple differential differential cross sections with medium modifications on the meson mass increase dramatically relative to the free values. We see that for pseudoscalar coupling with medium effects on the meson masses and coupling constants the results of the scattering observables are almost the same as when we only include medium effects on the coupling constants. This trend is seen in the results of pseudovector coupling as well. We attribute this to the high momentum transfer involved in the reaction which dominates over the meson masses in the NN form factor given by Eq. (2.97). Its also observed that only m^*_{meson} and g^*_{meson} dramatically change the scattering observables when compared to the free calculations. Medium effects on the proton masses only shift the curves to a lower energy. This observation is seen for both pseudoscalar and pseudovector coupling.

In reference to figs. (3.14) to (3.28) and (3.32) to (3.46) we see that the spin transfer observables calculated with pseudoscalar and pseudovector coupling and the various medium effects included generally seem to have the same form as the free predictions. This appears to be the trend for all knockout states. The analyzing power calculated with pseudoscalar coupling

and the inclusion of various medium effects deviates slightly from the free values. If we however use a pseudovector coupling the medium modified results for the analyzing power are virtually the same as the free predictions. If we take all medium-modified quantities into account then we observe a strong reduction in D_{nn} and $D_{s's}$ relative to the free predictions. We see the same result if we use medium-modified meson masses and coupling constants or only medium-modified coupling constants. This observation holds for pseudoscalar and pseudovector coupling. In general the medium-modified spin observables calculated with pseudovector coupling included tend to be closer to the free values than is the case for pseudoscalar πNN coupling.

3.4 Synopsis of the numerical analysis

In this chapter we presented results of calculated $(p, 2p)$ triple differential cross sections and complete sets of spin transfer observables. Calculations were performed for incident energy of 400 MeV with scattering angles $32.5°$ and $-50, 0°$ on a target of ^{40}Ca, and knock out states $1d_{\frac{5}{2}}$, $1d_{\frac{3}{2}}$ and $2s_{\frac{1}{2}}$ respectively. We discussed results of various checks performed on our code. We compared results of scattering observables obtained with the trace method to those calculated with the brute force approach. A systematic study of nuclear medium modifications on the proton mass, σ, ρ and ω meson masses on $(p, 2p)$ scattering observables was made. Pseudoscalar and pseudovector coupling of the πNN vertex have been included in the calculations and the results which include the different contributions of the various medium effects were compared.

We showed that identical results are obtained for calculations of spin observables based on both the the brute force method and the trace method. This inspires confidence that our trace method, which is a more transparent and elegant formalism, is accurate. We also observe very little differences between the results predicted with the initial energy prescription and the final energy prescription (apart for the cross sections). With the inclusion of a pseudoscalar coupling we see some significant differences between the medium modified and free predictions of the scattering observables. With pseudovector coupling we see that the trends in the shape of the medium modified scattering observables are quite similar to those seen with pseudoscalar coupling. We however see that with pseudovector coupling the analyzing power is virtually the same as the free values. Pseudovector coupling also seems to bring most of the spin observables closer to the free predictions. This is due to cancelations of the scaling factors for the

medium-modified meson masses and πNN coupling constants which appear in the Eq. (2.97). Unpolarized triple differential cross sections calculated with a pseudovector coupling appear to be reduced relative to the pseudoscalar predictions. For a complete experimental study of nuclear medium effects one should consider all possible spin observables, as this study shows that spin transfer observables, other than the analyzing power, are quite sensitive to the introduction of different medium effects.

Some refinements to the present model are clearly required. For example nuclear distortions on the projectile and scattered protons need to be included for calculations at the lower energy regime where distortion effects become important. There is also still a big uncertainty as to which momentum transfer to use for the NN-interaction [Cha98, Man00]. Finally the simplistic IA1 form of the NN t-matrix needs to be replaced by the more general IA2 representation [Ven99].

The model presented in this thesis is useful for the experimental $(p, 2p)$ program at RCNP where data are currently being collected at an energy region which is high enough for one to ignore the effects of nuclear distortions on the projectile and scattered protons. Future comparisons with data could give guidelines as to the choice between pseudoscalar and pseudovector for the πNN coupling.

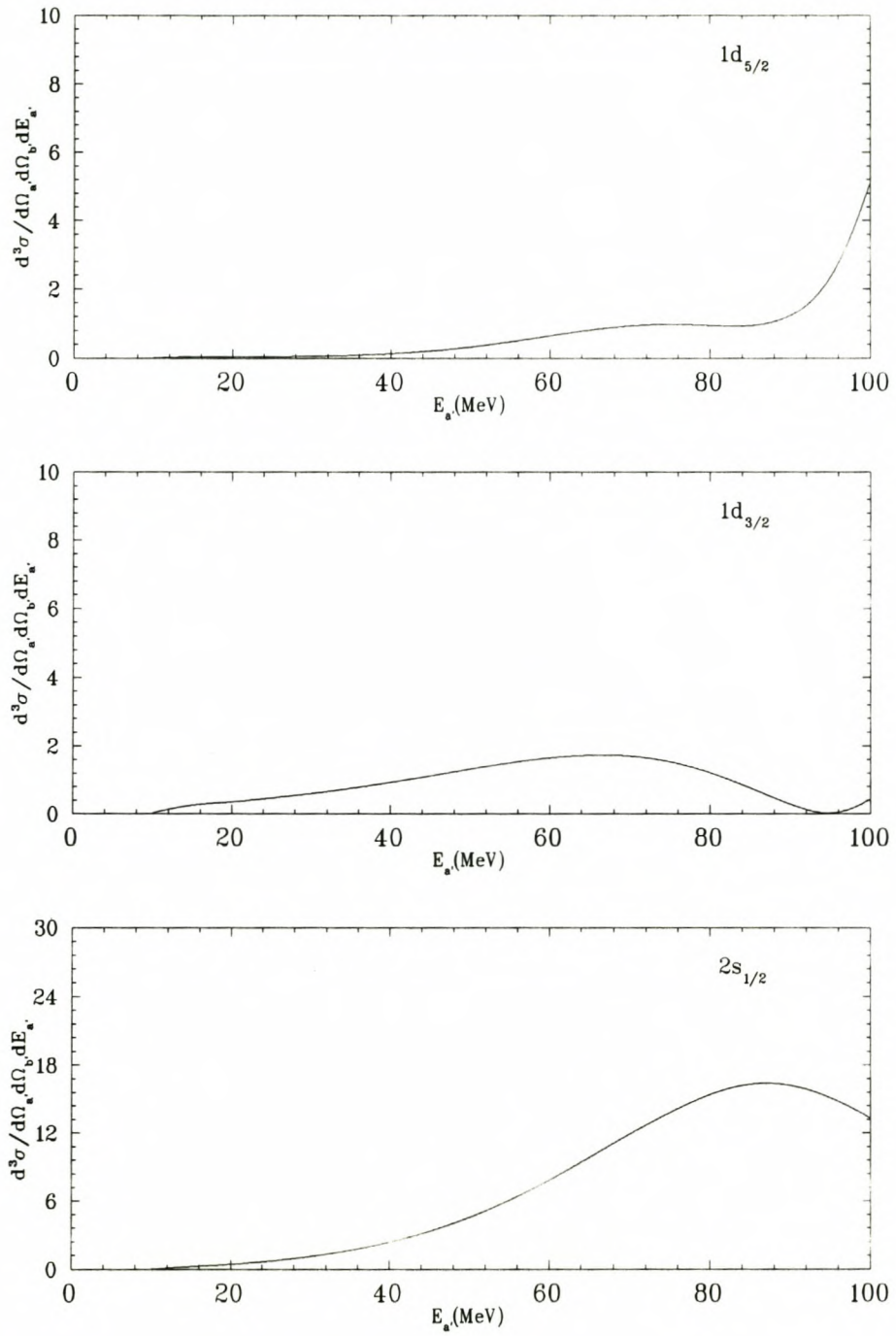

Figure 3.3: Plots comparing the calculated unpolarized triple differential cross sections for the $1d_{\frac{5}{2}}$, $1d_{\frac{3}{2}}$ and $2s_{\frac{1}{2}}$ states based on the brute force and trace methods. The results obtained with both brute force and trace method are exactly the same (solid line). Triple differential cross sections are in units of $\mu b/sr^2 MeV$.

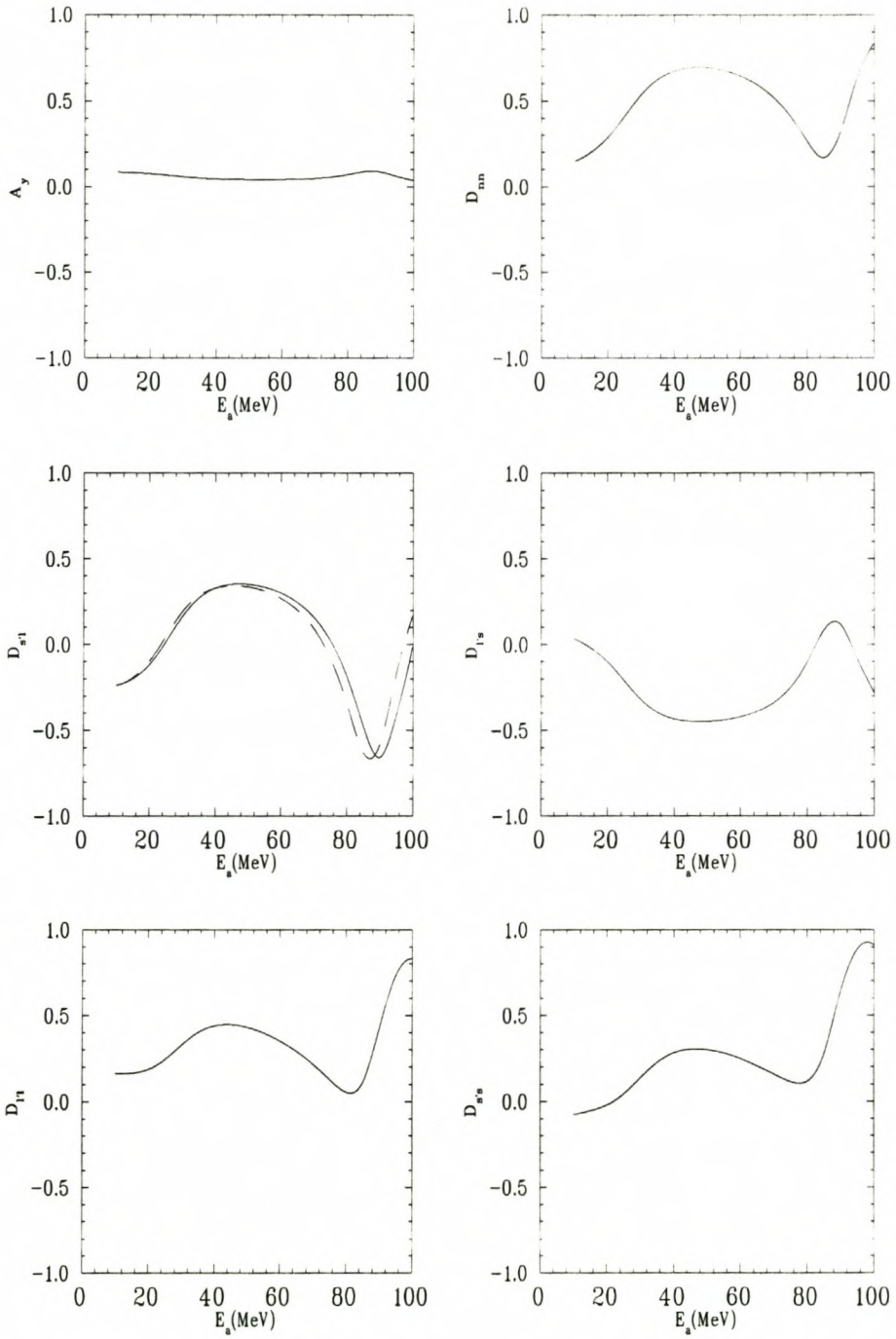

Figure 3.4: Plots comparing complete sets of $(p, 2p)$ spin transfer observables for the $1d_{\frac{5}{2}}$ state based on the brute force (solid line) and trace methods (dashed line).

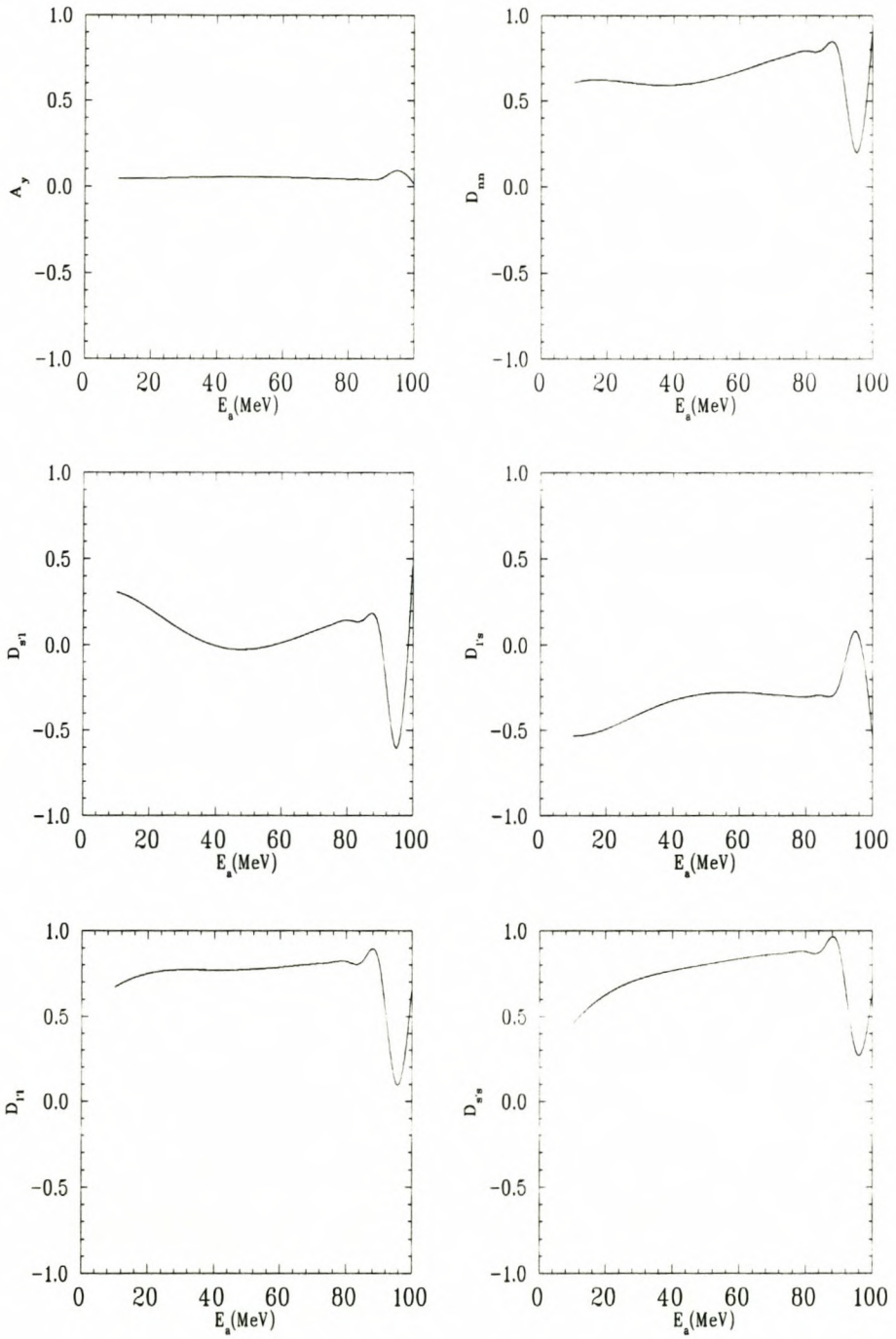

Figure 3.5: Plots comparing complete sets of $(p, 2p)$ spin transfer observables for the $1d_{\frac{3}{2}}$ state based on the brute force and trace methods. The results of both the brute force and trace method are exactly the same (solid line).

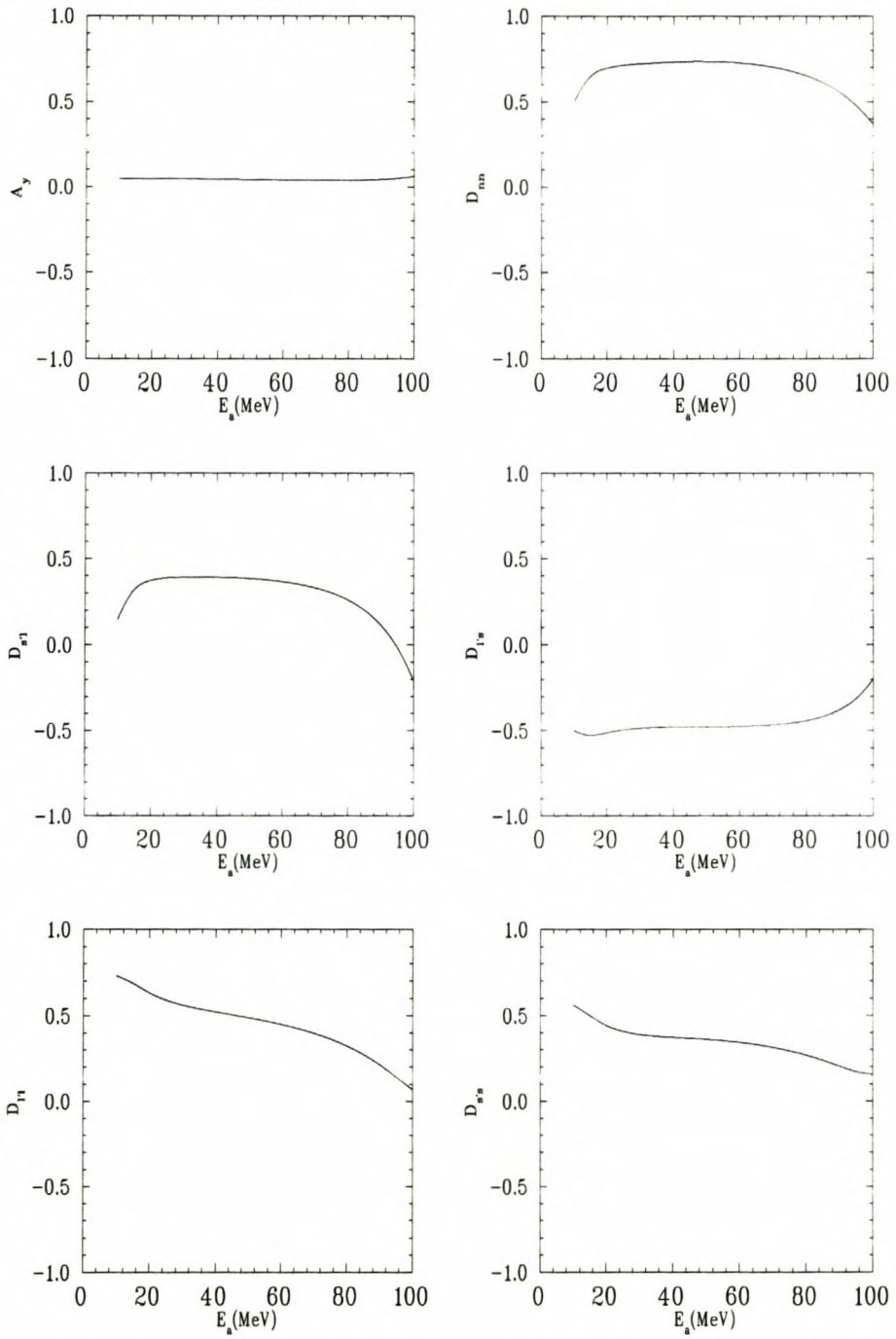

Figure 3.6: Plots comparing complete sets of $(p, 2p)$ spin transfer observables for the $2s_{\frac{1}{2}}$ state based on the brute force and trace methods. The results obtained with both the brute force and trace method are exactly the same (solid line).

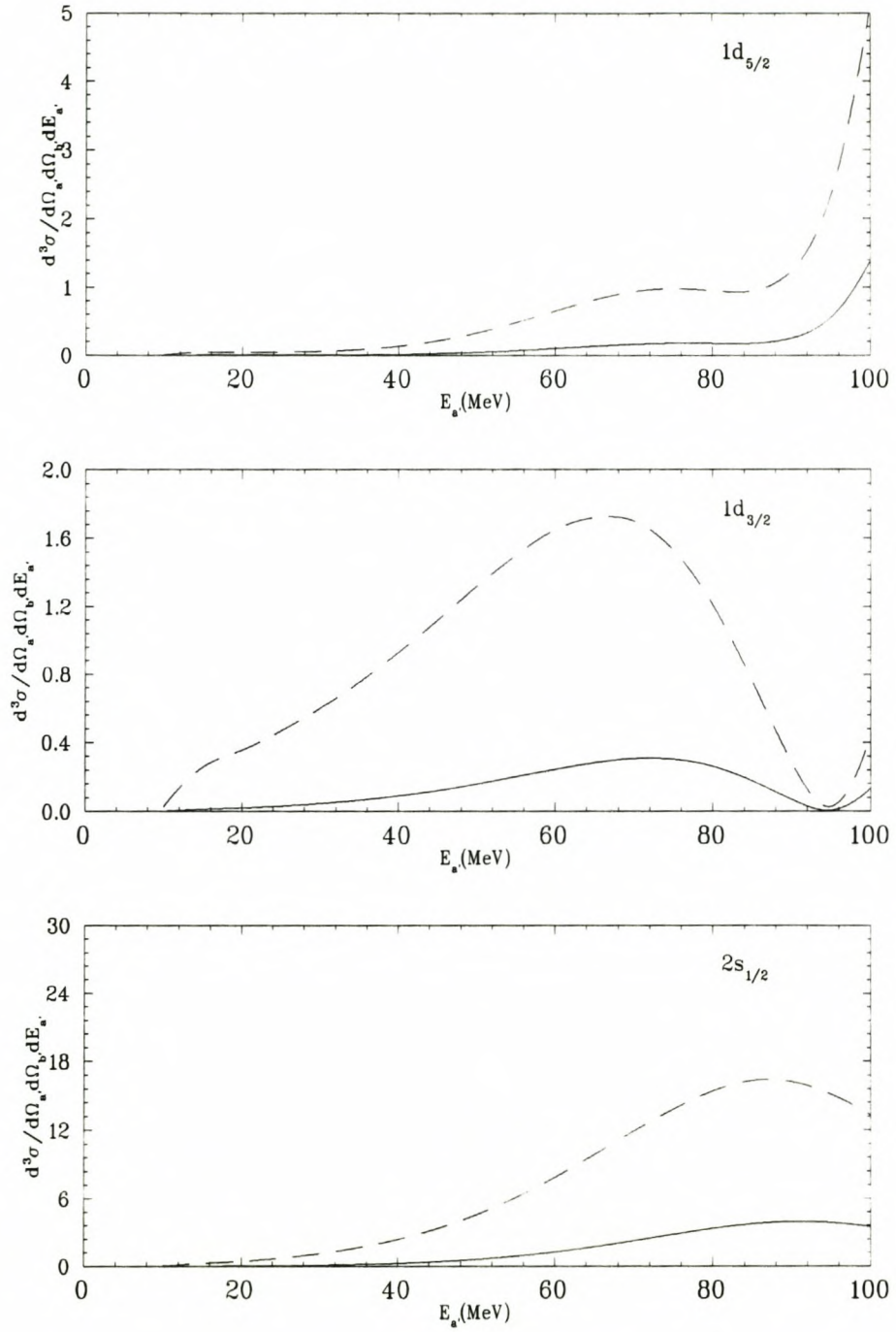

Figure 3.7: Plots comparing the calculated unpolarized triple differential cross sections for the $1d_{\frac{5}{2}}$, $1d_{\frac{3}{2}}$ and $2s_{\frac{1}{2}}$ states based on the initial and final energy prescriptions. The solid line represents the results obtained with the initial energy prescription while the dashed line shows the results of the final state energy prescription.

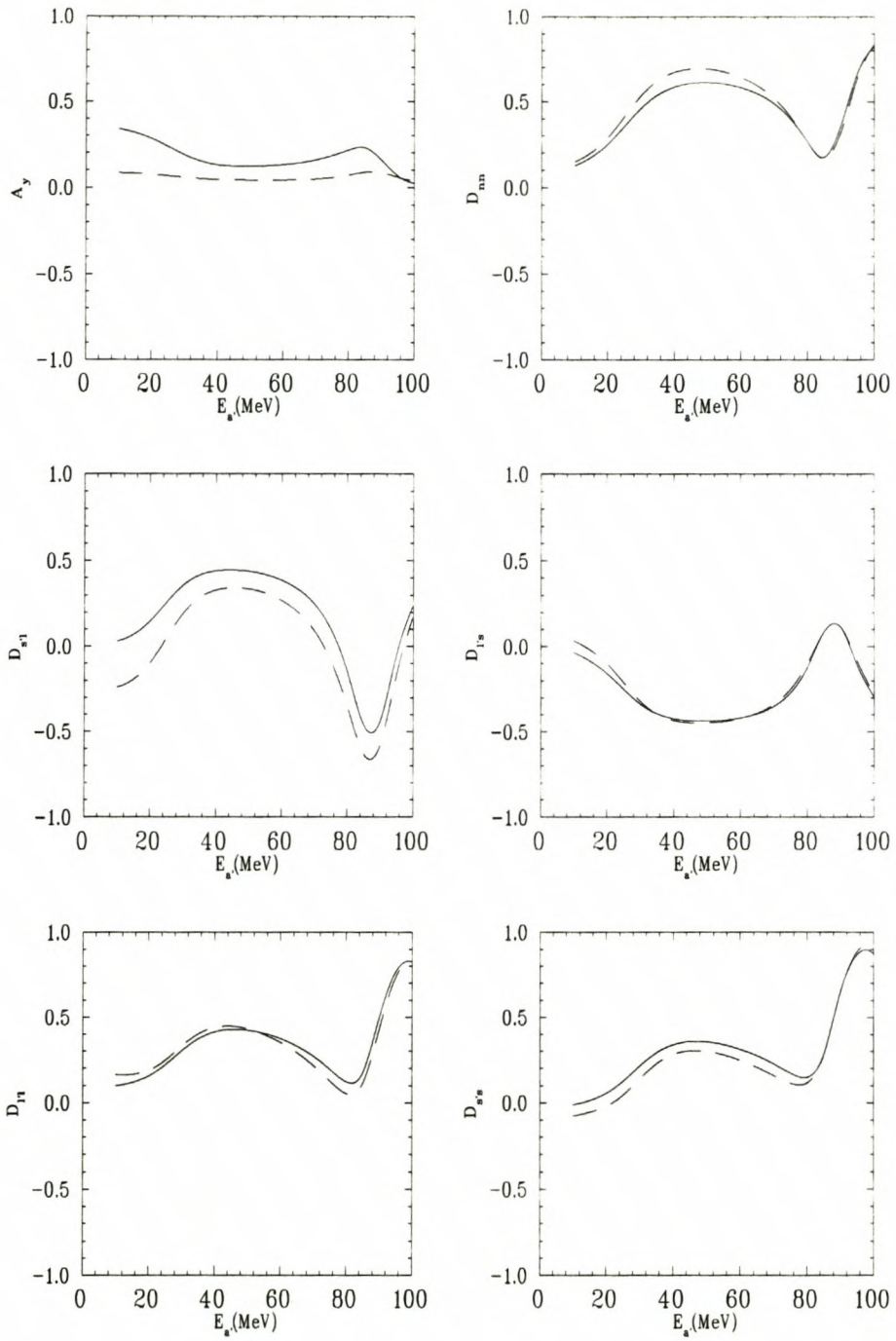

Figure 3.8: Plots comparing complete sets of $(p, 2p)$ spin transfer observables for the $1d_{\frac{5}{2}}$ state based on the initial (solid line) and final energy prescriptions (dashed line).

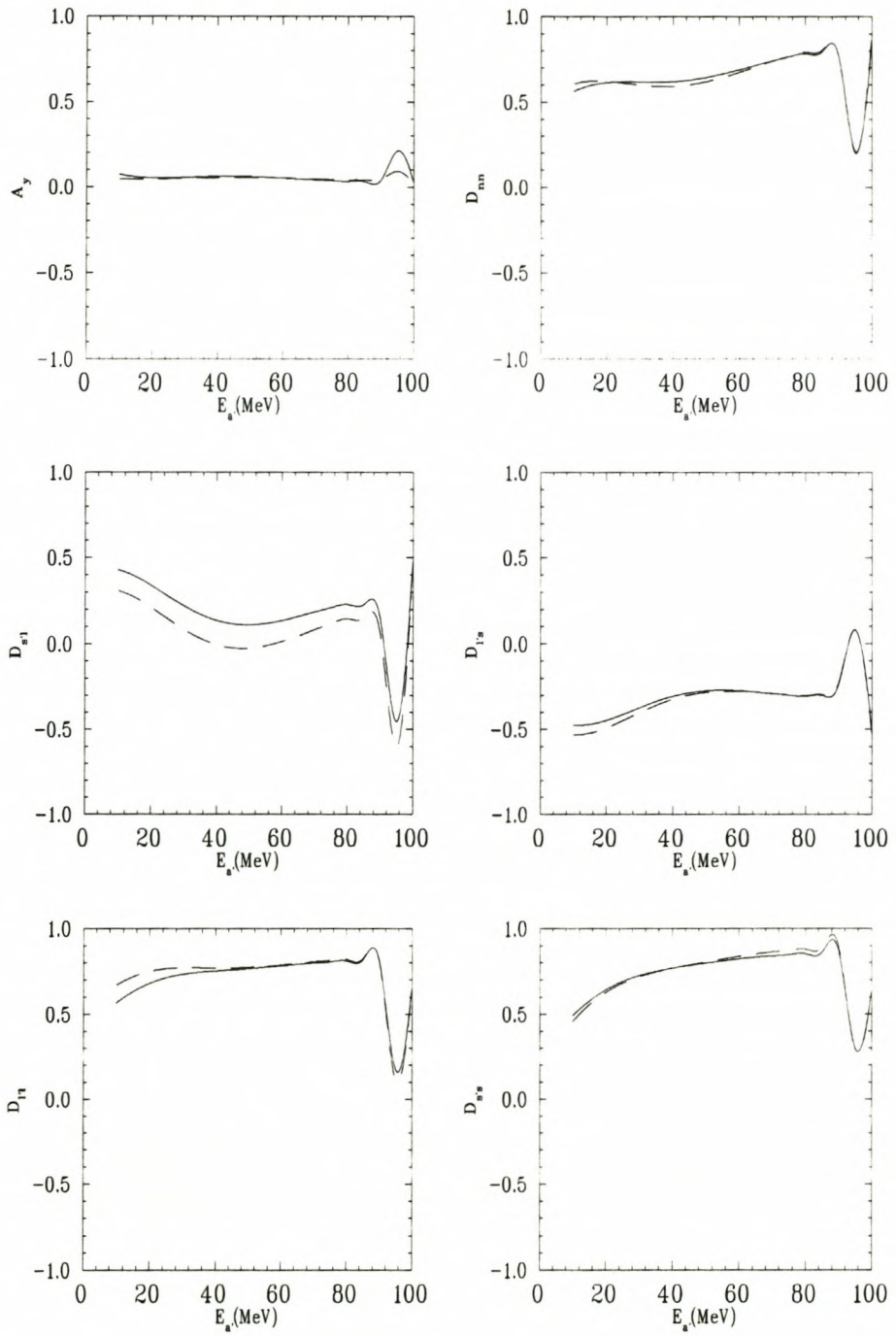

Figure 3.9: Plots comparing complete sets of $(p, 2p)$ spin transfer observables for the $1d_{\frac{3}{2}}$ state based on the initial (solid line) and final energy prescriptions (dashed line).

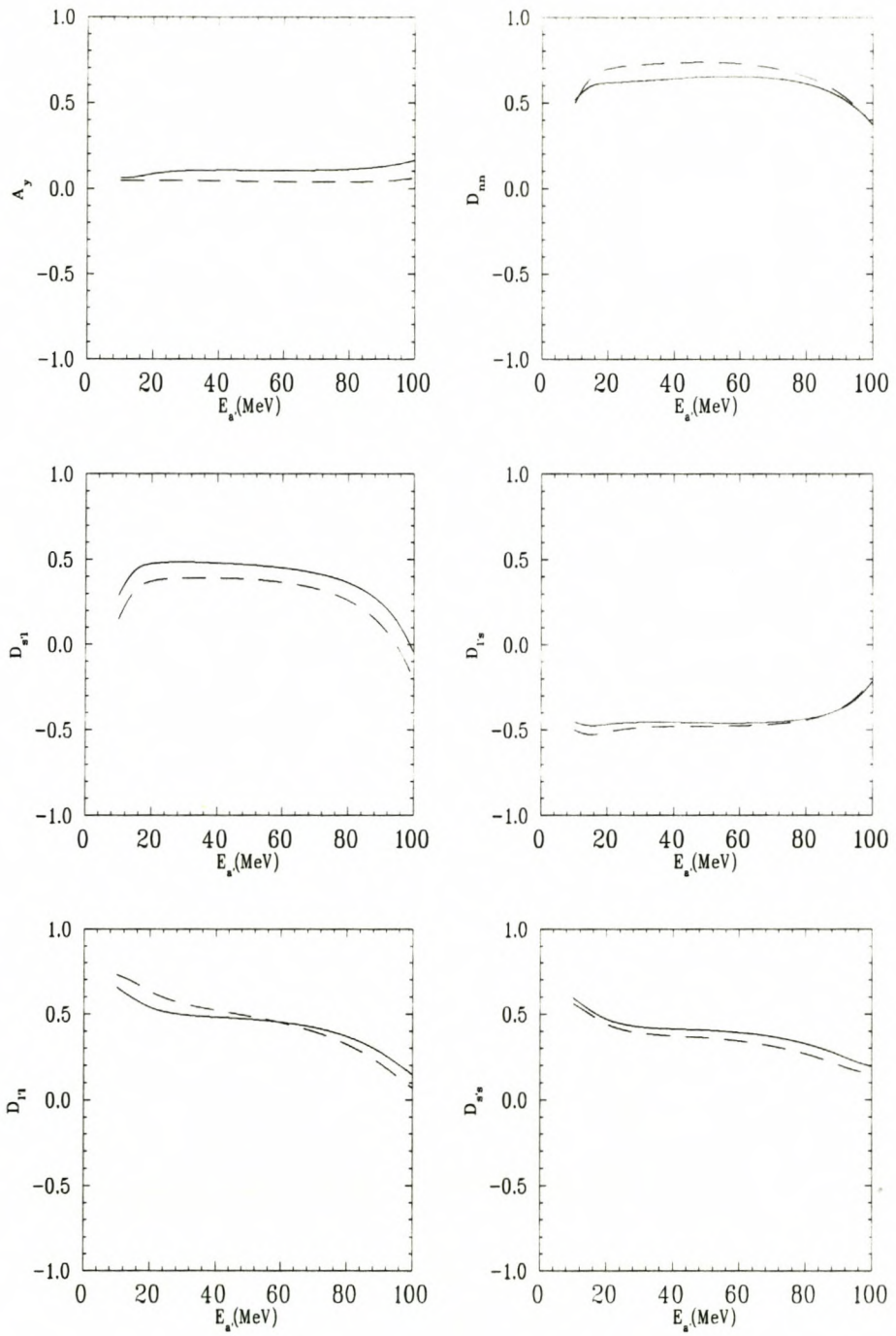

Figure 3.10: Plots comparing complete sets of $(p, 2p)$ spin transfer observables for the $2s_{\frac{1}{2}}$ state based on the initial (solid line) and final energy prescriptions (dashed line).

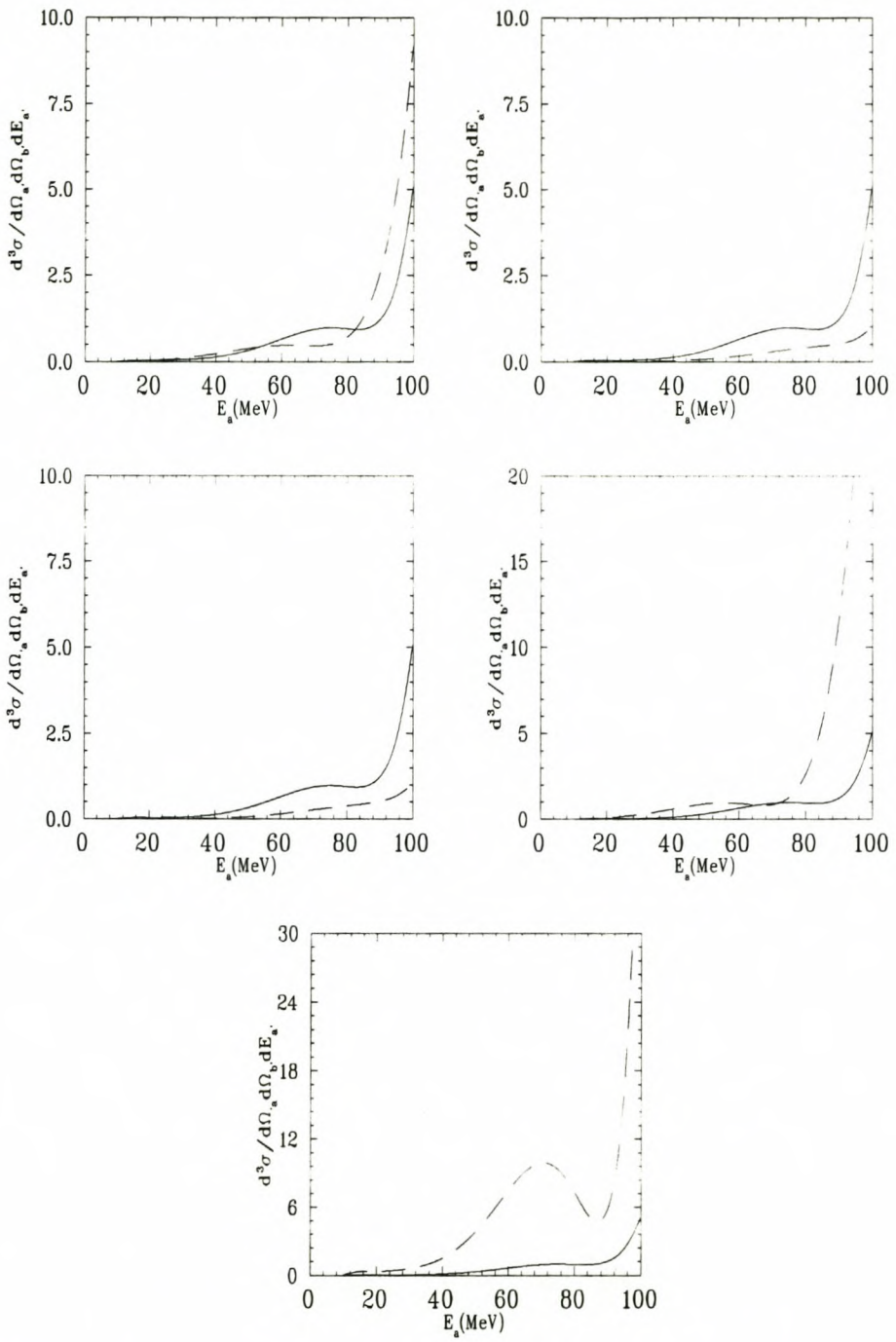

Figure 3.11: Plots of $(p, 2p)$ triple differential cross sections for the $1d_{\frac{5}{2}}$ state obtained with the trace method which include no medium effects (solid line) compared with calculations including medium modifications (dashed line). The plots from right to left, and top to bottom show calculations with M_p^*, m_{meson}^* and g_{meson}^* effect, m_{meson}^*, g_{meson}^* and free M_p, g_{meson}^* and free M_p and m_{meson}, M_p^* and free m_{meson} and g_{meson}, m_{meson}^* and free M_p and g_{meson} respectively for pseudoscalar πNN coupling.

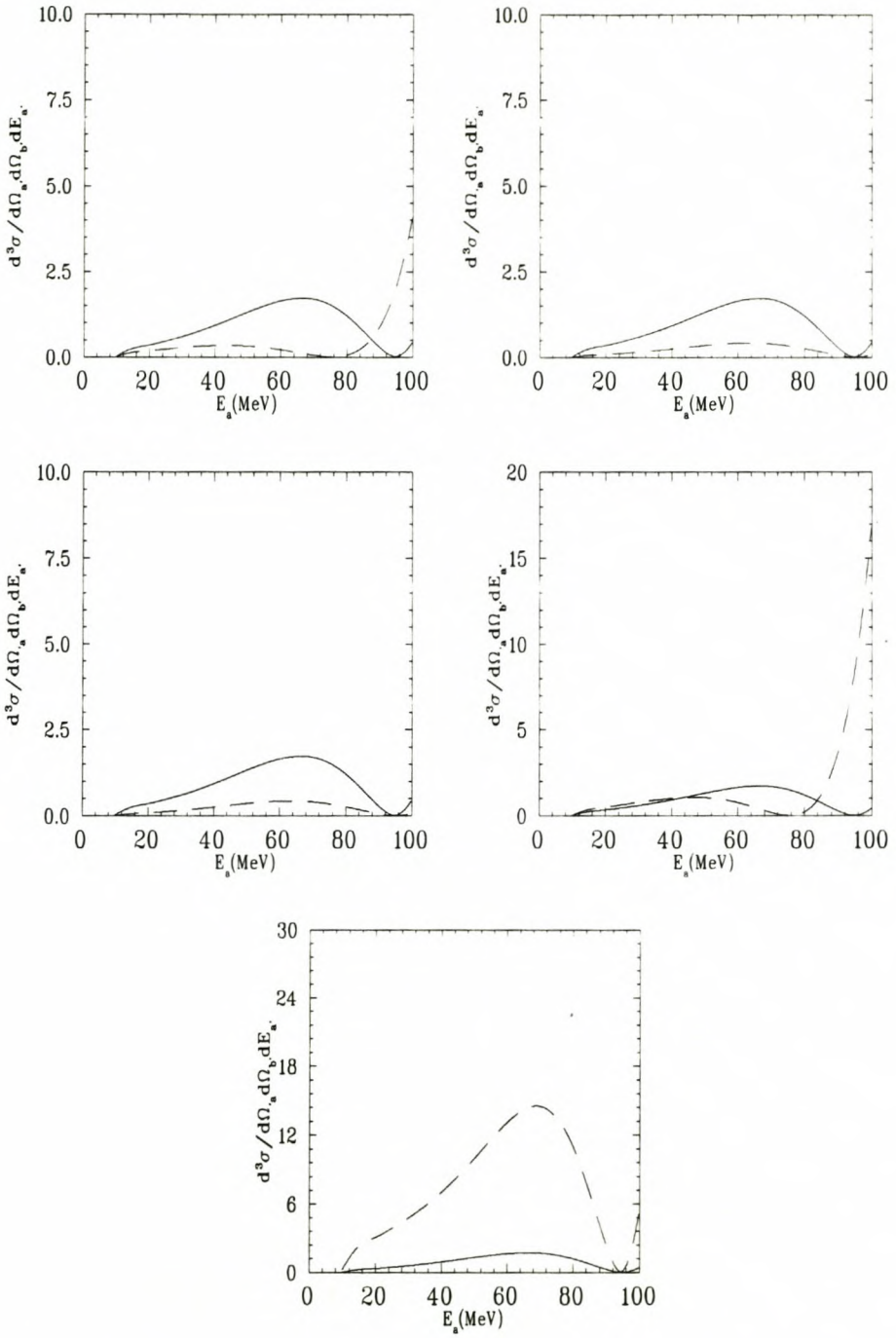

Figure 3.12: Plots of $(p, 2p)$ triple differential cross sections for the $1d_{\frac{3}{2}}$ state obtained with the trace method which exclude medium effects (solid line) compared with calculations including medium modifications (dashed line). The plots from right to left, and top to bottom show calculations with M_p^*, m_{meson}^* and g_{meson}^* effect, m_{meson}^*, g_{meson}^* and free M_p, g_{meson}^* and free M_p and m_{meson}, M_p^* and free m_{meson} and g_{meson}, m_{meson}^* and free M_p and g_{meson} respectively for pseudoscalar πNN coupling.

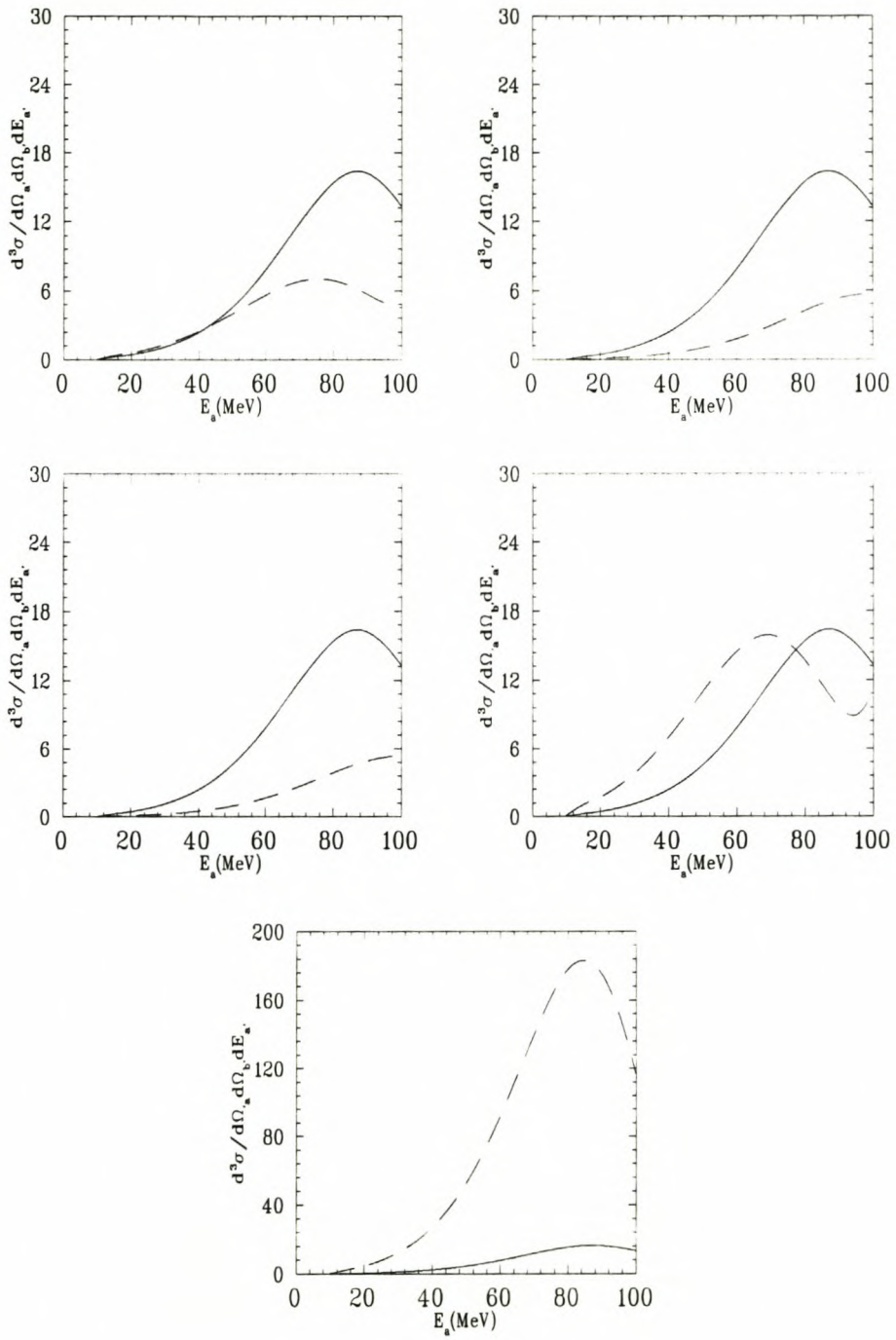

Figure 3.13: Plots of $(p, 2p)$ triple differential cross sections for the $2s_{\frac{1}{2}}$ state obtained with the trace method which exclude medium effects (solid line) compared with calculations including medium modifications (dashed line). The plots from right to left, and top to bottom show calculations with M_p^*, m_{meson}^* and g_{meson}^* effect, m_{meson}^*, g_{meson}^* and free M_p, g_{meson}^* and free M_p and m_{meson}, M_p^* and free m_{meson} and g_{meson}, m_{meson}^* and free M_p and g_{meson} respectively for pseudoscalar πNN coupling.

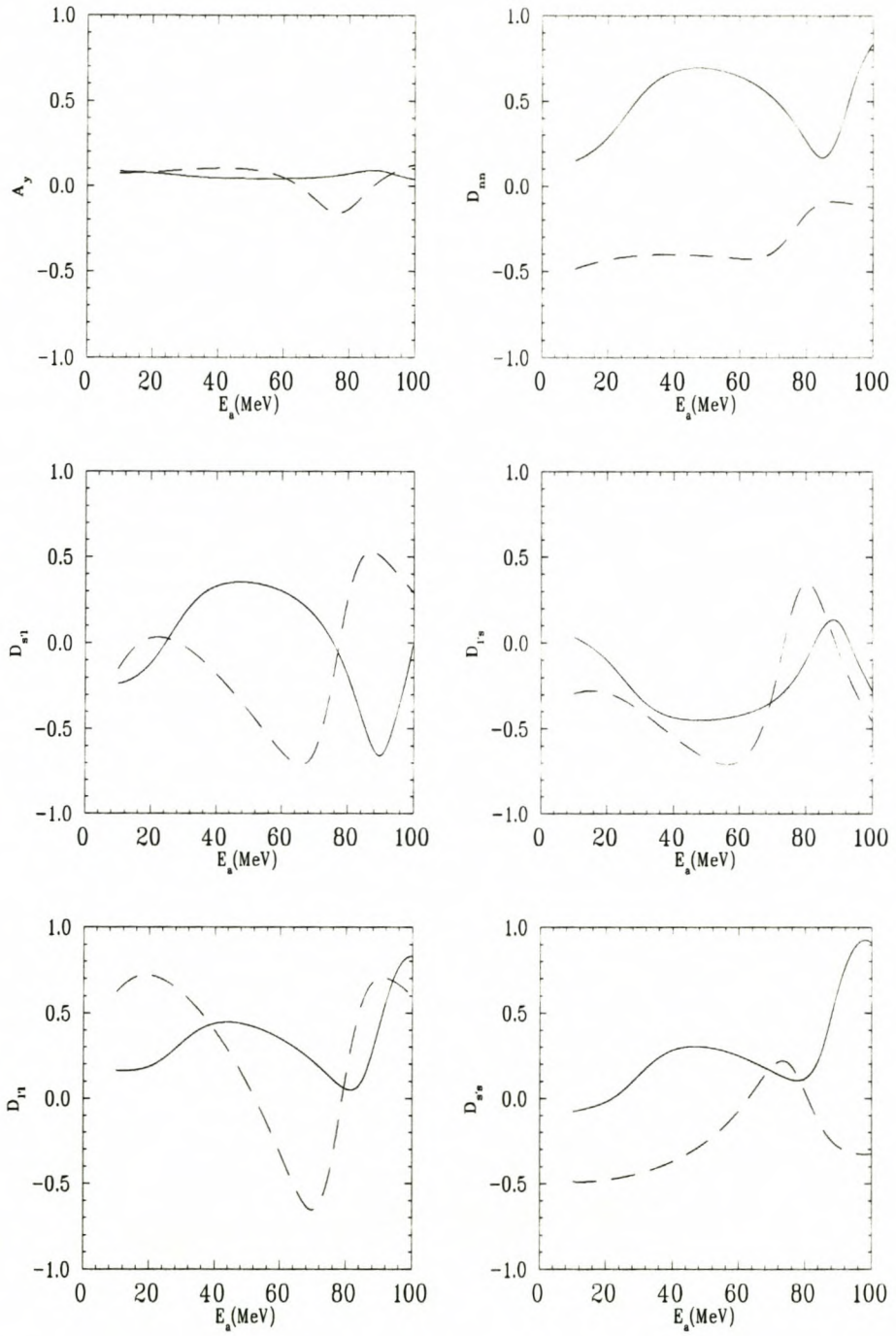

Figure 3.14: Plots of $(p, 2p)$ spin transfer observables for the $1d_{\frac{5}{2}}$ state obtained using the trace method which exclude medium effects (solid line) compared with calculations including medium modified M_p^*, m_{meson}^* and g_{meson}^* (dashed line) for pseudoscalar πNN coupling.

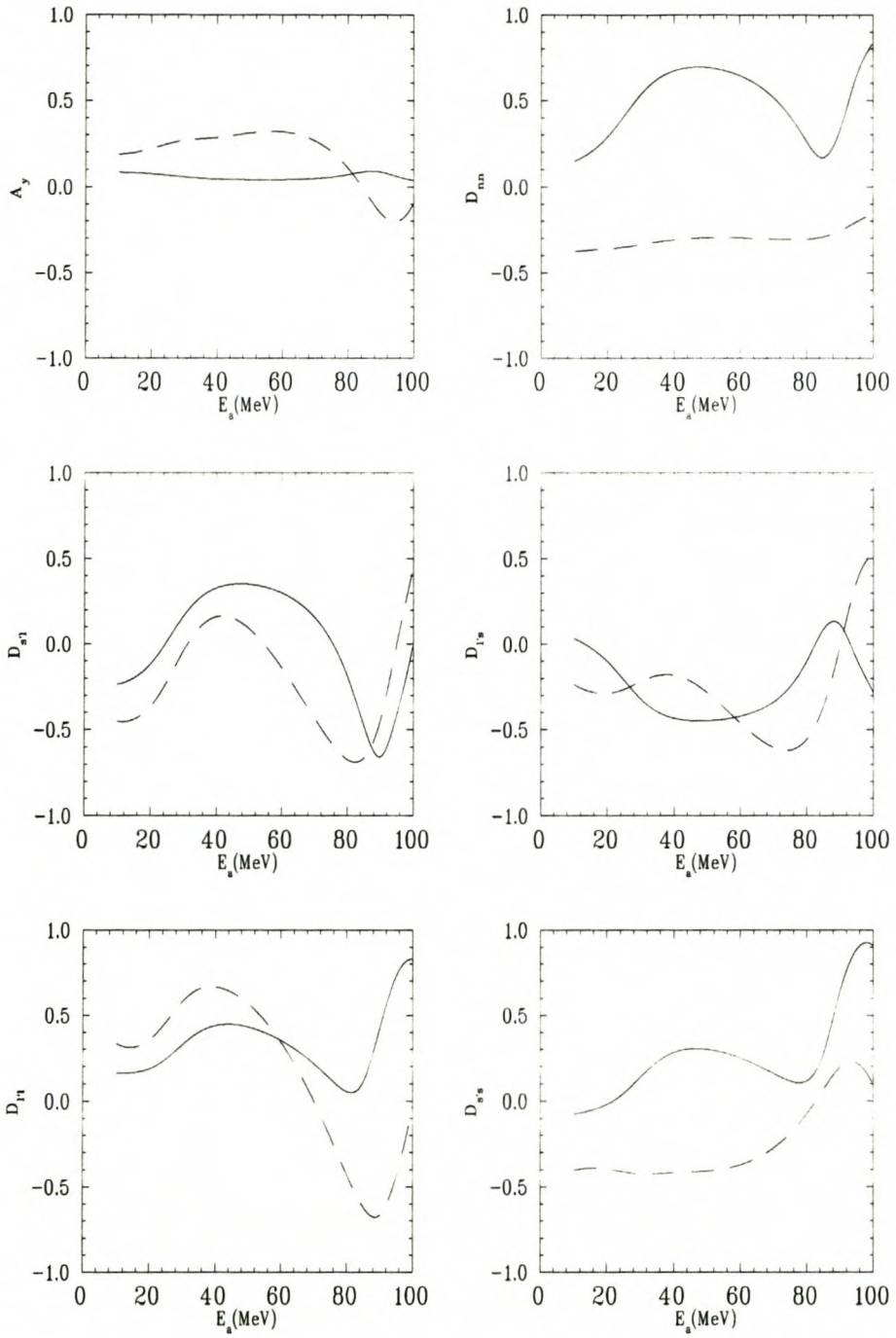

Figure 3.15: Plots of $(p, 2p)$ spin transfer observables for the $1d_{\frac{5}{2}}$ state obtained using the trace method which exclude medium effects (solid line) compared with calculations which include free M_p and medium modified m^*_{meson} and g^*_{meson} (dashed line) for pseudoscalar πNN coupling.

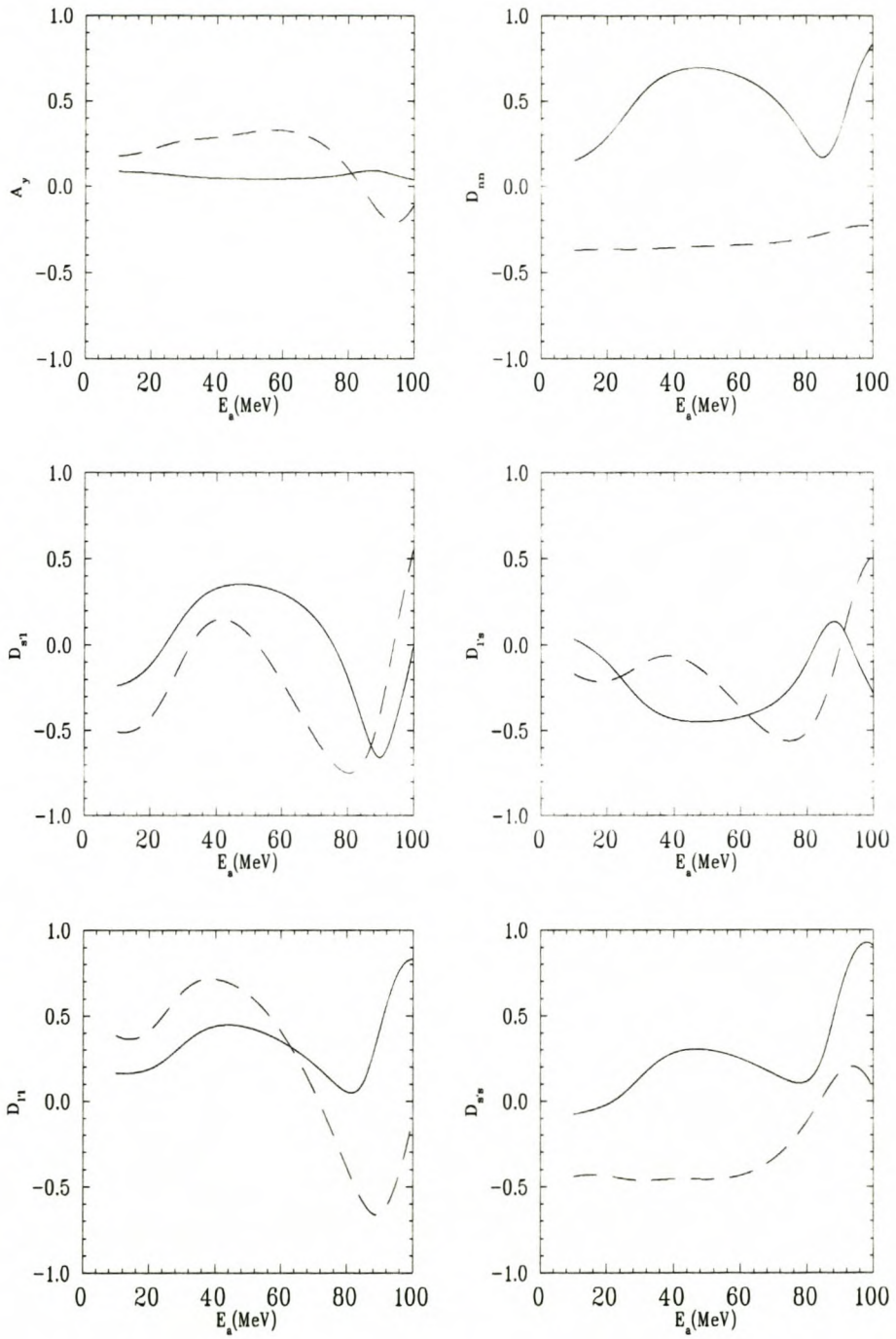

Figure 3.16: Plots of $(p, 2p)$ spin transfer observables for the $1d_{\frac{5}{2}}$ state obtained using the trace method which exclude medium effects (solid line) compared with calculations which include free M_p and m_{meson} with medium modified g^*_{meson} (dashed line) for pseudoscalar πNN coupling.

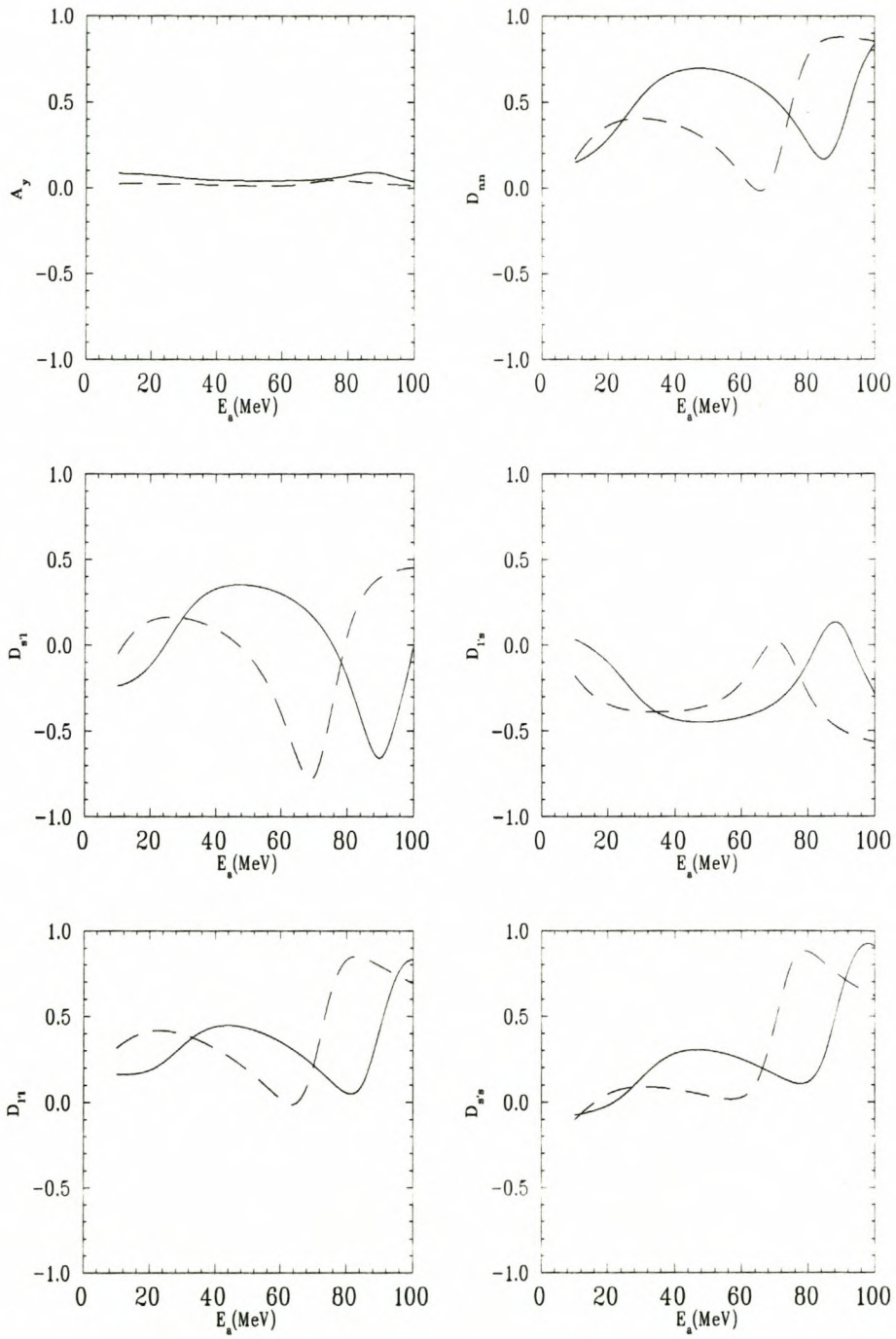

Figure 3.17: Plots of $(p, 2p)$ spin transfer observables for the $1d_{\frac{5}{2}}$ state obtained using the trace method which exclude medium effects (solid line) compared with calculations which include free m_{meson} and g_{meson} with medium modified M_p^* (dashed line) for pseudoscalar πNN coupling.

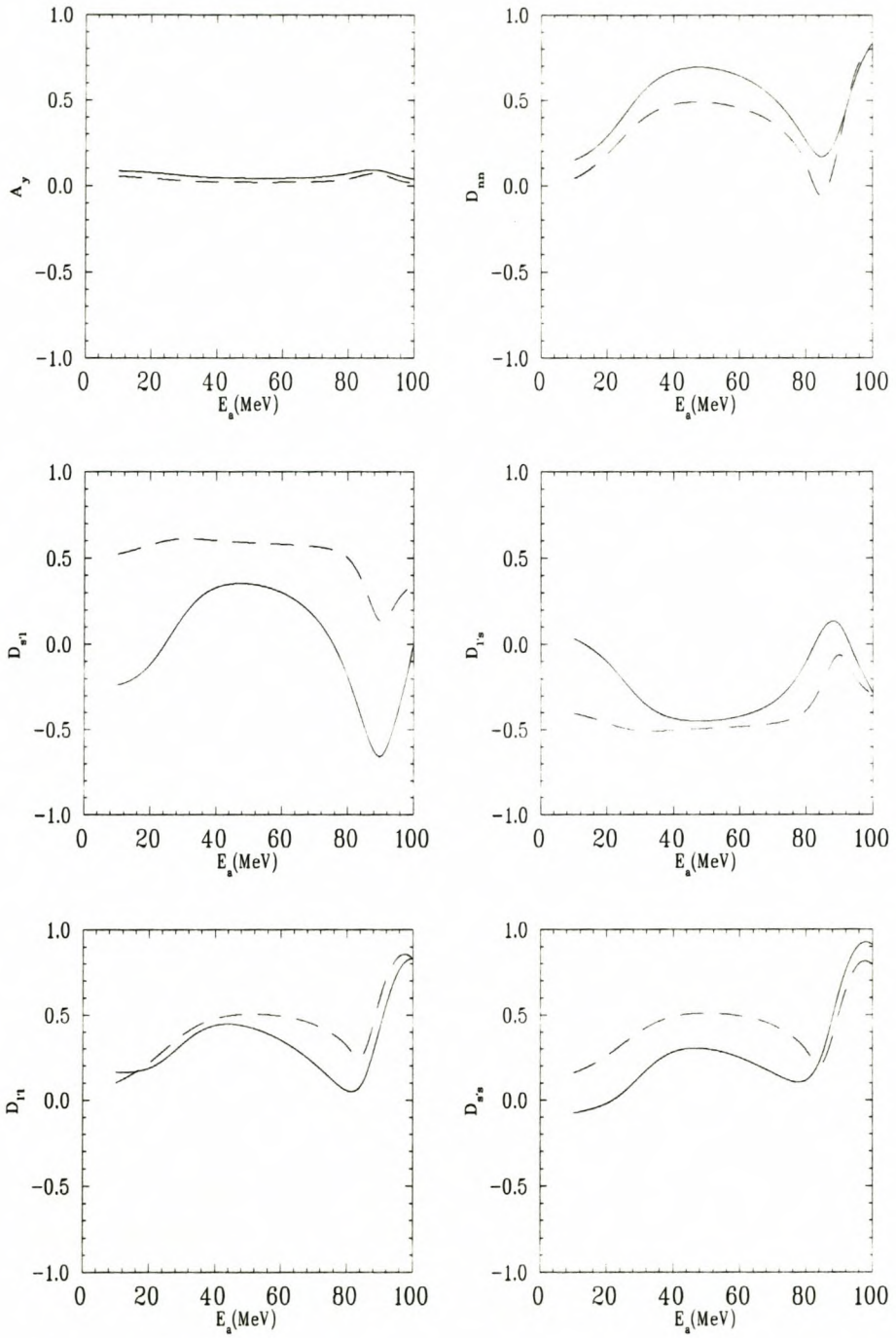

Figure 3.18: Plots of $(p, 2p)$ spin transfer observables for the $1d_{\frac{5}{2}}$ state obtained using the trace method which exclude medium effects (solid line) compared with calculations which include free M_p and g_{meson} with medium modified m^*_{meson} (dashed line) for pseudoscalar πNN coupling.

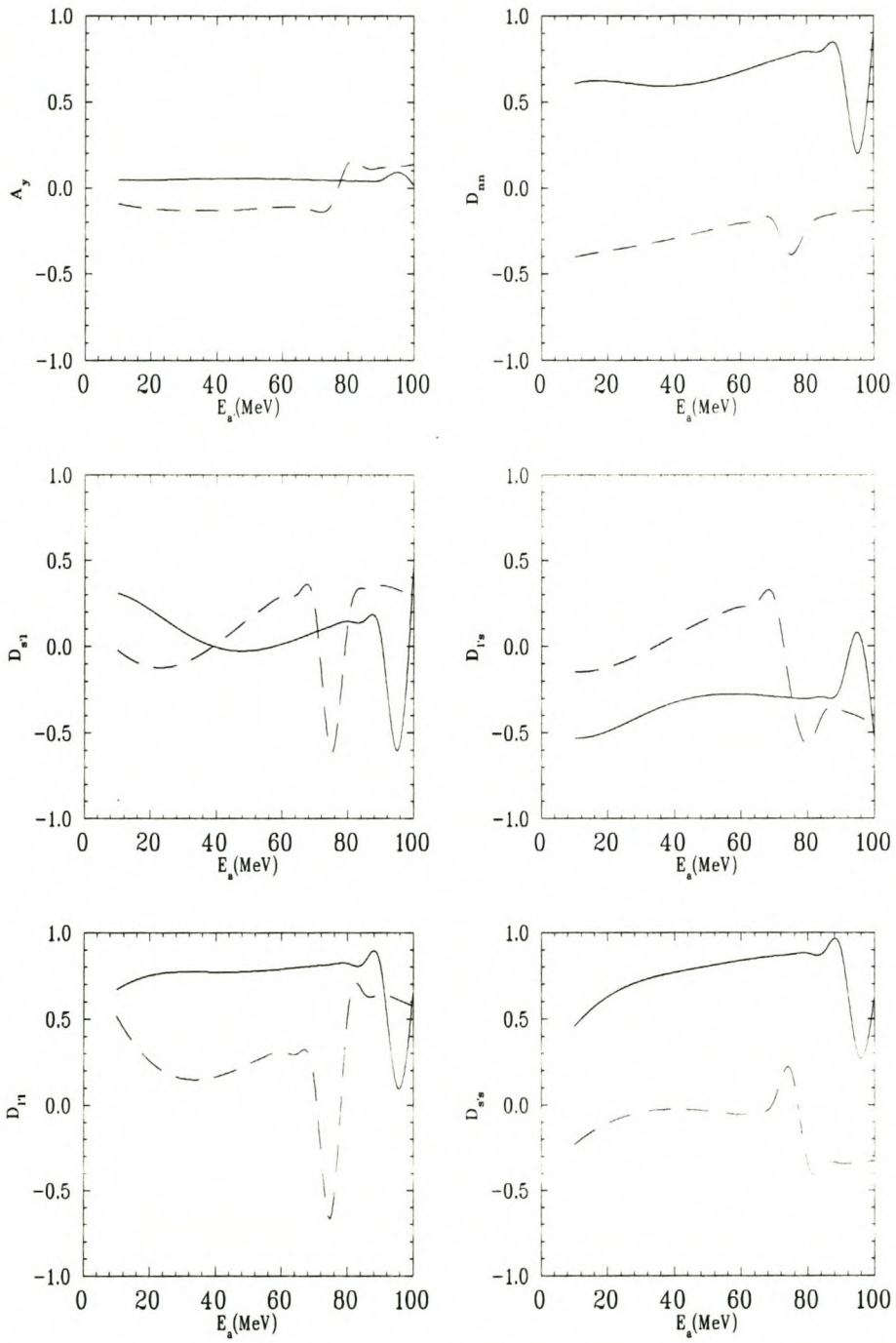

Figure 3.19: Plots of $(p, 2p)$ spin transfer observables for the $1d_{\frac{3}{2}}$ state obtained using the trace method which exclude medium effects (solid line) compared with calculations including medium modified M_p^*, m_{meson}^* and g_{meson}^* (dashed line) pseudoscalar coupling.

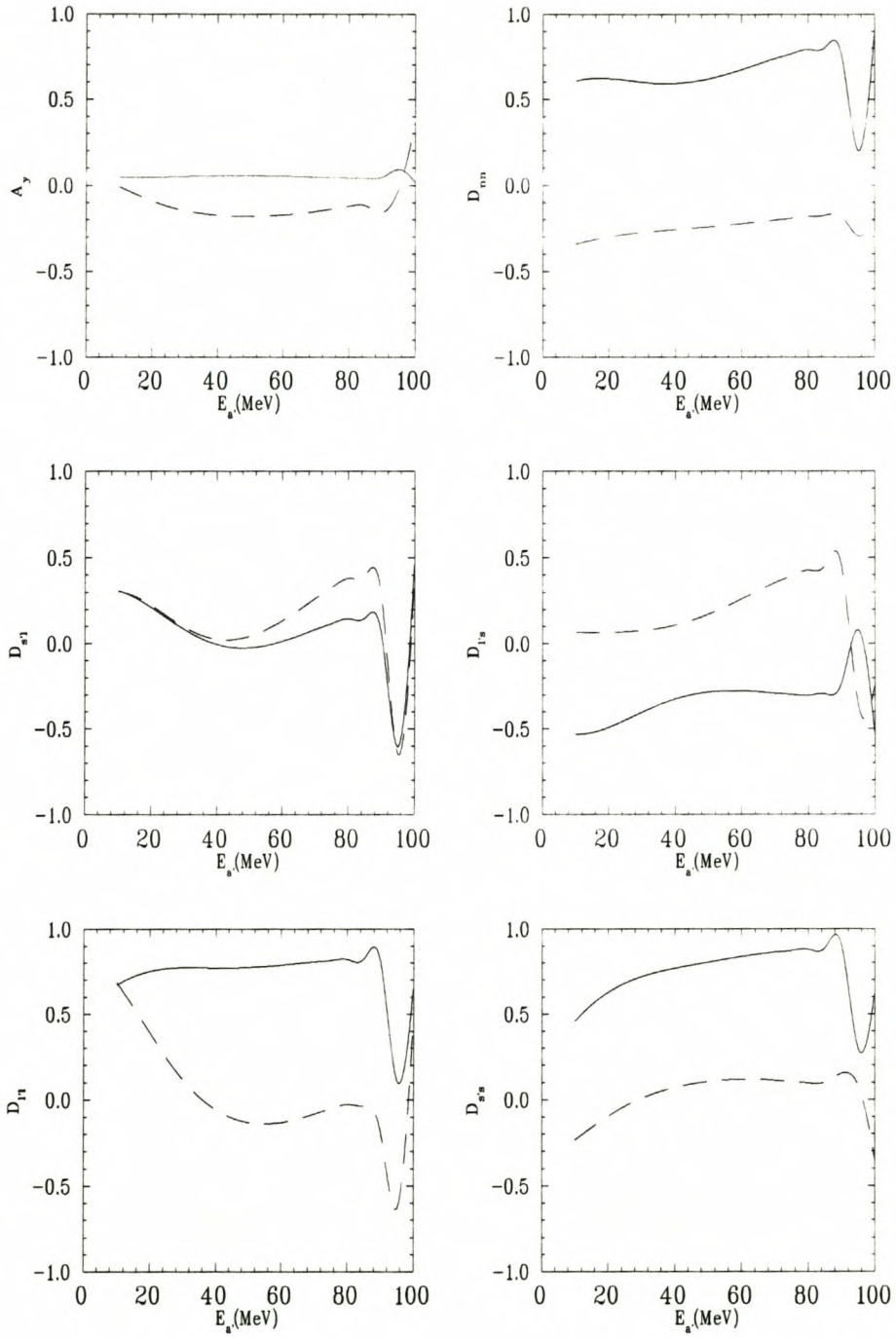

Figure 3.20: Plots of $(p, 2p)$ spin transfer observables for the $1d_{\frac{3}{2}}$ state obtained using the trace method which exclude medium effects (solid line) compared with calculations which include free M_p and medium modified m^*_{meson} and g^*_{meson} (dashed line) for pseudoscalar πNN coupling.

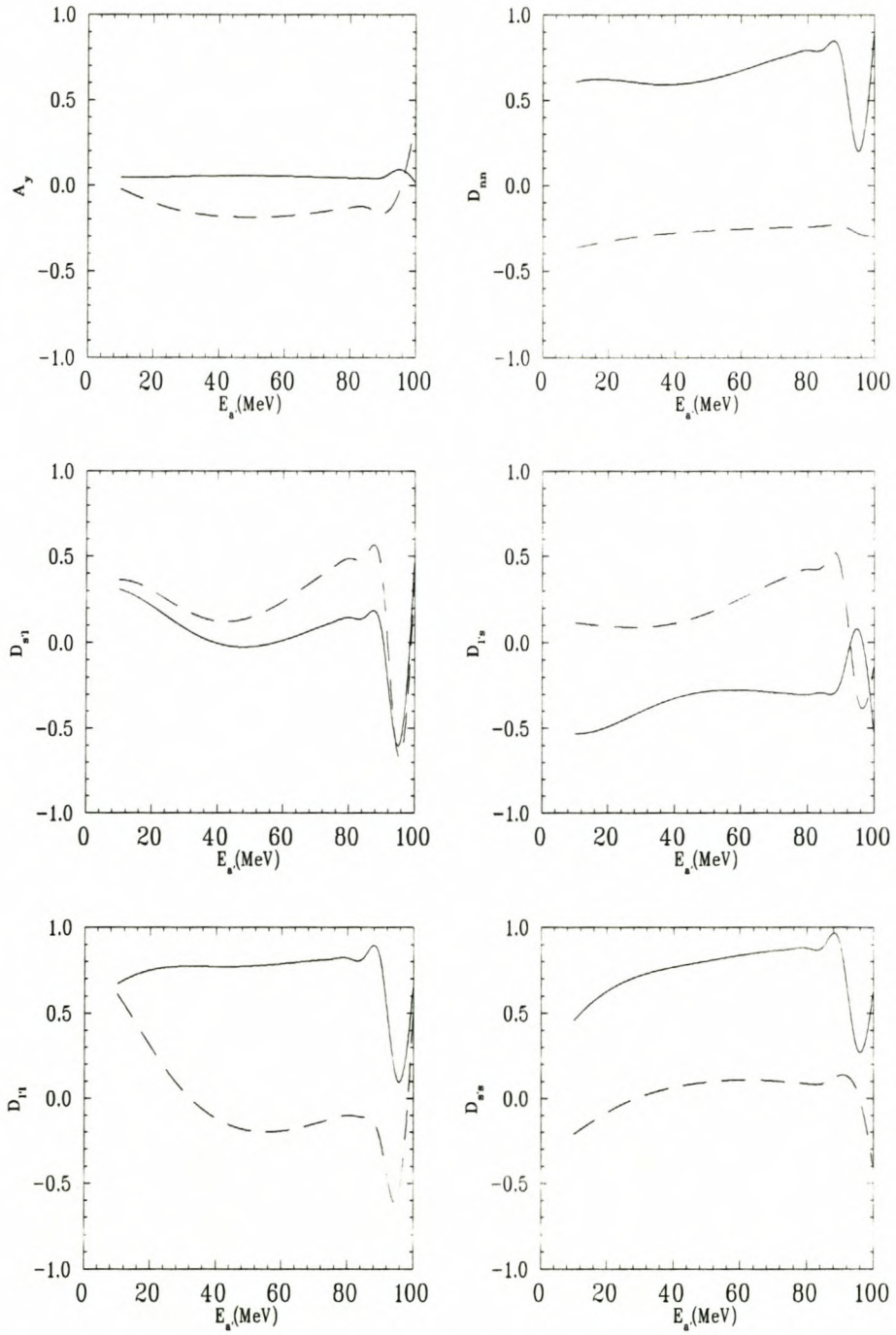

Figure 3.21: Plots of $(p, 2p)$ spin transfer observables for the $1d_{\frac{3}{2}}$ state obtained using the trace method which exclude medium effects (solid line) compared with calculations which include free M_p and m_{meson} with medium modified g^*_{meson} (dashed line) for pseudoscalar πNN coupling.

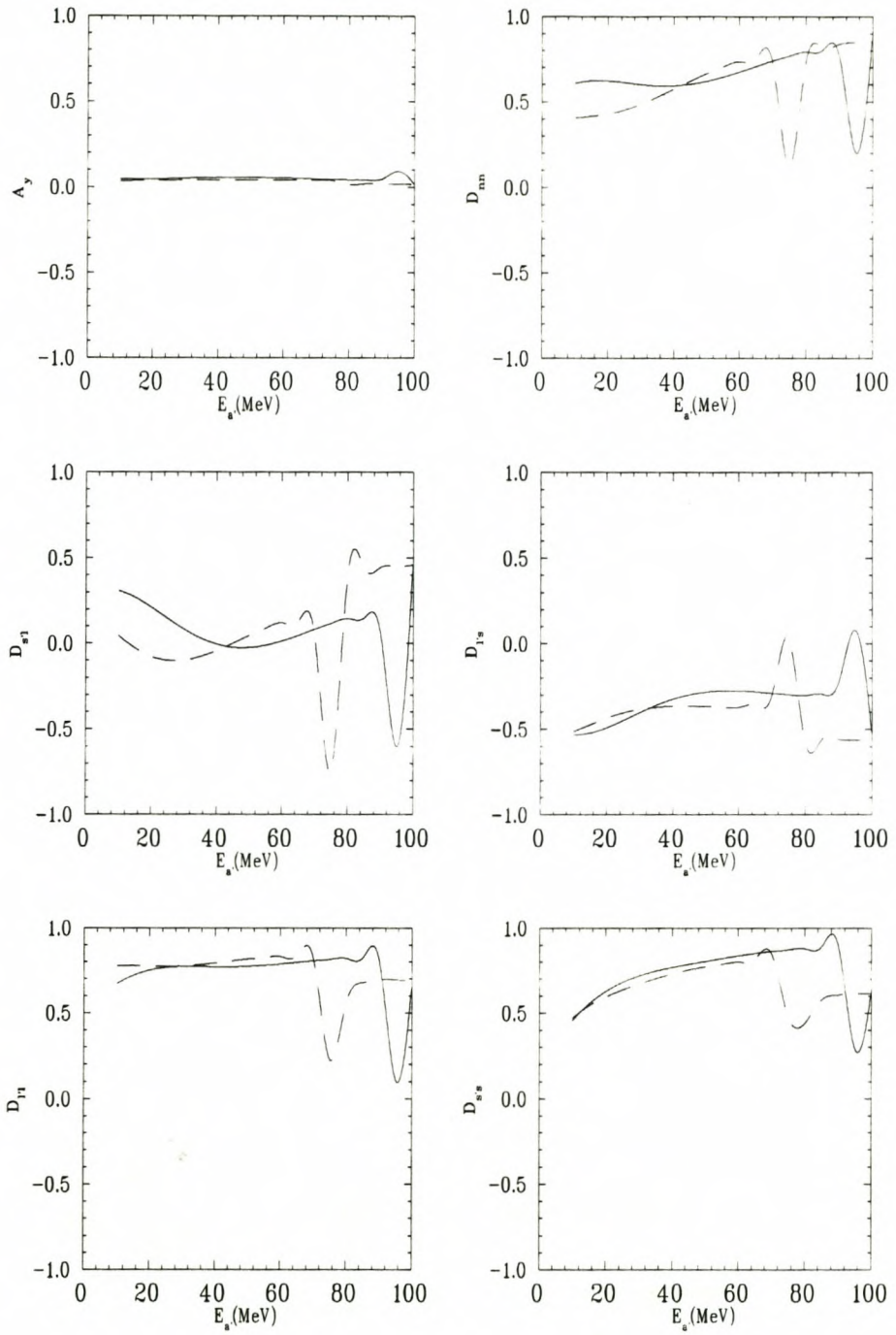

Figure 3.22: Plots of $(p, 2p)$ spin transfer observables for the $1d_{\frac{3}{2}}$ state obtained using the trace method which exclude medium effects (solid line) compared with calculations which include free m_{meson} and g_{meson} with medium modified M_p^* (dashed line) for pseudoscalar πNN coupling.

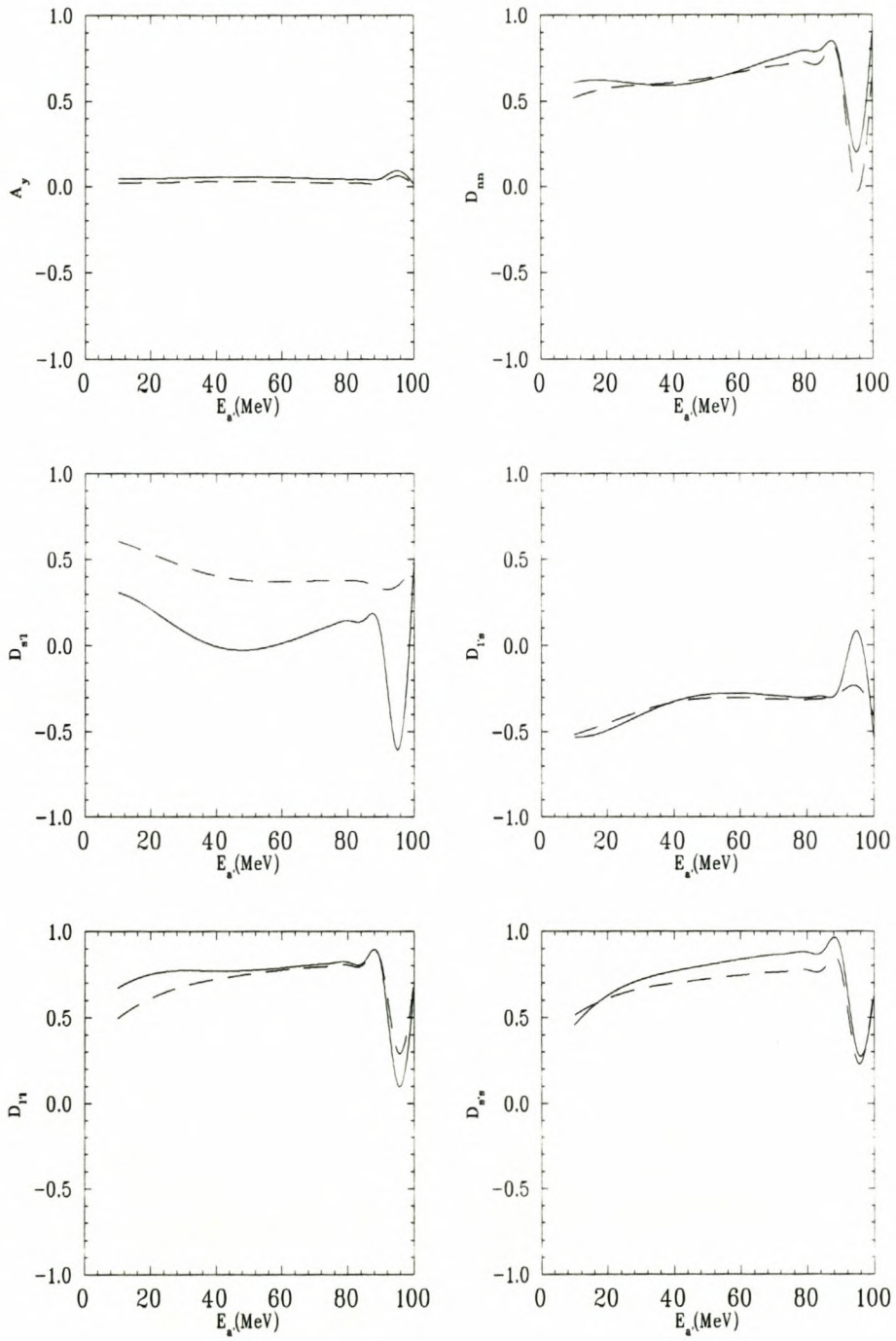

Figure 3.23: Plots of $(p, 2p)$ spin transfer observables for the $1d_{\frac{3}{2}}$ state obtained using the trace method which exclude medium effects (solid line) compared with calculations which include free M_p and g_{meson} with medium modified m^*_{meson} (dashed line) for pseudoscalar πNN coupling.

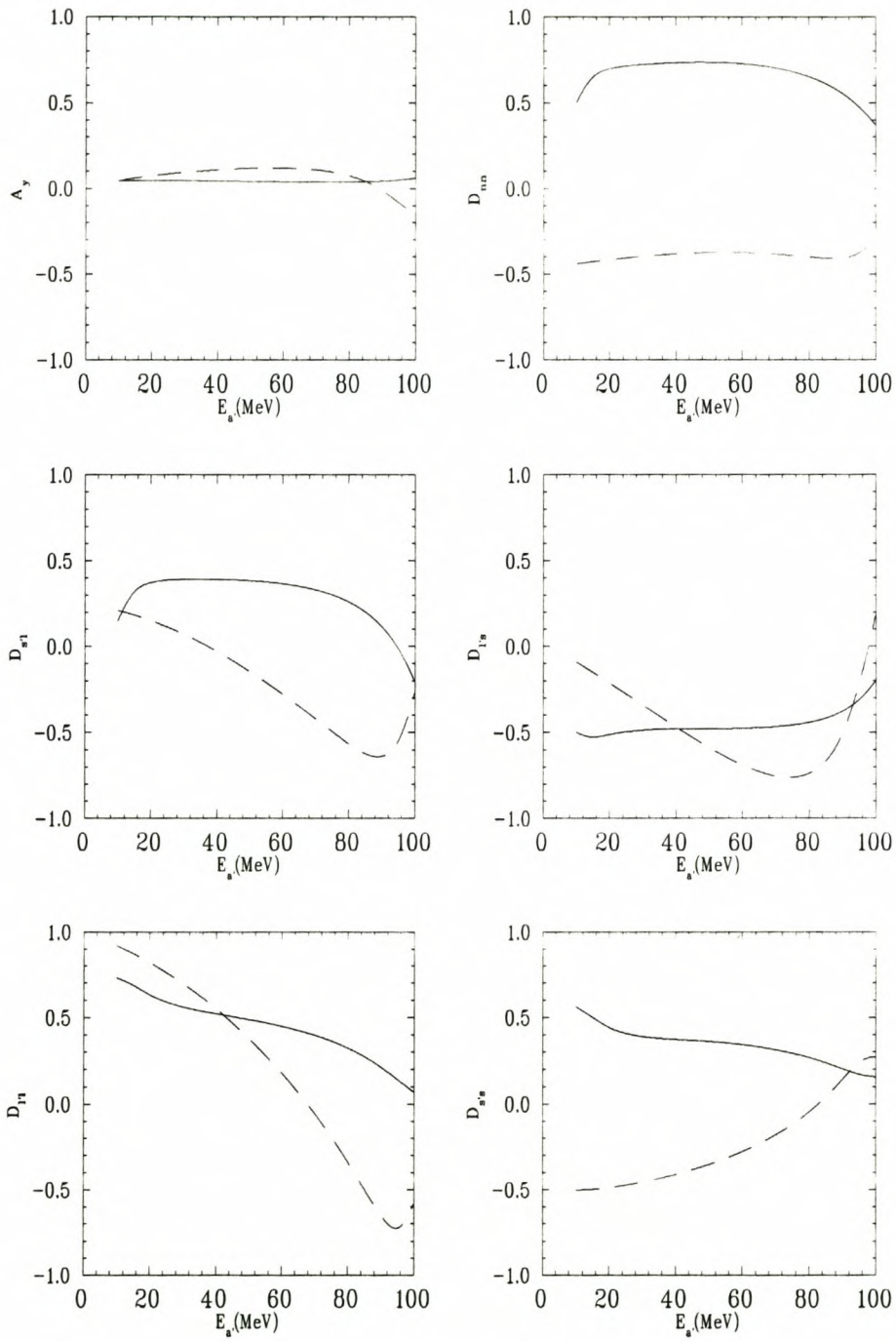

Figure 3.24: Plots of $(p, 2p)$ spin transfer observables for the $2s_{\frac{1}{2}}$ state obtained using the trace method which exclude medium effects (solid line) compared with calculations including medium modified M_p^*, m_{meson}^* and g_{meson}^* (dashed line) for pseudoscalar πNN coupling.

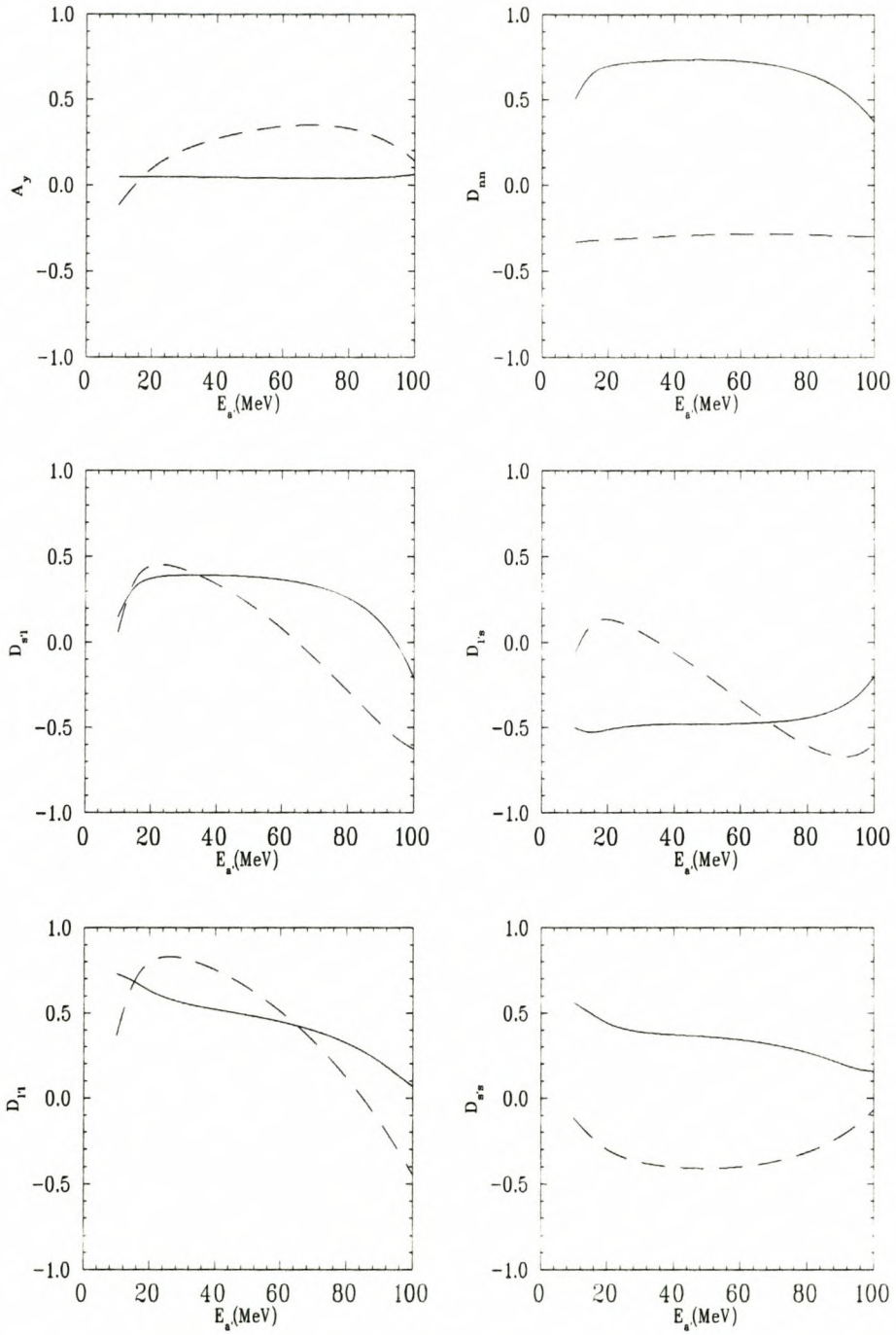

Figure 3.25: Plots of $(p, 2p)$ spin transfer observables for the $2s_{\frac{1}{2}}$ state obtained using the trace method which exclude medium effects (solid line) compared with calculations which include free M_p and medium modified m^*_{meson} and g^*_{meson} (dashed line) for pseudoscalar πNN coupling.

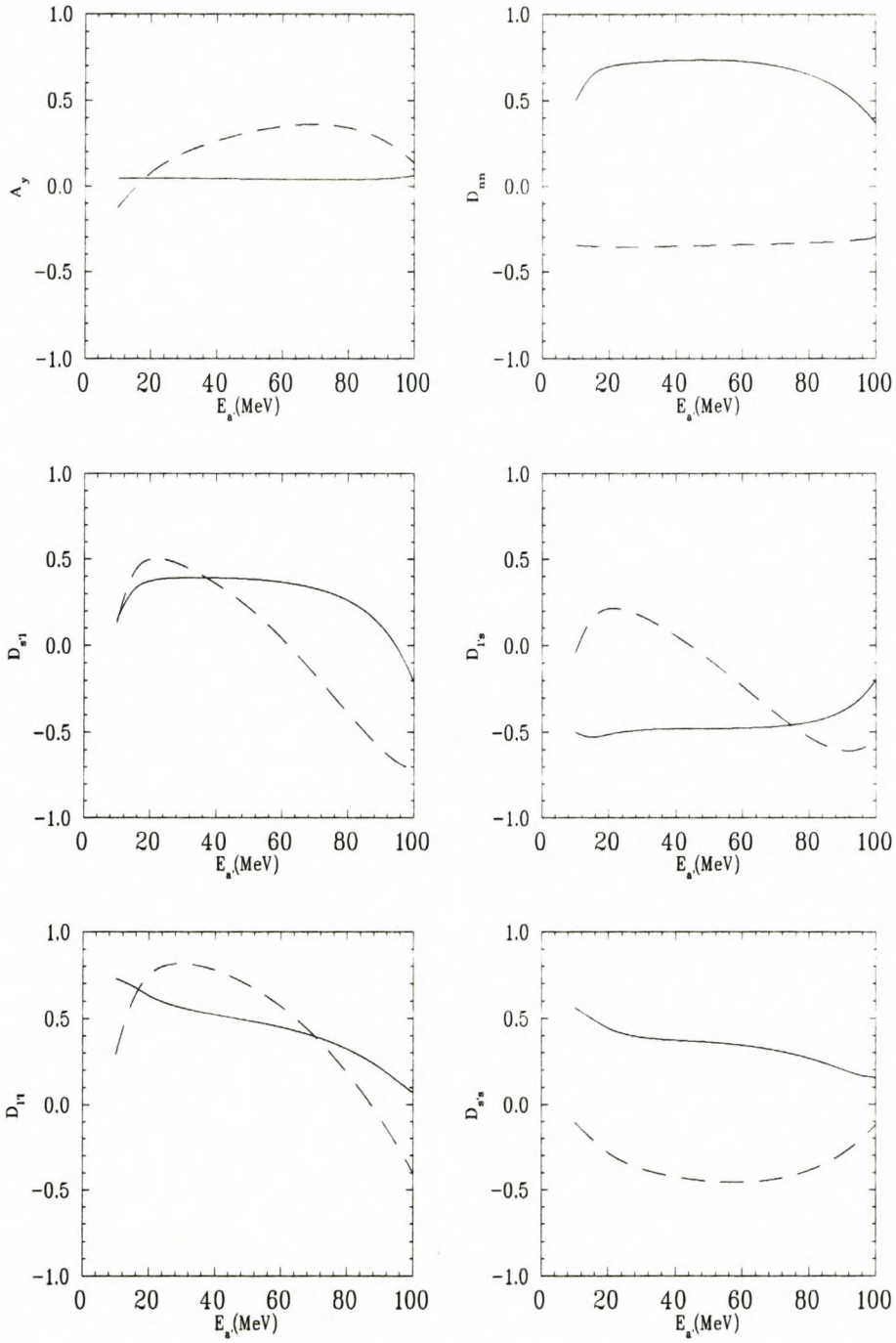

Figure 3.26: Plots of $(p, 2p)$ spin transfer observables for the $2s_{\frac{1}{2}}$ state obtained using the trace method which exclude medium effects (solid line) compared with calculations which include free M_p and m_{meson} with medium modified g^*_{meson} (dashed line) for pseudoscalar πNN coupling.

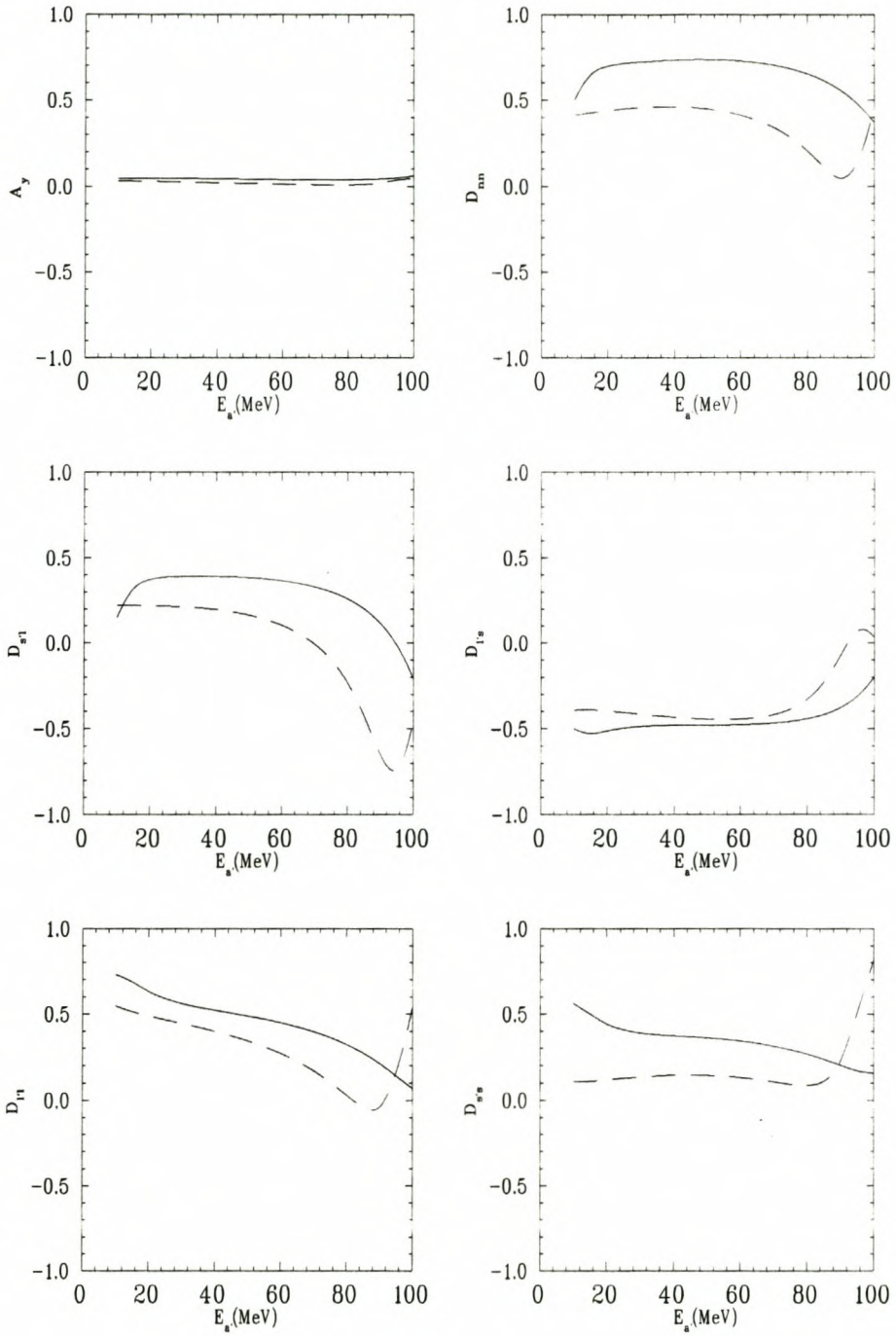

Figure 3.27: Plots of $(p, 2p)$ spin transfer observables for the $2s_{\frac{1}{2}}$ state obtained using the trace method which exclude medium effects (solid line) compared with calculations which include free m_{meson} and g_{meson} with medium modified M_p^* (dashed line) for pseudoscalar πNN coupling.

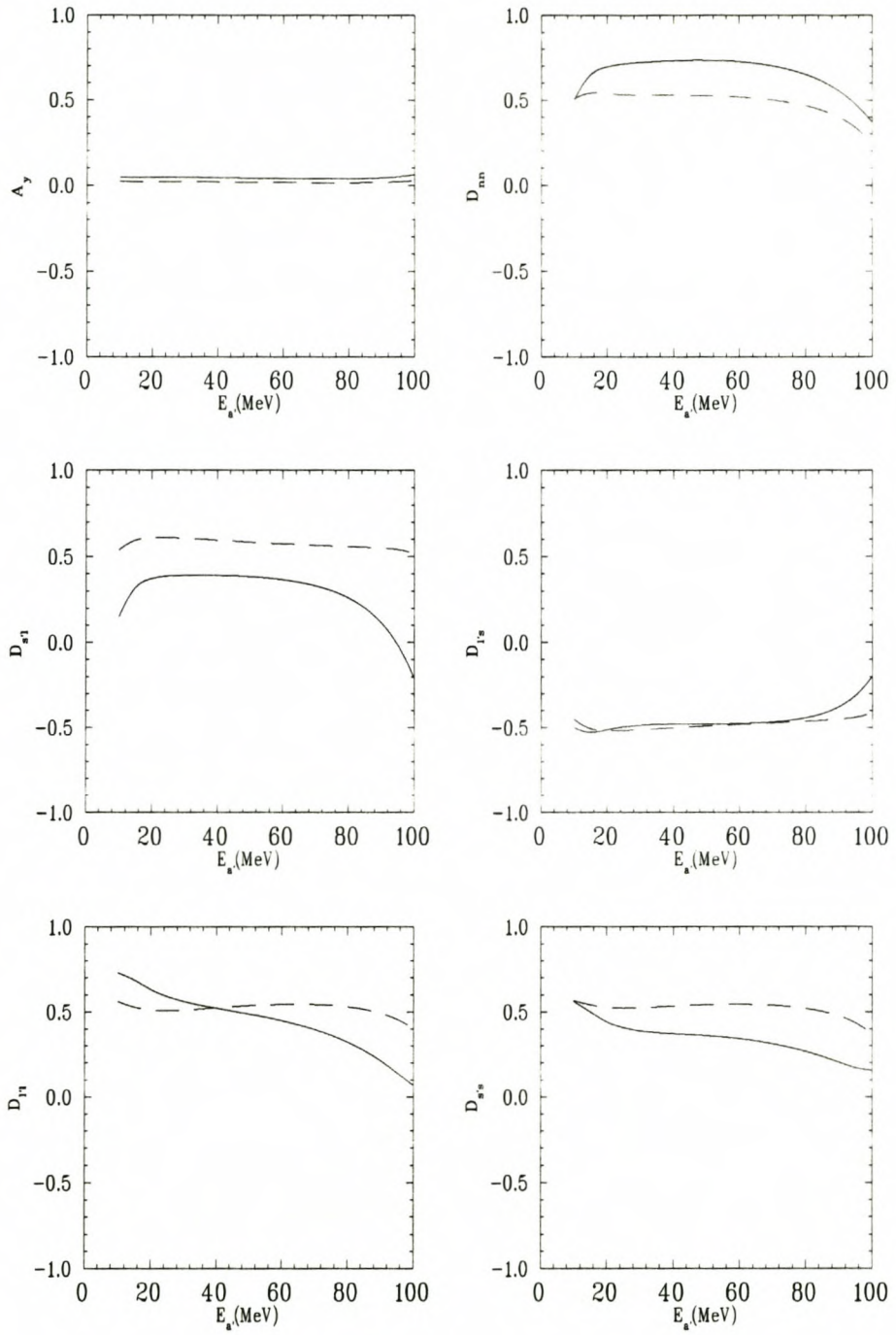

Figure 3.28: Plots of $(p, 2p)$ spin transfer observables for the $2s_{\frac{1}{2}}$ state obtained using the trace method which exclude medium effects (solid line) compared with calculations which include free M_p and g_{meson} with medium modified m^*_{meson} (dashed line) for pseudoscalar πNN coupling.

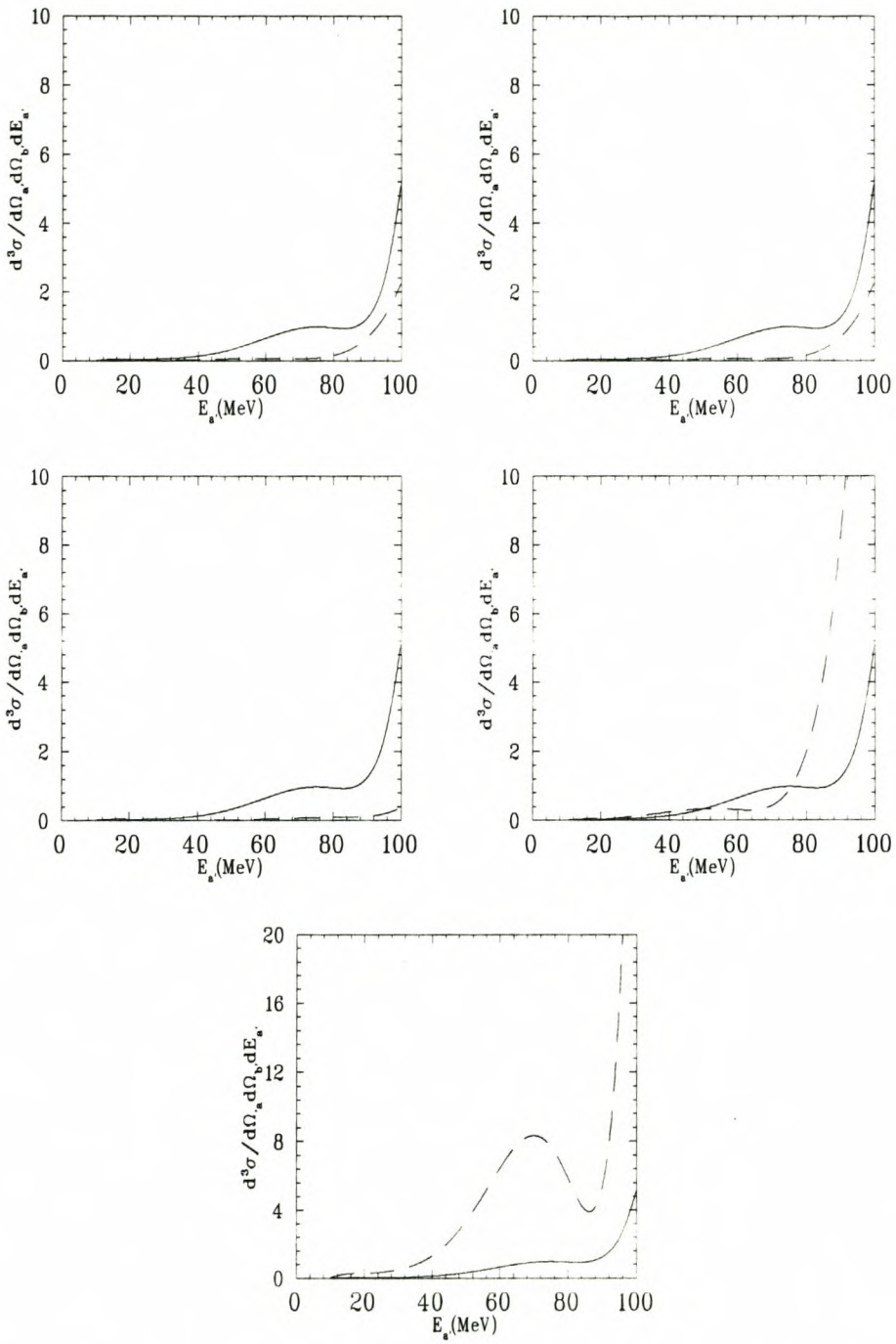

Figure 3.29: Plots of $(p, 2p)$ triple differential cross sections for the $1d_{\frac{5}{2}}$ state obtained with the trace method excluding medium effects (solid line) compared with calculations which include medium modifications (dashed line). The plots from right to left, and top to bottom show calculations with M_p^*, m_{meson}^* and g_{meson}^* effect, m_{meson}^*, g_{meson}^* and free M_p, g_{meson}^* and free M_p and m_{meson}, M_p^* and free m_{meson} and g_{meson}, m_{meson}^* and free M_p and g_{meson} respectively for pseudovector πNN coupling.

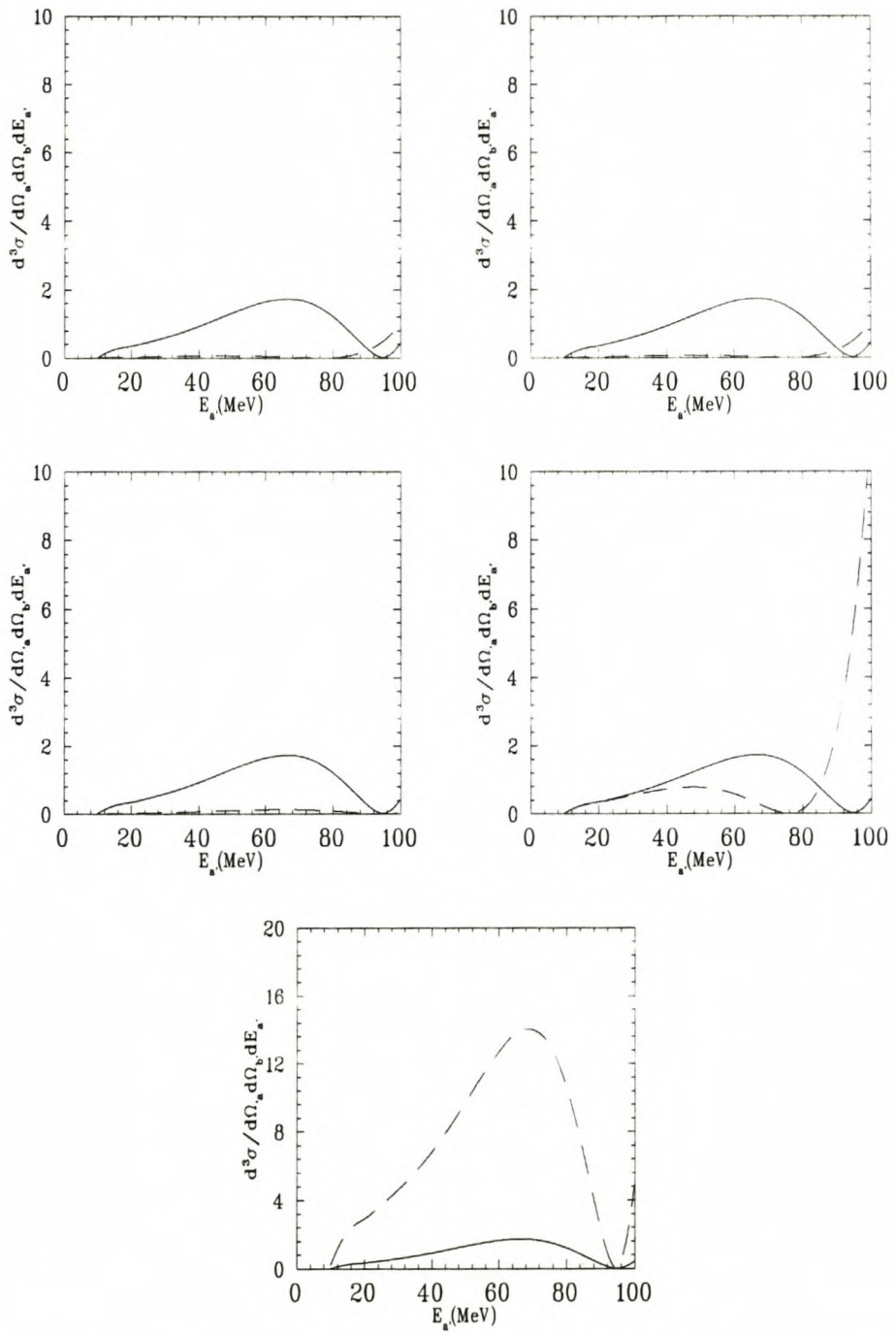

Figure 3.30: Plots of $(p, 2p)$ triple differential cross sections for the $1d_{\frac{3}{2}}$ state obtained with the trace method excluding medium effects (solid line) compared with calculations which include medium modifications (dashed line). The plots from right to left, and top to bottom show calculations with M_p^*, m_{meson}^* and g_{meson}^* effect, m_{meson}^*, g_{meson}^* and free M_p, g_{meson}^* and free M_p and m_{meson}, M_p^* and free m_{meson} and g_{meson}, m_{meson}^* and free M_p and g_{meson} respectively for pseudovector πNN coupling.

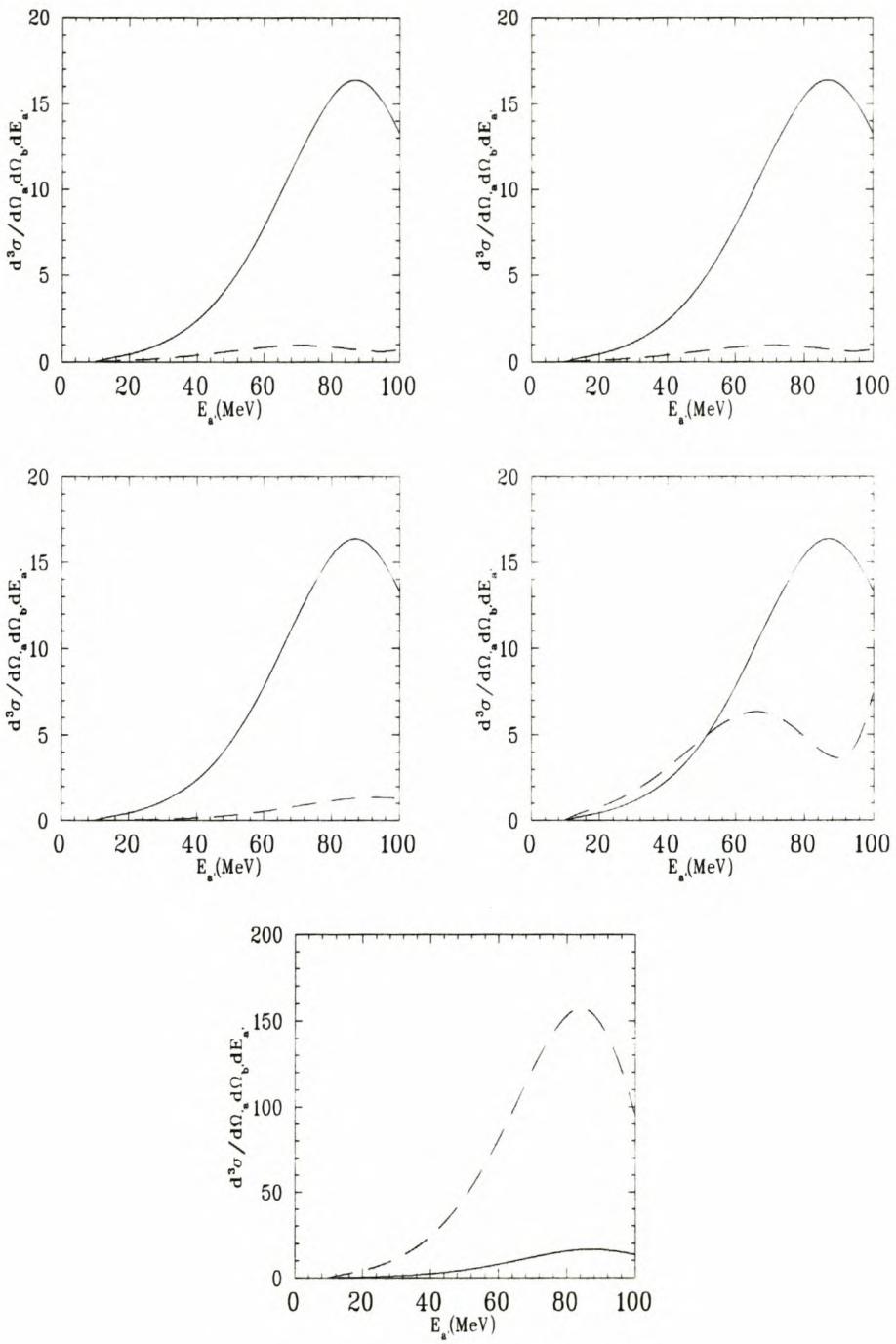

Figure 3.31: Plots of $(p, 2p)$ triple differential cross sections for the $2s_{\frac{1}{2}}$ state obtained with the trace method excluding medium effects (solid line) compared with calculations which include medium modifications (dashed line). The plots from right to left, and top to bottom show calculations with M_p^*, m_{meson}^* and g_{meson}^* effect, m_{meson}^*, g_{meson}^* and free M_p, g_{meson}^* and free M_p and m_{meson}, M_p^* and free m_{meson} and g_{meson}, m_{meson}^* and free M_p and g_{meson} respectively for pseudovector πNN coupling.

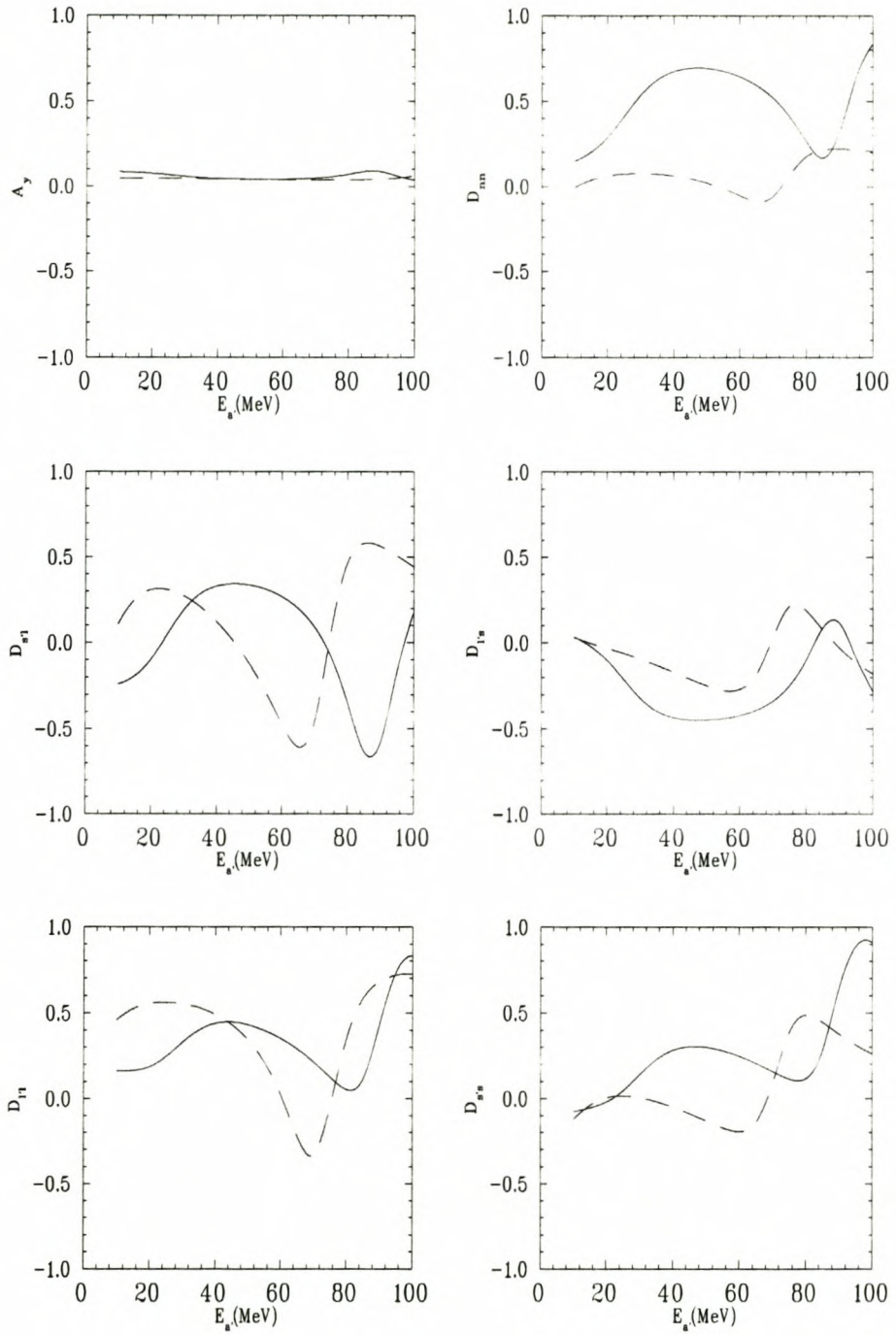

Figure 3.32: Plots of $(p, 2p)$ spin transfer observables for the $1d_{\frac{5}{2}}$ state obtained using the trace method excluding medium effects (solid line) compared with calculations which include medium modified M_p^*, m_{meson}^* and g_{meson}^* effect (dashed line) for pseudovector πNN coupling.

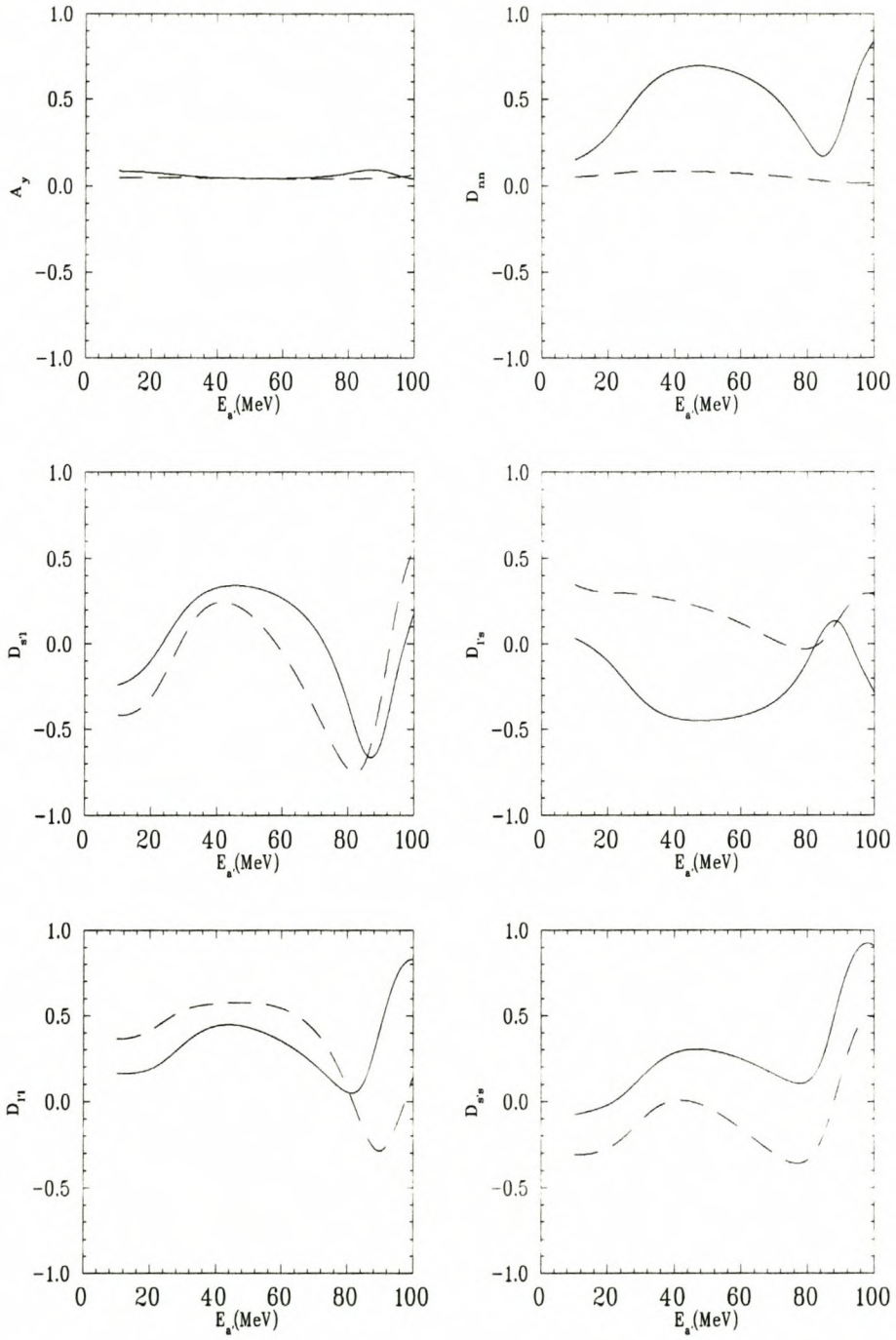

Figure 3.33: Plots of $(p, 2p)$ spin transfer observables for the $1d_{\frac{5}{2}}$ state obtained using the trace method excluding medium effects (solid line) compared with calculations which include free M_p and medium modified m^*_{meson} and g^*_{meson} (dashed line) for pseudovector πNN coupling.

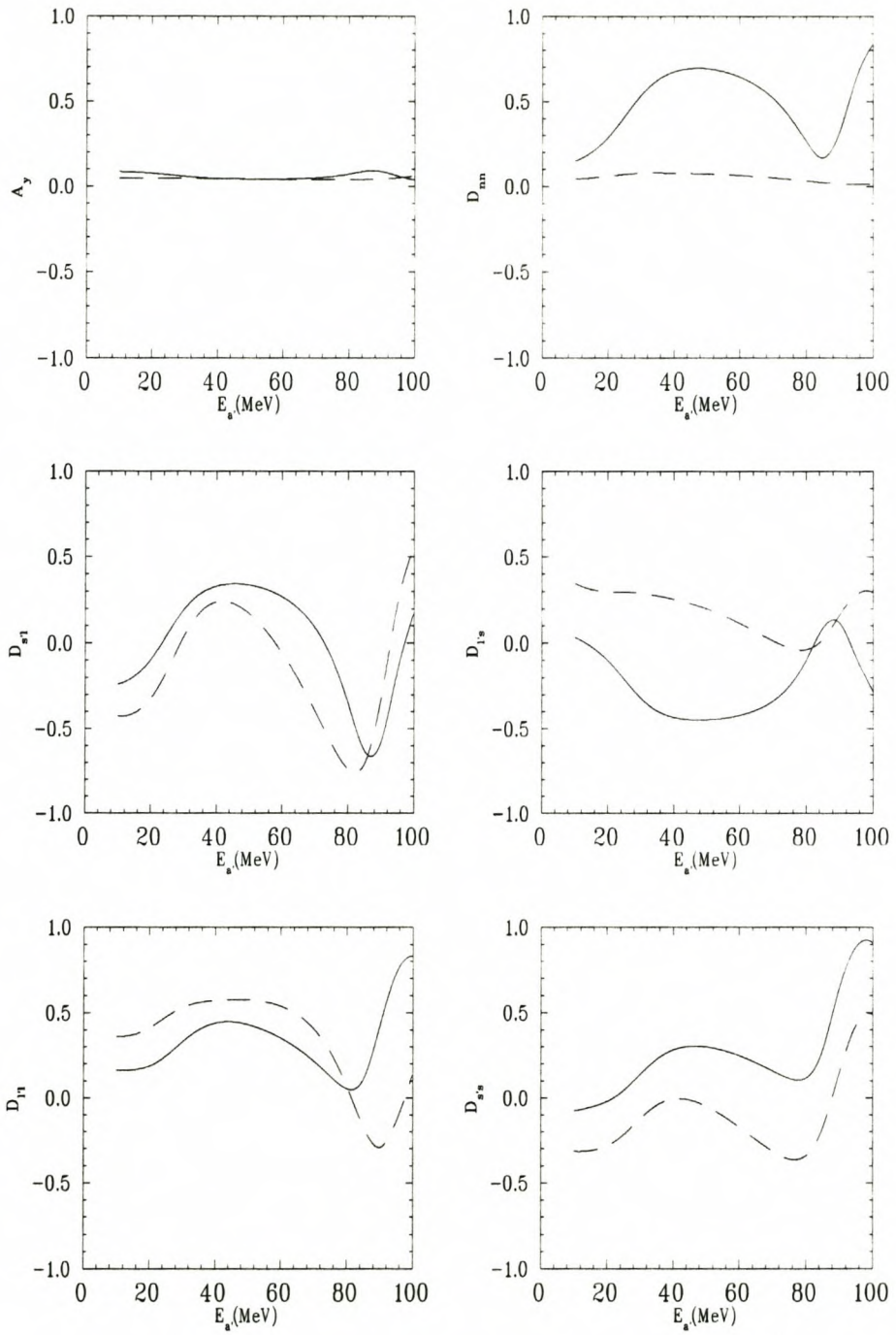

Figure 3.34: Plots of $(p, 2p)$ spin transfer observables for the $1d_{\frac{5}{2}}$ state obtained using the trace method excluding medium effects (solid line) compared with calculations which include free M_p and m_{meson} with medium modified g^*_{meson} (dashed line) for pseudovector πNN coupling.

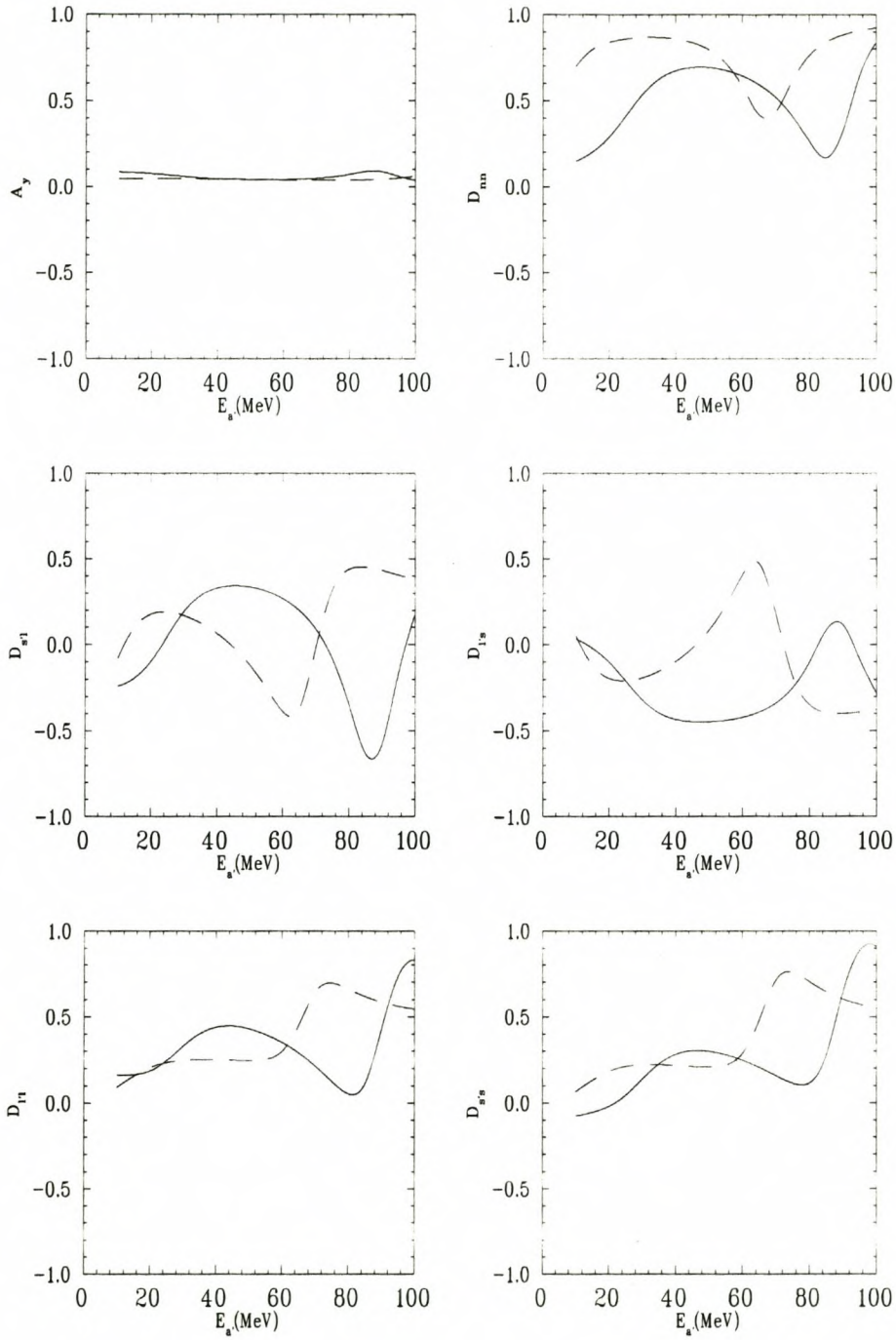

Figure 3.35: Plots of $(p, 2p)$ spin transfer observables for the $1d_{\frac{5}{2}}$ state obtained using the trace method excluding medium effects (solid line) compared with calculations which include free m_{meson} and g_{meson} with medium modified M_p^* (dashed line) for pseudovector πNN coupling.

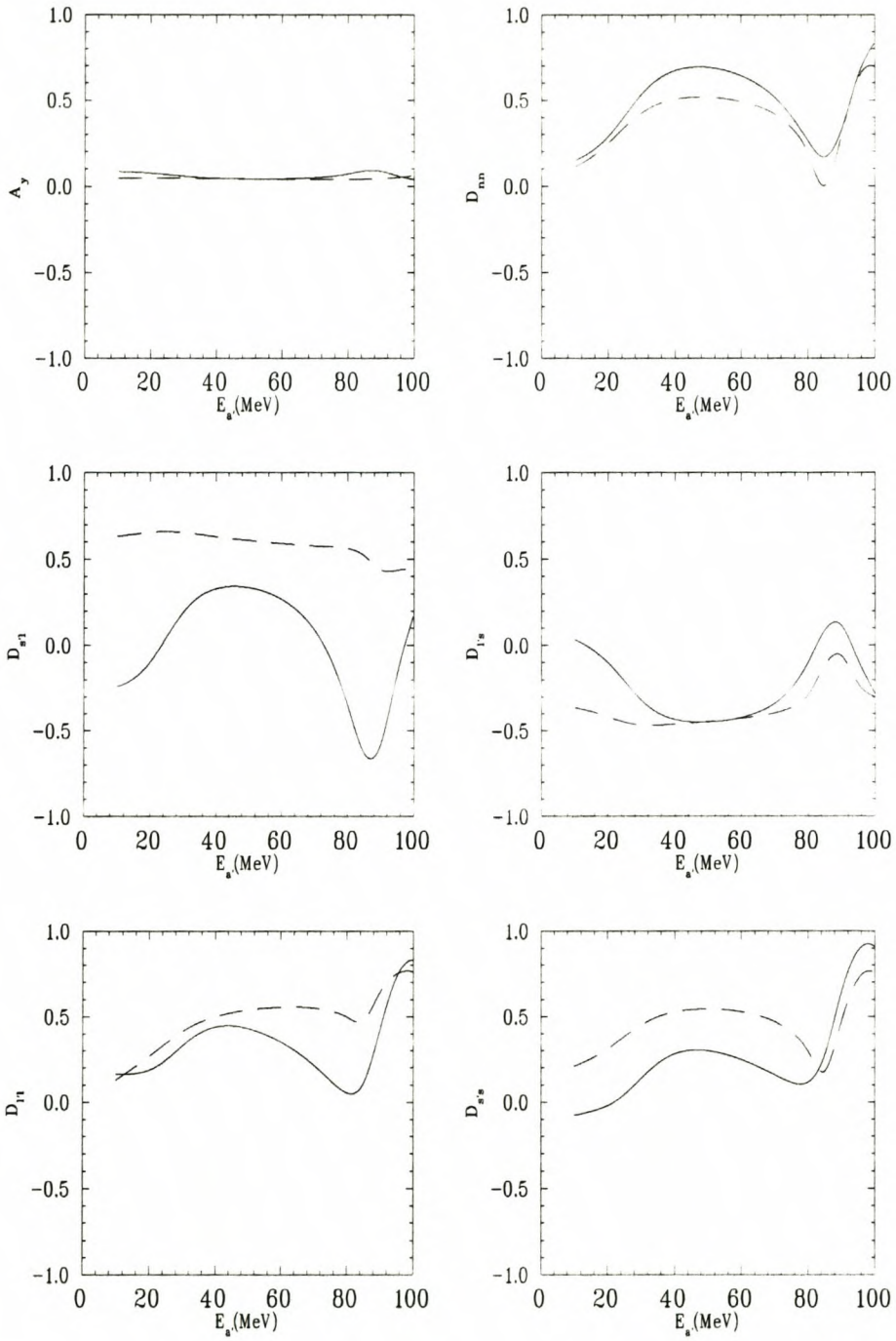

Figure 3.36: Plots of $(p, 2p)$ spin transfer observables for the $1d_{\frac{5}{2}}$ state obtained using the trace method excluding medium effects (solid line) compared with calculations which include free M_p and g_{meson} with medium modified m^*_{meson} (dashed line) for pseudovector πNN coupling.

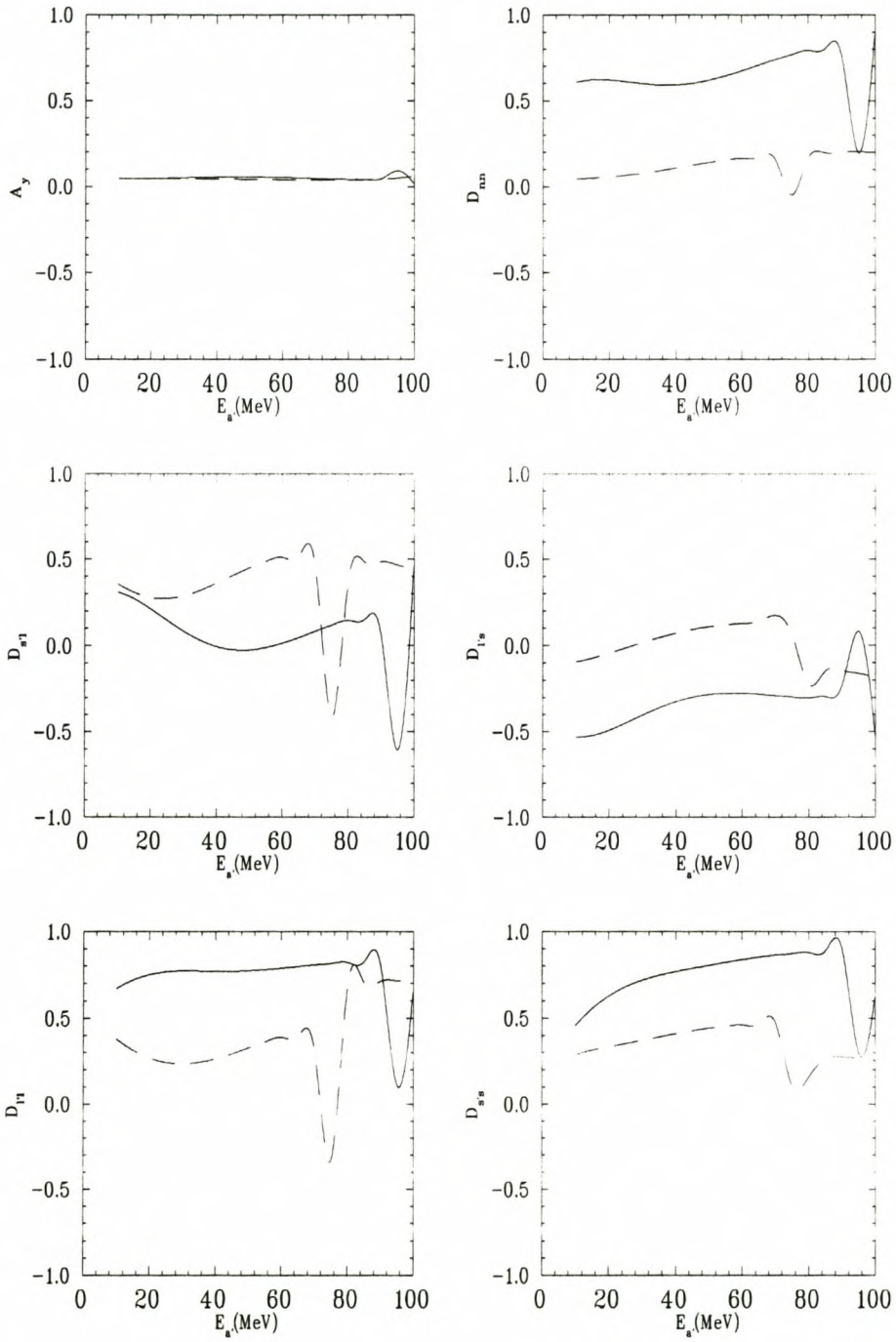

Figure 3.37: Plots of $(p, 2p)$ spin transfer observables for the $1d_{\frac{3}{2}}$ state obtained using the trace method excluding medium effects (solid line) compared with calculations which include medium modified M_p^*, m_{meson}^* and g_{meson}^* effect (dashed line) for pseudovector πNN coupling.

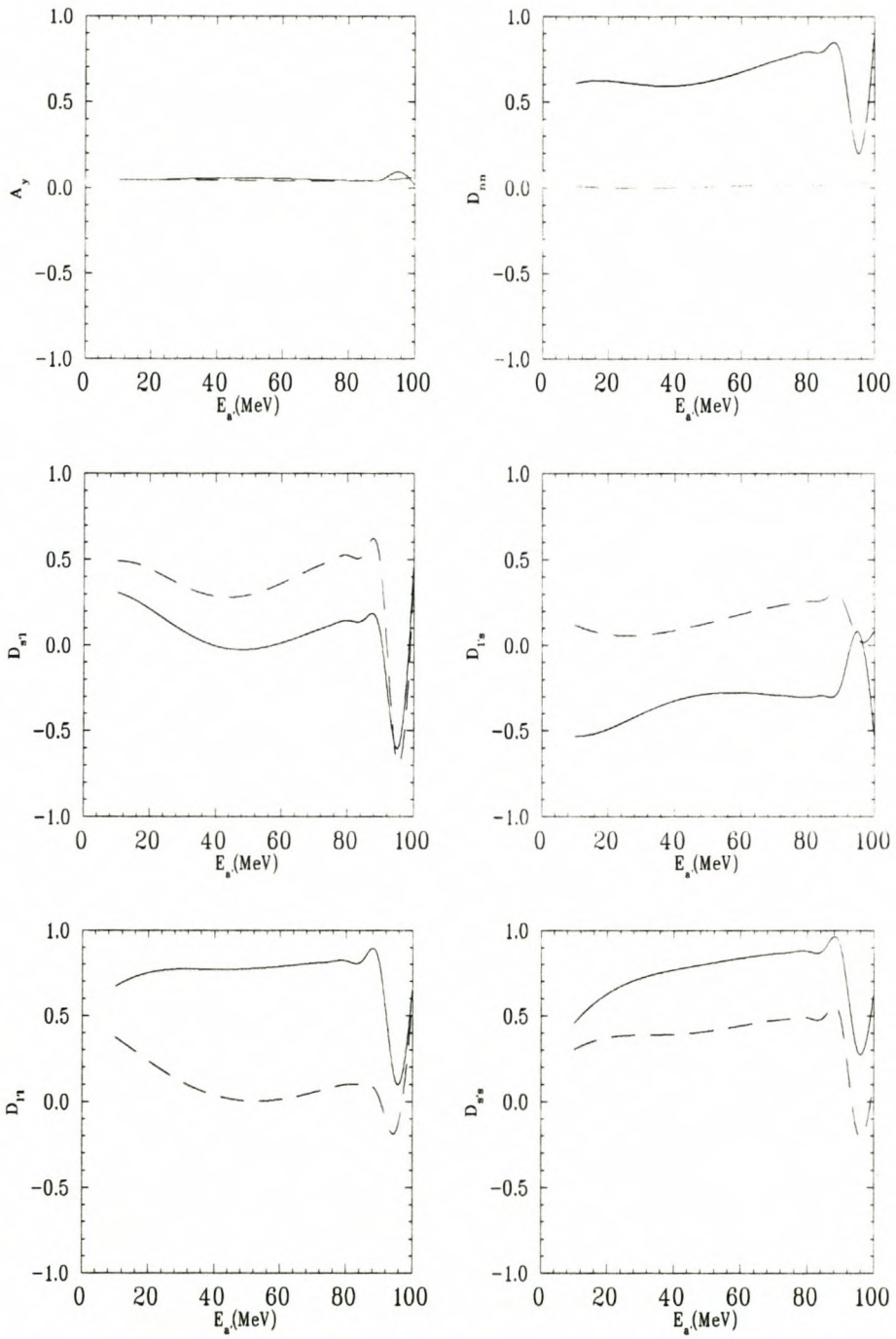

Figure 3.38: Plots of $(p, 2p)$ spin transfer observables for the $1d_{\frac{3}{2}}$ state obtained using the trace method excluding medium effects (solid line) compared with calculations which include free M_p and medium modified m^*_{meson} and g^*_{meson} (dashed line) for pseudovector πNN coupling.

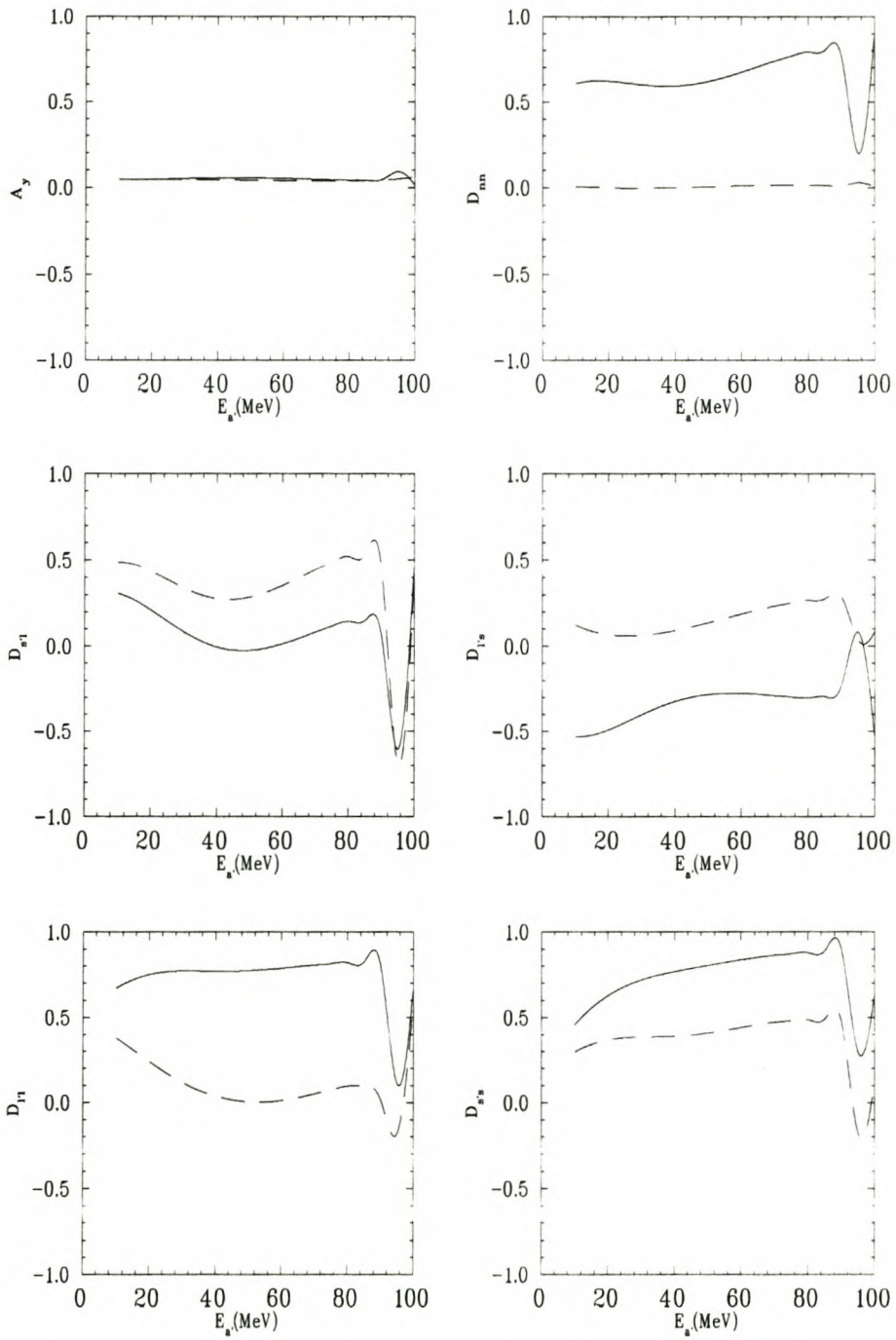

Figure 3.39: Plots of $(p, 2p)$ spin transfer observables for the $1d_{\frac{3}{2}}$ state obtained using the trace method excluding medium effects (solid line) compared with calculations which include free M_p and m_{meson} with medium modified g^*_{meson} (dashed line) for pseudovector πNN coupling.

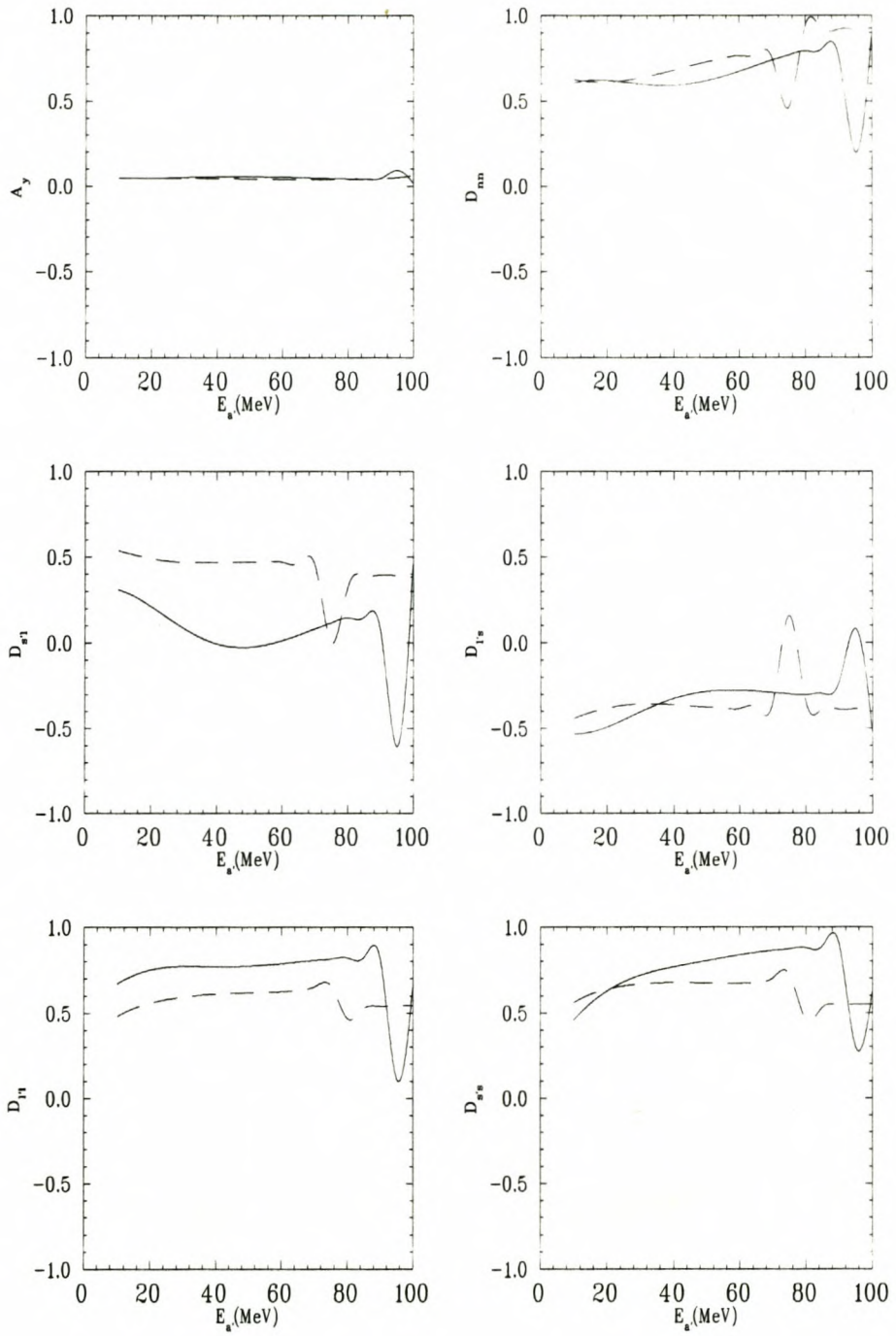

Figure 3.40: Plots of $(p, 2p)$ spin transfer observables for the $1d_{\frac{3}{2}}$ state obtained using the trace method excluding medium effects (solid line) compared with calculations which include free m_{meson} and g_{meson} with medium modified M_p^* (dashed line) for pseudovector πNN coupling.

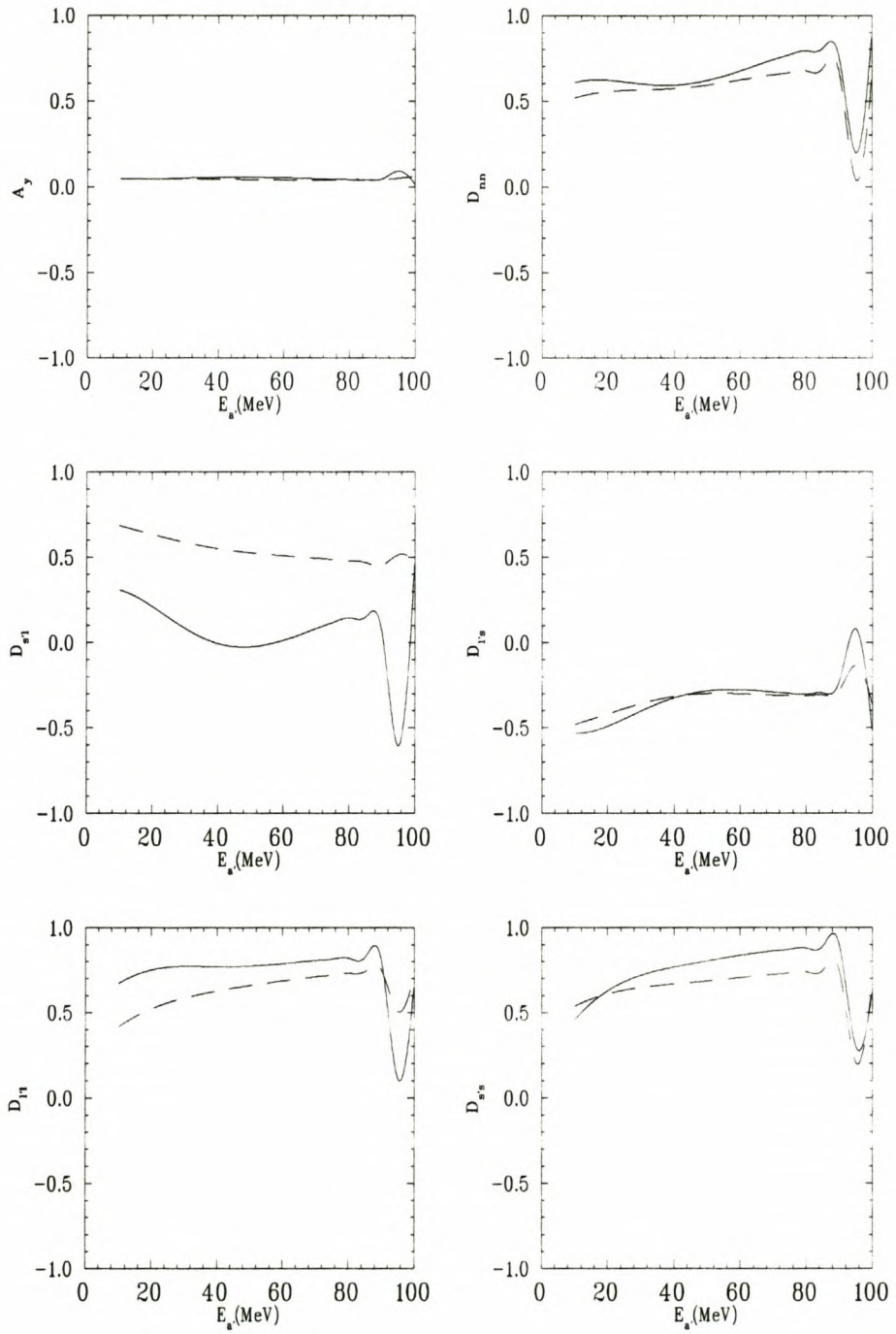

Figure 3.41: Plots of $(p, 2p)$ spin transfer observables for the $1d_{\frac{3}{2}}$ state obtained using the trace method excluding medium effects (solid line) compared with calculations which include free M_p and g_{meson} with medium modified m^*_{meson} (dashed line) for pseudovector πNN coupling.

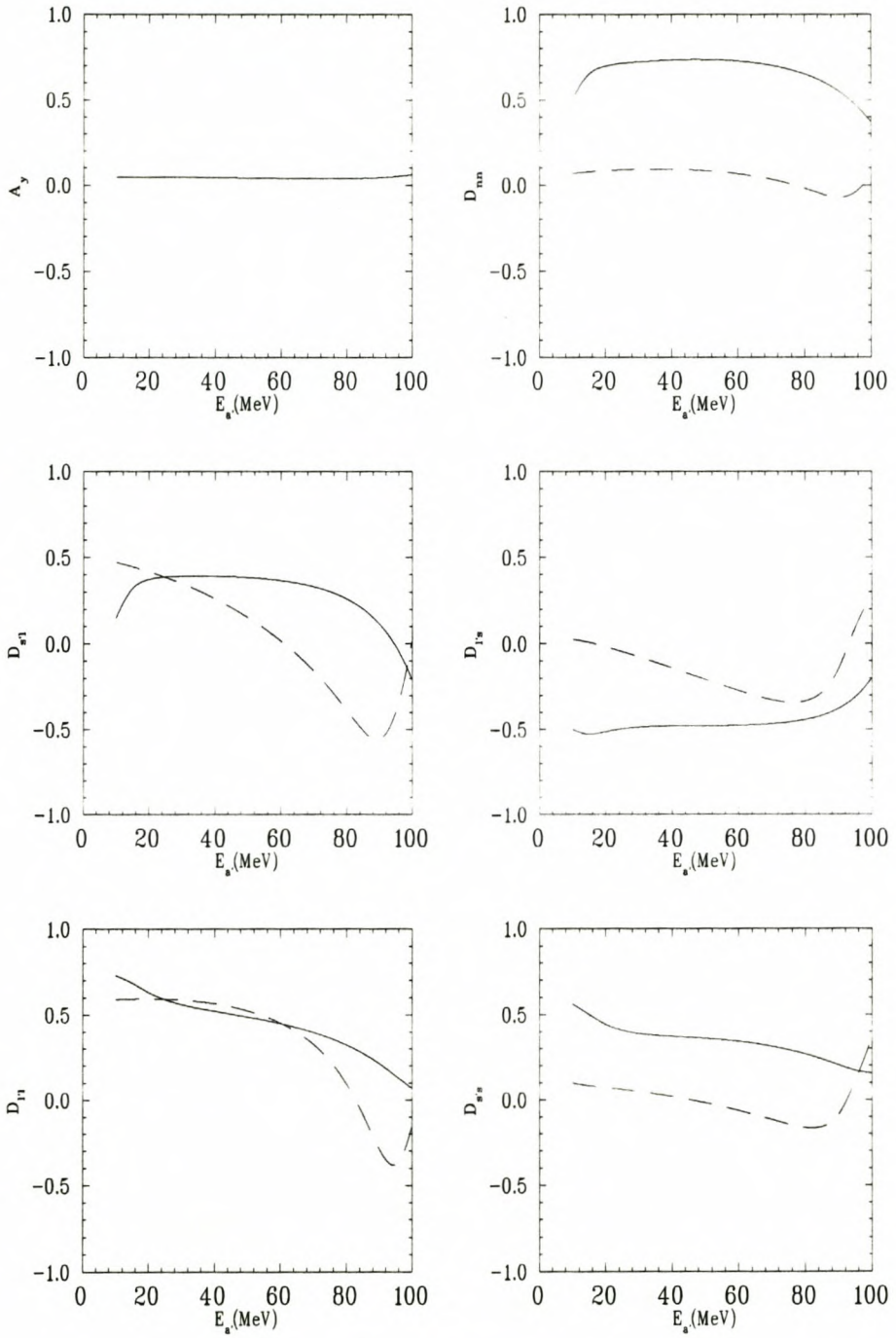

Figure 3.42: Plots of $(p, 2p)$ spin transfer observables for the $2s_{\frac{1}{2}}$ state obtained using the trace method excluding medium effects (solid line) compared with calculations which include medium modified M_p^*, m_{meson}^* and g_{meson}^* effect (dashed line) for pseudovector πNN coupling.

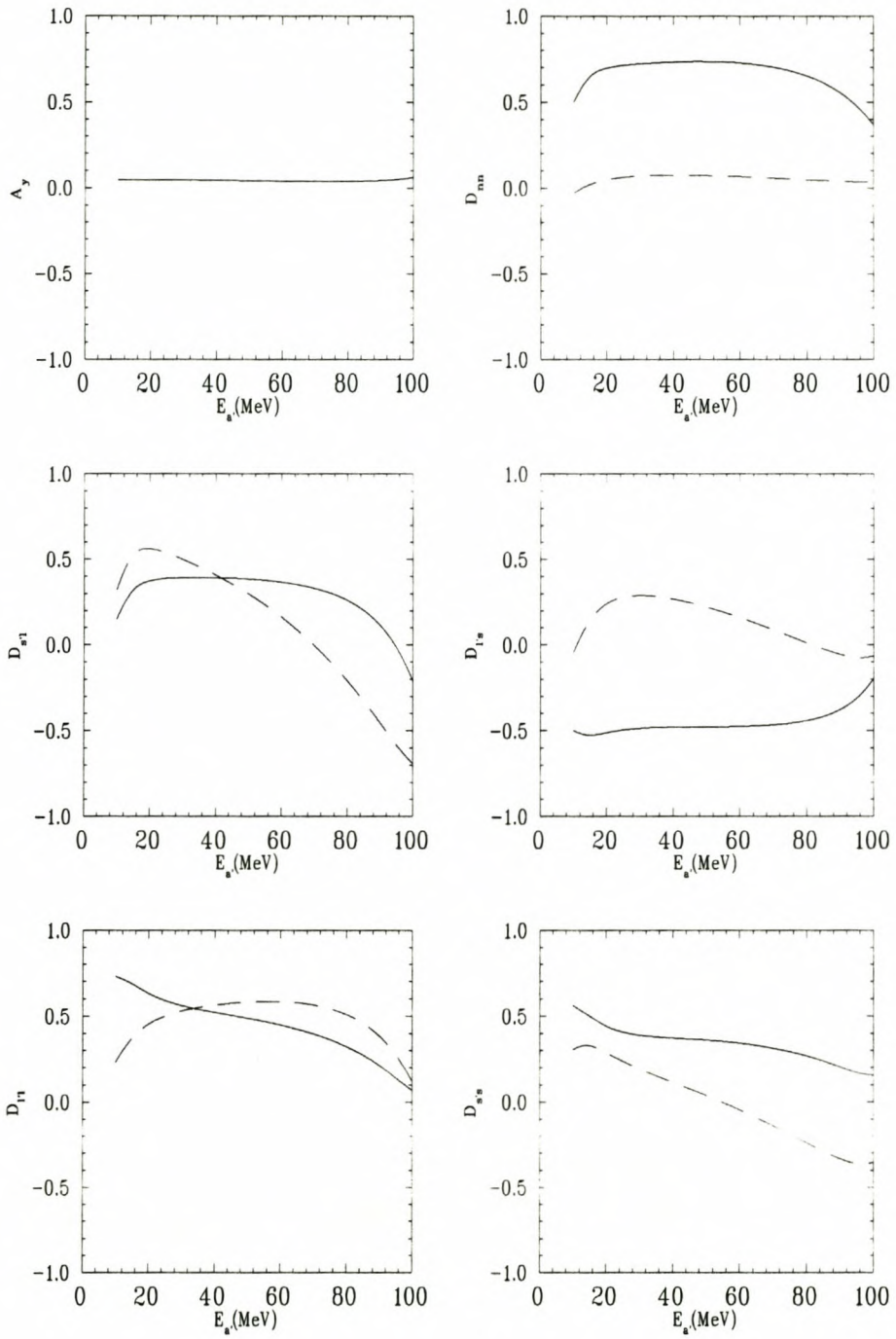

Figure 3.43: Plots of $(p, 2p)$ spin transfer observables for the $2s_{\frac{1}{2}}$ state obtained using the trace method excluding medium effects (solid line) compared with calculations which include free M_p and medium modified m^*_{meson} and g^*_{meson} (dashed line) for pseudovector πNN coupling.

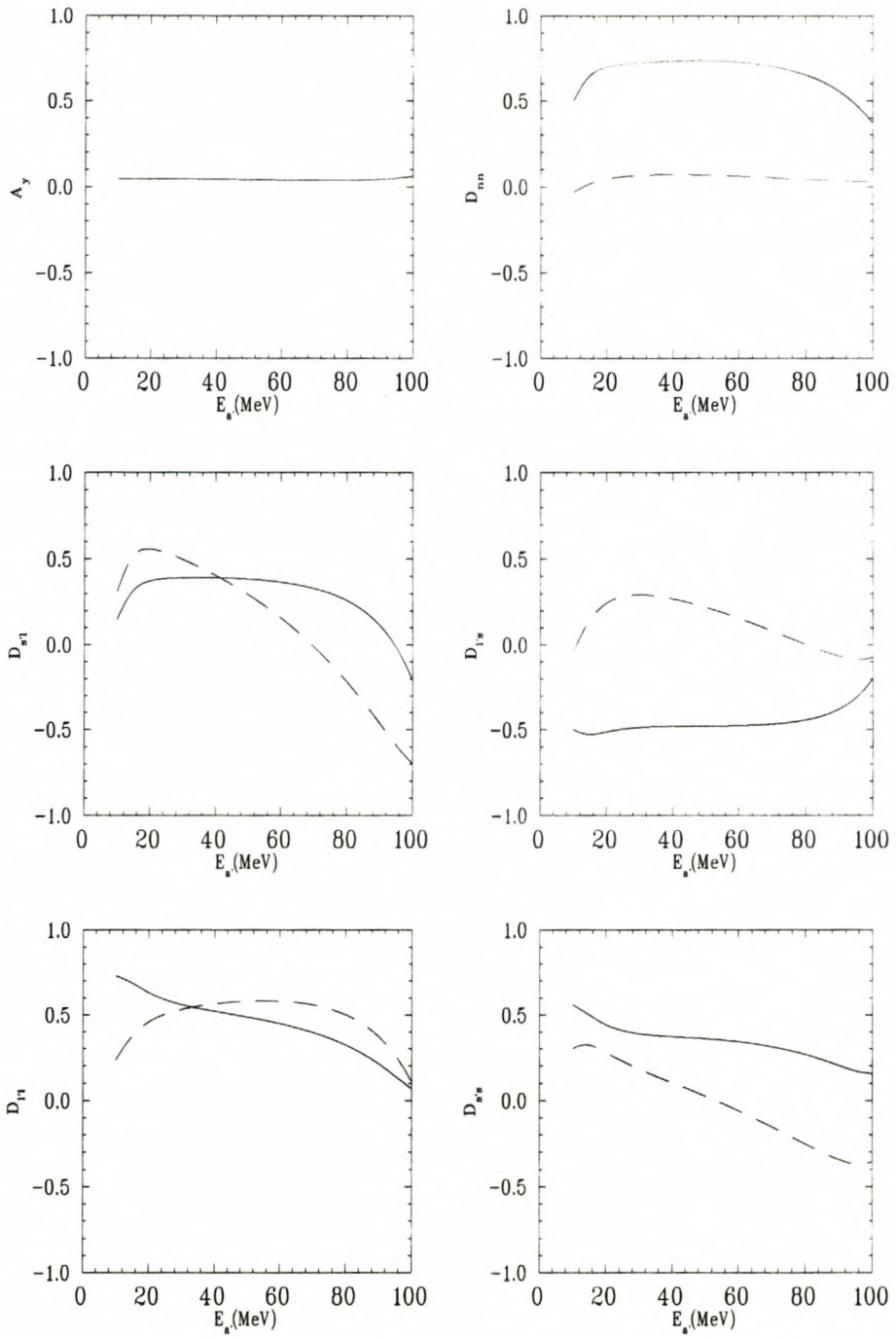

Figure 3.44: Plots of $(p, 2p)$ spin transfer observables for the $2s_{\frac{1}{2}}$ state obtained using the trace method excluding medium effects (solid line) compared with calculations which include free M_p and m_{meson} with medium modified g^*_{meson} (dashed line) for pseudovector πNN coupling.

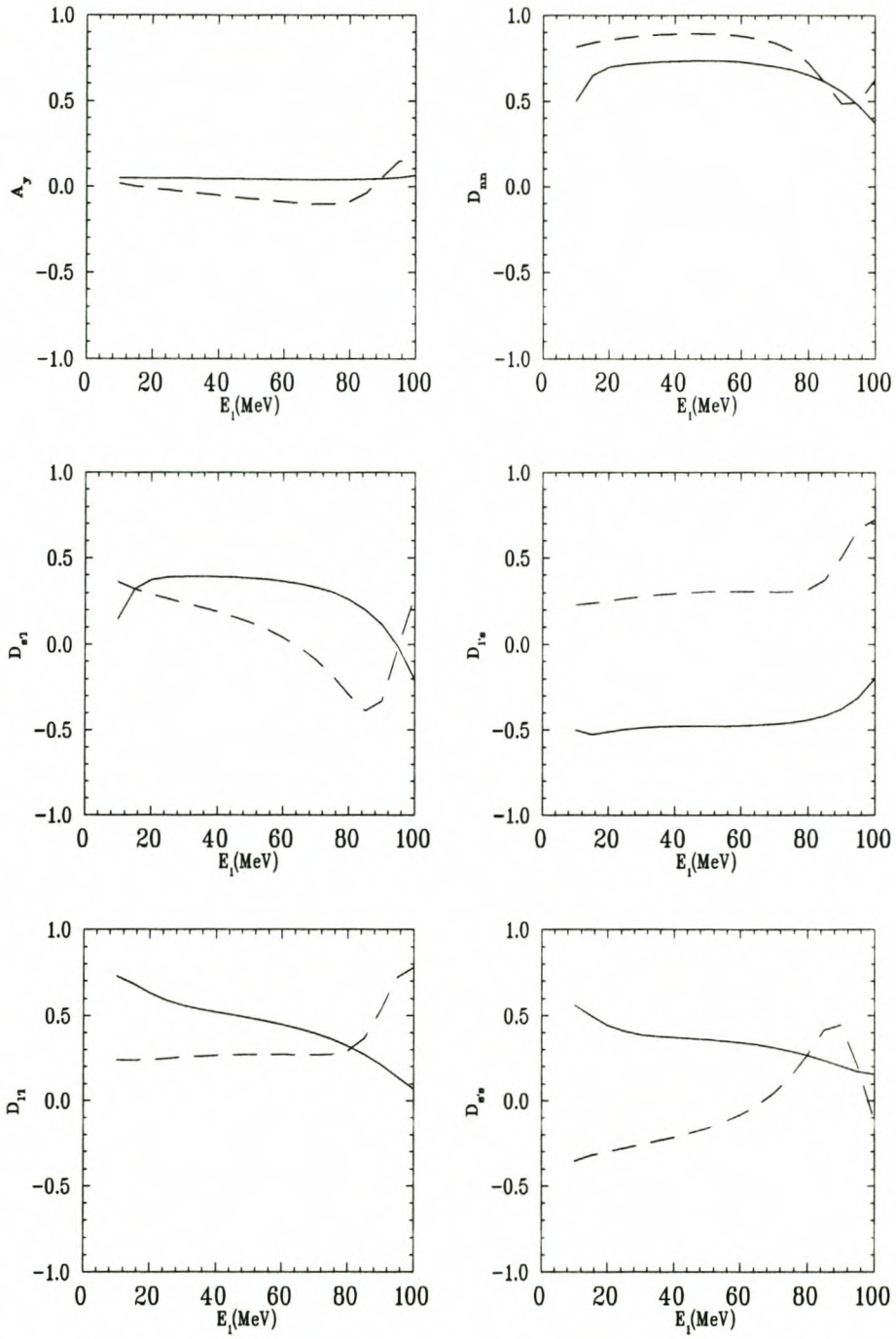

Figure 3.45: Plots of $(p, 2p)$ spin transfer observables for the $2s_{\frac{1}{2}}$ state obtained using the trace method excluding medium effects (solid line) compared with calculations which include free m_{meson} and g_{meson} with medium modified M_p^* (dashed line) for pseudovector πNN coupling.

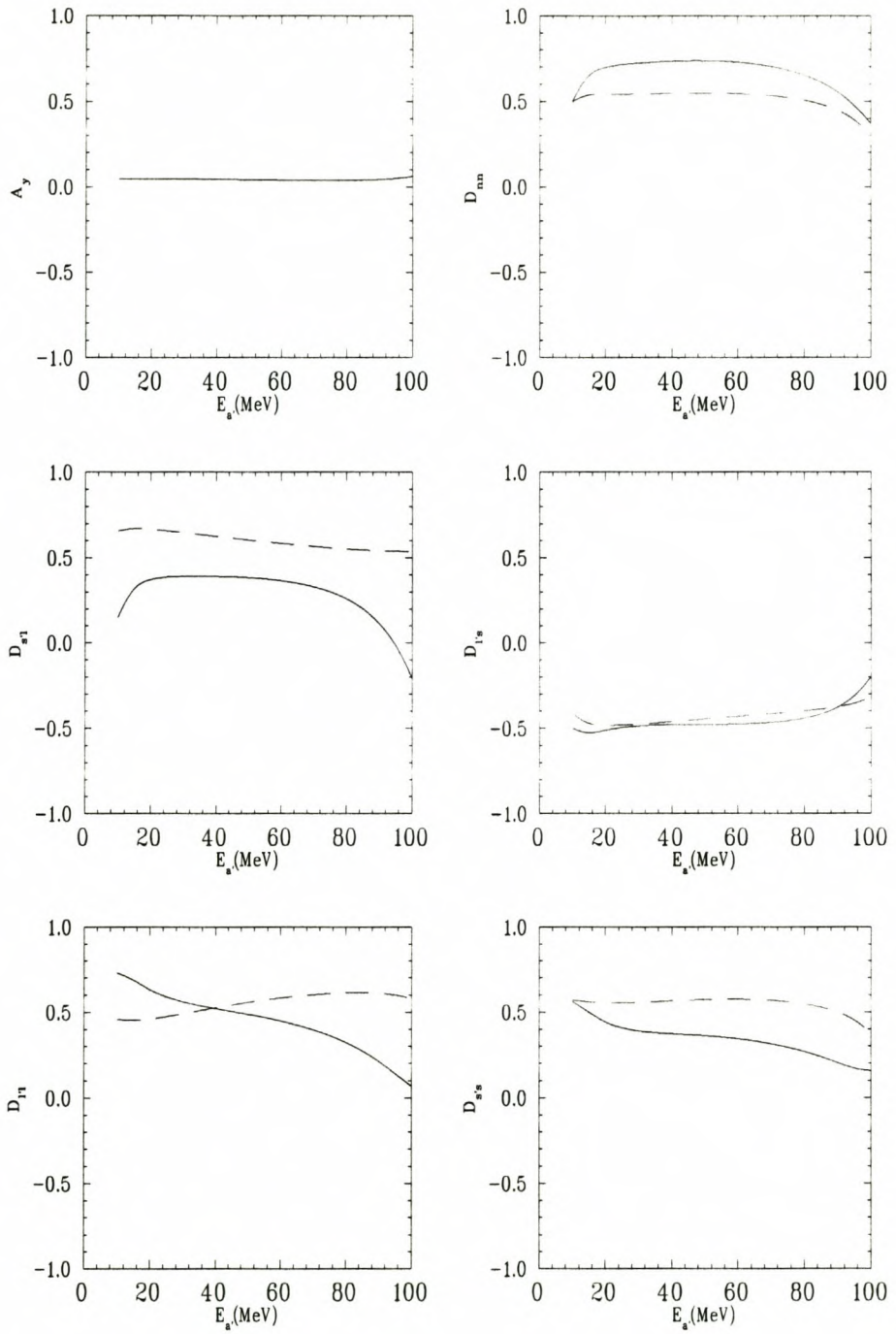

Figure 3.46: Plots of $(p, 2p)$ spin transfer observables for the $2s_{\frac{1}{2}}$ state obtained using the trace method excluding medium effects (solid line) compared with calculations which include free M_p and g_{meson} with medium modified m^*_{meson} (dashed line) for pseudovector πNN coupling.

Chapter 4

Summary and conclusions

The work presented in this dissertation represents a first step towards calculating complete sets of $(p, 2p)$ spin transfer observables. We have investigated the difference between the various kinematic prescriptions used in obtaining the NN t-matrix. Furthermore, we have looked at the effects of various nuclear medium modified parameters on the spin transfer observables. In addition to this, we have included both pseudoscalar and pseudovector coupling for the πNN vertex. Clearly the work presented in this dissertation represents a benchmark for future distorted wave models, which will allow an accurate calculation of complete sets of spin transfer observables at both the low and high energy regime, as well as allow us to include medium effects on the scattered wave function correctly.

Our formalism formulation, which is based on the relativistic impulse approximation model, allows us to write the transition amplitude $|T_{L_b J_b}(\mu_a, \mu_{a'}, \mu_{b'}, M_b)|^2$ in a form which we can directly use to calculate spin transfer observables. This is refered to as the trace method. We have also presented an alternative method which involves calculating $T_{L_b J_b}(\mu_a, \mu_{a'}, \mu_{b'}, M_b)$ first, which we refer to as the brute force approach. The trace method allows one to separate the spin dependent and independent components of the interaction into two separate terms. Because we focus on the high energy regime, it is reasonable to only consider the relativistic plane wave functions as describing the propagation of the scattered particles. The relativistic Love-Franey model is used to include a Lorentz invariant form of the NN-interaction. Medium effects are included through the Brown-Rho scaling law. Pseudoscalar and pseudovector coupling are included for the πNN vertex. Radial boundstate wave functions are calculated with the Dirac-Hartree approximation.

Our formalism has then been included in a numerical code, which we used to calculate complete sets of $(p, 2p)$ spin transfer observables. In addition we also include calculations of

unpolarized triple differential cross sections. Results of checks performed on our code, as well as results obtained for the unpolarized triple differential cross sections and spin observables were presented and discussed. We also compared results for our newly developed trace method to those of the traditional brute force approach. Furthermore, differences between the initial and final energy prescription were investigated. Various medium modifications to the scattering observables were included and compared to the results obtained with free parameters. We also looked at the differences between pseudoscalar and pseudovector predictions of the $(p, 2p)$ scattering observables.

In conclusion:

- We have presented a simple, but nevertheless useful model, which has undergone stringent numerically checks.
- This model demonstrates the influence of the various medium-modified parameters and different πNN couplings on the different scattering observables, and thus provides us guidelines for new experiments.
- Future additions to our model will include nuclear distortion effects and the inclusion of the more general IA2 representation of the NN interaction which will allow us to perform calculations at low and high energies.

Appendix A

Mathematical identities

A.1 Matrix identities

Theorem : Any 2×2 matrix can be expressed as

$$M = \sum_{ij=1}^{2} (e_i^\dagger \otimes e_j) M_{ij} \tag{A.1}$$

where $e_1 = (1,0)$ and $e_2 = (0,1)$.

Proof : Let e_i represent the unit vectors $e_1 = (1,0)$ and $e_2 = (0,1)$. Suppose M is a 2×2 matrix. The following properties hold

$$\begin{aligned} e_1^\dagger \otimes e_1 &= \begin{pmatrix} 1 \\ 0 \end{pmatrix} \otimes (1,0) \\ &= \begin{pmatrix} 1 & 0 \\ \\ 0 & 0 \end{pmatrix} \end{aligned} \tag{A.2}$$

$$\begin{aligned} e_1^\dagger \otimes e_2 &= \begin{pmatrix} 1 \\ 0 \end{pmatrix} \otimes (0,1) \\ &= \begin{pmatrix} 0 & 1 \\ \\ 0 & 0 \end{pmatrix} \end{aligned} \tag{A.3}$$

$$e_2^\dagger \otimes e_1 = \begin{pmatrix} 0 \\ 1 \end{pmatrix} \otimes (1,0)$$

$$= \begin{pmatrix} 0 & 0 \\ \\ 1 & 0 \end{pmatrix} \tag{A.4}$$

$$e_2^\dagger \otimes e_2 = \begin{pmatrix} 0 \\ 1 \end{pmatrix} \otimes (0,1)$$

$$= \begin{pmatrix} 0 & 0 \\ \\ 0 & 1 \end{pmatrix}. \tag{A.5}$$

If M_{ij} is an entry of the matrix

$$M = \begin{pmatrix} M_{11} & M_{12} \\ \\ M_{21} & M_{22} \end{pmatrix} \tag{A.6}$$

then it follows from the equations above that one can write

$$M = \sum_{i,j=1}^{2} (e_i^\dagger \otimes e_j) M_{ij}. \tag{A.7}$$

Bibliography

[Arn86] R. A. Arndt and D. Roper, VPI and Scattering Analysis Interactive Dialin Program and Data Base.

[Bro91] G. E. Brown and M. Rho, Phys. Rev. Lett. 66, 2720 (1991).

[Bjo64] J. D. Bjorken and S. Drell, Relativistic Quantum Mechanics (McGram-Hill, New York, 1964).

[Cha98] N. S. Chant, Private communication (1998).

[Coo89] E. D. Cooper and O. V. Maxwell, Nucl. Phys. A 493, 468 (1989).

[Cow00] A. A. Cowley, Private Communication (1999).

[Fra90] J. B. Fraleigh and R. A. Beauregard, Linear Algebra (Addison-Wesley publishing company, New York, 1990).

[Gre90] W. Greiner, Relativistic Quantum Mechanics (Springer-Verlag, Berlin, 1990).

[Gre92] W. Greiner, Quantum Electrodynamics(Springer-Verlag, Berlin, 1992).

[Gro93] F. Gross, Relativistic Quantum Mechanics and Field Theory (John Wiley and Sons, Inc., 1993).

[Hil99] G. C. Hillhouse, Relativistic Descriptions of Polarization Transfer, Ph. D Thesis, University of Stellenbosch (1999), unpublished.

[Hor81] C. J. Horowitz and Brian Serot, Nucl. Phys. A 368, 503 (1981).

[Hor85] C. J. Horowitz, Phys. Rev. C 31, 1340 (1985).

[Hor88] C. J. Horowitz and D. P. Murdock, Phys. Rev. C 37, 2032 (1988).

[Ike95] Y. Ikebata, Phys. Rev. C 52, 890 (1995).

[Its80] C. Itzykson and J. Zuber, Quantum Field Theory, (McGraw-Hill Inc. 1980).

[Kit76] P. Kitching, C. A. Miller, D. A. Hutcheon, A. N. James, W. J. McDonald, J. M. Cameron, W. C. Olsen and G. Roy, Phys. Rev. Lett. 37, 1600 (1976).

[Kre95] G. Krein, Th. A. J. Maris, B. B. Rodrigues and E. A. Veit, Phys. Rev. C 51, 2646 (1995).

[Kud86] Y. Kudo and K. Miyazaki, Phys. Rev. C 34, 1192 (1986).

[Lan91] K. Langanke, J. A. Maruhn, S. E. Koonin, Computational Nuclear Physics 1 (Springer-Verlag Berlin, 1991).

[LF81] W. G. Love and M. A. Franey, Phys. Rev. C 24, 1073 (1981).

[Math70] J. Mathews and R. L. Walker, Mathematical Methods of Physics, 2nd ed., (Addison-Wesley Publishing Company, Inc., 1970).

[Mat82] T. Matsui, and B. D. Serot. Ann. Phys. (N.Y.) 83. 107 (1982).

[Man96] J. Mano, M. Arima, Y. Kudo and H. Tsunoda, Prog. Theo. Phys., Vol 96, no. 5(1996).

[Man98] J. Mano and Y. Kudo, Prog. Theo. Phys. Vol. 100, no. 1 (1998).

[Man00] J. Mano, Private communication (2000).

[Max96] O. V. Maxwell, Nucl. Phys. A 600, 509 (1996).

[Max98] O. V. Maxwell, Nucl. Phys. A 638, 747 (1998).

[McN83] J. A. McNeil, L. Ray and S. J. Wallace, Phys. Rev. C 27, 2123 (1983).

[Mur87] D. P. Murdock, Proton Scattering as a Probe of Relativity in Nuclei, Ph.D Thesis, Massachussetts Institute of Technology (1987), unpublished.

[Nor99] T. Noro, Private communication (1999).

[Nor00] T. Noro, Private communication (2000).

[Num92] Numerical Recipes in Fortran 2nd ed., (Cambridge University Press, 1992).

[Pal81] M. K. Pal, Theory of Nuclear Structures (Scientific and Academic Editions, New Delhi, 1981.)

[Sak85] J. J. Sakurai, Modern Quantum Mechanics, Addison and Wesley Publicating Corporation Incorporated, New York, (1985).

[Ser86] B. D. Serot and J. D. Walecka, in Advances in Nuclear Physics, ed. J. W. Negel and E. Vogt (Plenum, New York, 1986), Vol. 16, p. 1.

[Var88] D. A. Varshalovich, A. N. Moskalev and V. K. Khersonskii, Quantum Theory of Angular Momentum, World Scientific Publishing Co., Inc. (N.J) (1988).

[Ven99] B. I. S. van der Ventel, G. C. Hillhouse, P. R. de Kock, and S. J. Wallace, Phys. Rev. C 60, 064618 (1999).

[Wal74] J. D. Walecka, Ann. Phys. 83, 491 (1974).

[Zha99] F. Zhang, Matrix Theory, Basic Results and Techniques, (Springer-Verlag, New York, 1999).